

The Development and Deployment of FOTOS: A Fast Observation of Trace Organics System

Dissertation
zur Erlangung des Grades
„Doktor der Naturwissenschaften“
im Promotionsfach Chemie

am Fachbereich Chemie, Pharmazie und Geowissenschaften
der Johannes Gutenberg-Universität Mainz

Aaron Michael Johnson
geb. in Saint Joseph, Missouri, USA

Mainz, 2011

Dekan:

1. Berichtstatter:

2. Berichtstatter:

Tag der mündlichen Prüfung: 29.06.2011

Zusammenfassung

Flüchtige organische Bestandteile (engl.: VOC) sind in der Atmosphäre in Spuren vorhanden, spielen aber trotzdem eine wichtige Rolle in der Luftchemie: sie beeinflussen das Ozon der Troposphäre, städtischen Smog, Oxidationskapazität und haben direkte und indirekte Auswirkungen auf die globale Klimaveränderung. Eine wichtige Klasse der VOC sind die Nicht-Methan-Kohlenwasserstoffe (engl.: NMHC), die überwiegend von anthropogenen Quellen kommen. Aus diesem Grund ist für Luftchemiker ein Messinstrument nötig, das die VOC, die NMHC eingeschlossen, mit einer höheren Zeitaufösung misst, besonders für Echtzeitmessungen an Bord eines Forschungsflugzeuges. Dafür wurde das System zur schnellen Beobachtung von organischen Spuren (engl.: FOTOS) entworfen, gebaut für den Einsatz in einem neuen Wissenschaftlichen Flugzeug, das in großen Höhen und über weite Strecken fliegt, genannt HALO. In der Folge wurde FOTOS in zwei Messkampagnen am Boden getestet.

FOTOS wurde entworfen und gebaut mit einem speziell angefertigten, automatisierten, kryogenen Probensystem mit drei Fallen und einem angepassten, erworbenen schnellen GC-MS. Ziel dieses Aufbaus war es, die Vielseitigkeit zu vergrößern und das Störungspotential zu verringern, deshalb wurden keine chemischen Trocknungsmittel oder adsorbierenden Stoffe verwendet. FOTOS erreichte eine Probenfrequenz von 5.5 Minuten, während es mindestens 13 verschiedene C₂- bis C₅-NMHC maß. Die Drei-Sigma-Detektionsgrenze für n- und iso-Pentan wurde als 2.6 und 2.0 pptv ermittelt, in dieser Reihenfolge. Labortests bestätigten, dass FOTOS ein vielseitiges, robustes, hochautomatisiertes, präzises, genaues, empfindliches Instrument ist, geeignet für Echtzeitmessungen von VOC in Probenfrequenzen, die angemessen sind für ein Forschungsflugzeug wie HALO.

Um die Leistung von FOTOS zu bestätigen, wurde vom 26. Januar bis 4. Februar 2010 ein Zwischenvergleich gemacht mit dem GC-FID-System am Meteorologischen Observatorium Hohenpeißenberg, einer WMO-GAW-globalen Station. Dreizehn verschiedene NMHC wurden innerhalb des Rahmens der GWA Data Quality Objectives (DQO) analysiert und verglichen. Mehr als 80% der Messungen von sechs C₃- bis C₅-NMHC erfüllten diese DQO. Diese erste Messkampagne im Feld hob die Robustheit und Messgenauigkeit von FOTOS hervor, zusätzlich zu dem Vorteil der höheren Probenfrequenz, sogar in einer Messung am Boden.

Um die Möglichkeiten dieses Instrumentes im Feld zu zeigen, maß FOTOS ausgewählte leichte NMHC während einer Messkampagne im Borealen Waldgebiet, HUMPPA-COPEC 2010. Vom 12. Juli bis zum 12. August 2010 beteiligte sich eine internationale Gruppe von Instituten und Instrumenten an Messungen physikalischer und chemischer Größen der Gas- und Partikelphasen der Luft über dem Borealen Wald an der SMEAR II-Station nahe Hyytiälä, Finnland. Es wurden mehrere Hauptpunkte von Interesse im Mischungsverhältnis der Alkane und im Isomerenverhältnis von Pentan identifiziert, insbesondere sehr unterschiedliche Perioden niedriger und hoher Variabilität, drei Rauchschwaden von Biomassen-Verbrennung von russischen Waldbränden und zwei Tage mit extrem sauberer Luft aus der Polarregion. Vergleiche der NMHC mit anderen anthropogenen Indikatoren zeigten mehrere Quellen anthropogener Einflüsse am Ort auf und erlaubten eine Unterscheidung zwischen lokalen und

weiter entfernten Quellen. Auf einen minimalen natürlichen Beitrag zum 24h-Kreislauf von NO_x wurde geschlussfolgert aus der Korrelation von NO_x mit Alkanen. Altersschätzungen der Luftmassen durch das Isomerenverhältnis von Pentan wurden erschwert durch sich verändernde Verhältnisse der Quellen und durch Besonderheiten der Photochemie während des Sommers im hohen Norden. Diese Messungen zeigten den Wert des Messens leichter NMHC, selbst in abgelegenen Regionen, als einen zusätzlichen spezifischen Marker von anthropogenem Einfluss.

Abstract

Volatile Organic Compounds (VOCs) are present in the atmosphere at trace levels, but nevertheless play an important role in atmospheric chemistry: influencing tropospheric ozone, urban smog, oxidation capacity, and having direct and indirect effects on global climate change. An important class of VOC is non-methane hydrocarbons (NMHCs), which have a predominantly anthropogenic source. Therefore, an instrument capable of higher time resolution measurement of VOCs, including the NMHCs, is desirable for atmospheric chemists, especially for in situ measurement aboard research aircraft. To this end, the Fast Observation of Trace Organics System (FOTOS) was designed, built for use aboard the new High Altitude Long Range Scientific Aircraft (HALO), and subsequently tested in two ground campaigns.

FOTOS was designed and constructed with a custom, automated, three-trap cryogenic sampling system and a modified, commercial, fast GC-MS. The goal of this design was to maximize versatility and minimize potential for artifacts, therefore no chemical drying agents or adsorbents were employed. FOTOS achieved 5.5 minute sampling frequency while measuring at least 13 different C₂ to C₅ NMHCs. The three sigma detection limit for n- and iso-pentane was determined to be 2.6 and 2.0 pptv, respectively. Laboratory tests confirmed that FOTOS was a versatile, robust, highly automated, precise, accurate, sensitive instrument, capable of in situ measurement of VOCs at sampling frequencies suitable for use aboard research aircraft, such as HALO.

In order to validate the performance of FOTOS, an intercomparison with the GC-FID system at the Meteorological Observatory at Hohenpeißenberg, a WMO-GAW global station, was performed from January 26th to February 4th, 2010. Thirteen different NMHCs were analyzed and compared within the framework of the GAW Data Quality Objectives (DQO). More than 80% of the measurements of six C₃ to C₅ NMHCs satisfied these DQO. This first field campaign highlighted the robustness and accuracy of FOTOS, in addition to the advantage of higher sampling frequency, even in a ground-based measurement.

To demonstrate the field capabilities of this new instrument, FOTOS measured select light NMHCs during a boreal forest campaign, HUMPPA-COPEC 2010. From July 12th to August 12th, 2010, an international consortium of institutes and instruments measured the physical and chemical properties of the gas and particle phase of the air over the boreal forest at the SMEAR II station near Hyytiälä, Finland. Several features of interest were identified in the alkane mixing ratios and the pentane isomer ratio, particularly contrasting periods of low and high variability, three biomass burning plumes from Russian wildfires, and two days of extremely clean air from the polar regions. Comparisons of NMHCs with other anthropogenic tracers revealed multiple sources of anthropogenic influence at the site and allowed for distinguishing between local and distant sources. Minimal natural contribution to the diel cycle of NO_x was deduced from correlations of NO_x with alkanes. Air mass age estimates by the pentane isomer ratio were complicated by varying source ratios and peculiarities of photochemistry during summer in the far north. These measurements revealed the value of measuring the light NMHCs, even in remote regions, as an additional specific marker of anthropogenic influence.

And as all have not faith, seek ye diligently and teach one another words of wisdom; yea, seek ye out of the best books words of wisdom; seek learning, even by study and by faith.

- Doctrine and Covenants 88:118

Teach ye diligently and my grace shall attend you, that you may be instructed more perfectly in theory, in principle, in doctrine, in the law of the gospel, in all things that pertain unto the kingdom of God, that are expedient for you to understand;

Of things both in heaven and in the earth, and under the earth; things which have been, things which are, things which must shortly come to pass; things which are at home, things which are abroad; the wars and the perplexities of the nations, and the judgments which are on the land; and a knowledge also of countries and of kingdoms —

That ye may be prepared in all things when I shall send you again to magnify the calling whereunto I have called you, and the mission with which I have commissioned you.

- Doctrine and Covenants 88: 78–80

The glory of God is intelligence, or, in other words, light and truth.

- Doctrine and Covenants 93:36

Contents

1	Introduction	1
1.1	The Air We Breathe	1
1.2	The Importance of VOCs	1
1.3	The Need for Higher Time Resolution	4
1.4	The Current Status of Fast GC	4
1.5	A New Instrument	6
2	A New, Fast GC-MS	9
2.1	GC in Atmospheric Science	9
2.2	HALO Specific Modifications	10
2.3	Sampling Overview	12
2.4	Cryogenic Trapping	16
2.5	Separation and Detection	23
2.6	Calibration	24
2.7	Data Quality Control Measures	26
2.8	Performance	28
2.9	Conclusions	34
3	MOHp Intercomparison	37
3.1	Measurement Standards	37
3.2	Sampling and Comparison Setup	38
3.3	Characteristic Results	39
3.4	Signal Agreement	40
3.5	Advantages of Higher Resolution	50
3.6	Envisioned Improvements	50
3.7	Conclusion	52
4	HUMPPA-COPEC 2010	53
4.1	The Boreal Forest	53
4.2	Sampling Setup	56
4.3	Data Coverage	57
4.4	Results Characterization	58
4.5	Specific Periods of Interest	61

4.6	Comparison with other Tracers	66
4.7	Air Mass Aging	72
4.8	Conclusion	74
5	Future Directions	77
6	Conclusions	81
	Lists of figures, tables and abbreviations	85
	Bibliography	93
	Acknowledgements	103
A	V25	105
A.1	A New Process Control System	106
A.2	Common Hardware and Construction	107
A.3	Input and Output Modules	107
A.4	Programming and Software	109
A.5	Performance and Capabilities	110
A.6	Conclusion	111
B	FastGCf2.pas	113
CV		135

Chapter 1

Introduction

1.1 The Air We Breathe

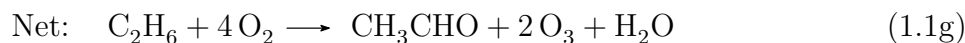
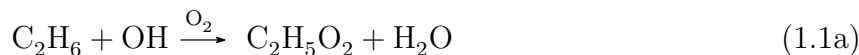
The atmosphere of the planet Earth has intrigued scientists for centuries. The analysis of the composition of ambient air began in 1676 with John Mayow and the discovery that normal air is composed of at least two main components. Since then, a great many scientists have sought to determine the composition of the atmosphere. Between 1767 and 1773, Joseph Priestly discovered at least seven different atmospherically relevant gases, including the nitrogen oxides, carbon monoxide and sulfur dioxide. As early as 1783, these investigations had become quite sophisticated and quantitative as Henry Cavendish determined the oxygen content of air to be 20.83% by volume, which is within almost a half percent of the current accepted value of 20.95% by volume. (For a more complete history of the discovery of elements and compounds of atmospheric importance, see Jacobson, 2002, Sect. 1.2.)

During the intervening centuries, the major constituents of the atmosphere have been well quantified: nitrogen (78.08%), oxygen (20.95%), and argon (0.93%). The abundances of these three gases are quite stable and equal around the globe. The next major component of the atmosphere is water vapor, which varies in abundance between 1 and 4% at Earth's surface. Due to this high variance, the contribution of water in air is usually removed (leaving "dry air") when calculating and reporting the abundance (i.e. mixing ratio, given in parts per volume, or mole fraction) of the other air constituents. The remaining 0.04% of the atmosphere is composed of the trace gases, the most abundant of which are CO₂, neon, helium, methane, krypton, and molecular hydrogen. The remaining tens of thousands of atmospheric constituents (Williams, 2004) are found at levels of about 0.5 parts per million by volume (ppmv), or $\mu\text{mol/mol}$, down to the parts per trillion by volume (pptv), or pmol/mol, level and below. The greatest number of this remaining set of trace gases are volatile organic compounds (VOCs).

1.2 The Importance of VOCs

Although VOCs are present at very low concentrations in the atmosphere, they play a critical role in its chemistry, affecting health, climate, and quality of life (see Williams, 2004, and

references therein). These impacts are wide ranging and include: the production of urban smog, direct health effects, and the formation of secondary organic aerosol (SOA). VOCs have been the subject of numerous books and review articles (e.g. Jacobson, 2002; Hewitt, 1999; Williams, 2004; Sillman, 1999). Of significant importance is the role of VOCs in ozone (O_3) production, illustrated by the example of ethane (C_2H_6) oxidation by the hydroxy radical (OH) shown in Eq. 1.1 (Jacobson, 2002).



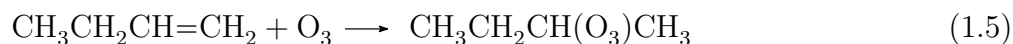
Hydrogen extraction from C_2H_6 by OH, and subsequent rapid combination with molecular oxygen (O_2), yields the ethylperoxy radical ($C_2H_5O_2$) (Eq. 1.1a). Reaction of $C_2H_5O_2$ with nitric oxide (NO) produces nitrogen dioxide (NO_2) and an ethoxy radical (C_2H_5O) (Eq. 1.1b). An oxygen molecule then extracts a hydrogen, forming acetaldehyde (a stable oxygenated VOC) and a hydroperoxy radical (HO_2) (Eq. 1.1c). The HO_2 and another NO then react, resulting in the regeneration of an OH radical plus another NO_2 molecule (Eq. 1.1d). Nitrogen dioxide photolyzes, regenerating NO radicals and producing atomic oxygen (Eq. 1.1e), which rapidly reacts with molecular oxygen producing ozone (Eq. 1.1f). In total, in the presence of NO and OH radicals, ethane oxidizes to acetaldehyde, producing two ozone molecules and a water molecule (Eq. 1.1g).

Although reaction with OH is the primary destruction pathway (“sink”) for VOCs, reaction with other atmospheric oxidants, including the nitrate radical (NO_3) and O_3 , are also significant, with reaction rates dependent on the chemical structure. Hydrogen extraction by NO_3 forms a peroxy radical, as with OH (Atkinson and Arey, 2003), which then follows the same reaction sequence as in Eq. 1.1. An example reaction of n-butane (C_4H_{10}) with NO_3 is shown in Eq. 1.2.



Saturated hydrocarbons do not react on appreciable time scales with O_3 (the atmospheric lifetime of alkane destruction from O_3 is greater than 4500 years, Atkinson and Arey, 2003), but those VOCs containing a double bond will add OH, NO_3 , and O_3 initially to

the double bond (Atkinson and Arey, 2003), seen in Eq. 1.3, 1.4, and 1.5 with 1-butane ($\text{CH}_3\text{CH}_2\text{CH}=\text{CH}_2$).



There are many different sources of VOCs, which can be broadly classified as either biogenic or anthropogenic. As byproducts of photosynthesis, plants release up to 1.2×10^{15} grams of carbon per year (gC yr^{-1}), predominately in the form of highly reduced, reactive compounds, such as isoprene or terpenes (respectively 44 and 11% of total emissions) (Fuentes et al., 2000; Guenther, 2002; Kesselmeier et al., 2002; Guenther et al., 1995). These emissions depend on plant type, age, and health, as well as light, temperature, and moisture conditions (Kesselmeier and Staudt, 1999; Guenther et al., 1995). Many studies have also shown direct emission by plants and animals for signaling purposes (Greene and Gordon, 2003; Krieger and Breer, 1999; Cremer et al., 2002; Shiojiri et al., 2002; Kessler and Baldwin, 2001). In contrast, anthropogenic emissions ($1.1\text{--}1.5 \times 10^{14} \text{ gC yr}^{-1}$) are dominated by more stable compounds, such as alkanes or aromatics, from the use and production of fossil fuels (respectively 24.7 and 20.2% of total emissions), domestic use of biofuels (20.0%), and contributions from the solvents industry (17%) (Butler et al., 2008; Schoenmakers et al., 2000; Olivier et al., 1999). The most difficult anthropogenic source to assess is that of burning biomass, which is dependent on a great number of factors, including fuel type, humidity, and burn rate (Andreae and Merlet, 2001; Lobert et al., 1990). Additionally, VOCs have a wide range of reactivities and atmospheric lifetimes, which allows VOC analysis to give unique insights into the chemical and transport history of a given air sample (Penkett et al., 2007; Williams et al., 2000).

One important class of VOC is the non-methane hydrocarbons (NMHCs). NMHCs are those compounds which contain only hydrogen and carbon. Methane is removed from this group due to its significantly higher concentration and longer lifetime, in addition to having predominately different sources to the other hydrocarbons. A large number of biogenic and anthropogenic VOC emissions are NMHCs, but those from natural sources (e.g. isoprene with a lifetime of about 1 hour) are much more reactive than those from anthropogenic sources (e.g. propane with a lifetime of 11 days) (Atkinson and Arey, 2003). Ambient concentrations of anthropogenic alkanes vary from a few ppbv in major urban areas (Baker et al., 2008), to hundreds of pptv at rural sites (this work), down to a few pptv in the lower stratosphere (Baker et al., 2010). Thus measurement of these longer-lived NMHCs provides an indicator for changes in primary anthropogenic emissions and the efficacy of emission reduction measures. As a marker of anthropogenic influence, NMHCs additionally provide an effective filter for measurements seeking to determine natural emissions of other trace gases. Therefore,

measurement of NMHCs provides highly desirable information in efforts focused on either anthropogenic and/or natural emissions.

1.3 The Need for Higher Time Resolution

For the past fifty years, VOCs have typically been measured by means of off-line gas chromatography (GC) analysis coupled with one of a range of detectors, e.g. Flame Ionization Detector (FID), Electron Capture Detector (ECD), Photo-Ionization Detector (PID) or mass spectrometry (MS) of samples collected in glass (Pollmann et al., 2008) or metal (Gebhardt et al., 2008; Colman et al., 2001) containers, or samples collected on absorbent cartridges (Williams et al., 2007b). These methods allow for wide coverage, including at remote sites with limited power or infrastructure (Pozzer et al., 2010), but have limitations in the compounds they are able to measure due to artifacts and storage effects (Pollmann et al., 2008; Baker et al., 2010; Colman et al., 2001). To circumvent these problems, many atmospheric observatories perform in situ GC analysis of VOCs (e.g. Plass-Dülmer et al., 2002). While these methods are more robust and inherently less prone to artifacts, they are generally limited in their time resolution and portability.

In order to explore the vertical properties of the atmosphere, atmospheric scientists have used a variety of airborne platforms including jet aircraft, microlights, balloons, and zeppelins (e.g. Eerdeken et al., 2009; Junkermann, 2005; Toon et al., 1999; Häsel et al., 2009). These airborne platforms, however, require higher performing instruments. Flask or cartridge sample collection during research flights is still possible, but the number of samples that can be collected is limited due to the space available for the sample containers. Typical laboratory GC-MS systems operate with 30–60 minute run times, making them unsuitable for aircraft deployment. For example, at a cruising speed of 275 m/s, a research aircraft would cross from Bremen, Germany to the coast of England in less than thirty minutes. That would result in at most one data point, if any. At a cycle time of five minutes, however, six measurements would be made, one every 82 km or roughly the distance from Bremen to the German coast. This simple example illustrates the need for a much higher time resolution than traditionally realized in order for an in situ GC to be used aboard a research aircraft. Apel et al. (2003) demonstrated the ability of a fast GC-MS system aboard an aircraft to measure a variety of light VOCs at rates acceptable for aircraft speeds, albeit with a large space requirement.

1.4 The Current Status of Fast GC

Since the introduction of gas chromatography in the 1960s, the principles related to increasing the speed of GC analysis have been understood (Matisová and Dömötöróvá, 2003). Beginning in the 1990s, a great deal of emphasis has been placed on reducing chromatography separation times due to commercial pressure to increase performance and throughput. Although largely arising from cost-cutting needs, these advances have benefits for the atmospheric applications of GC as well. The length of time required for a GC separation is a function

of the resolution achieved, selectivity of the method, and the sensitivity of detection. Thus, reducing the method to the minimum acceptable resolution, with the highest selectivity and sensitivity would result in the fastest possible analysis time (see Korytar et al., 2002, and references therein). Resolution can be reduced by such measures as shortening the GC column, optimizing the carrier gas velocity, higher and faster temperature programming, and pressure/flow programming (Leclercq and Cramers, 1985; Cramers and Leclercq, 1988). Selectivity can be increased by choosing the stationary phase and detection (e.g. FID, PID, ECD, MS) most suited for the target compounds. Furthermore, optimization of certain physical properties of the system result in shorter analysis times without losses to resolution. Methods capable of reducing analysis time without affecting resolution include using a narrower bore column (Desty et al., 1962), a lower molecular weight carrier gas, and eluting into a vacuum (see Matisová and Dömötöröová, 2003; Korytar et al., 2002, and references therein). Current technologies are capable of reproducibly manufacturing GC columns with inner diameters down to 0.1 mm. Although hydrogen gas is a more desirable carrier gas for chromatographic reasons, helium is often used due to safety concerns. The benefit of eluting into a vacuum can only be realized with a MS detector.

Mass spectrometry is a particularly well suited to GC analysis. As a well-developed and widely-used detection method, many robust commercial systems are readily available. There are many advantages to MS that also assist fast GC analysis. The vacuum necessary for MS function helps improve resolution, and thus reduces analysis time as mentioned previously. Many MS systems are capable of multiple ionization techniques, making them non-specific, while the measurement itself can be quite selective. The nature of MS allows the individual detection of multiple peaks with similar retention times, given the compounds have different masses and/or fragmentation patterns. By performing this mass separation, chromatographic resolution can be reduced, again decreasing analysis time. The reproducible retention times of eluted compounds in GC analysis facilitates running a MS in Select Ion Monitoring (SIM) mode. In SIM mode, only specific mass to charge (m/z) ratios are monitored, increasing sensitivity to the target compounds. The selected m/z ratios can be changed as the analysis progresses, providing an adapting selectivity in response to analyte elution. These attributes (non-specificity, selectivity, and sensitivity) together make MS a powerful detection method for fast GC analysis.

In addition to the GC analysis time, sampling frequency is dependent on speed of the sample collection and preparation (Maštovská and Lehotay, 2003). A common technique for obtaining short collection times is the use of cryogenics and resistively heated traps. Additionally, a second trapping of the analytes and focusing within a low volume trap prior injection is also widely used (e.g. Liu and Phillips, 1989; Apel et al., 2003; Baker et al., 2010). This has the effect of increasing the signal to noise, i.e. broad low peaks without secondary focusing quickly disappear below the detection horizon. Sampling rates can be increased by increasing sample flow (provided by efficient traps), reducing sample size (permitted by sensitive detectors), and running sample collection parallel to GC separation. The sensitivity

of the detector plays a large role in measurement time resolution. A more sensitive detector requires less sample. Less sample can be collected in a shorter period and can be separated on a narrower, shorter column. Splitless injection facilitates lower detection limits than split injections, but requires more specialization (Matisová and Dömötöröová, 2003).

To assist in sample trapping, chemical adsorbents have been used since the 1960s (Bellar et al., 1963) and become wide spread since then (Dettmer and Engewald, 2002). The advantage of using these adsorbents is that higher trapping temperatures are possible. The use of such adsorbents, however, has been shown to result in artifact contamination of the sample (Pollmann et al., 2006). Typically a molecule like ozone, present ambient air, will react with carbonaceous adsorbents to produce carbonyl compounds identical to those being detected. As an alternative to adsorbent trapping, inert substances such as glass wool or beads have been used in combination with cooling by liquid nitrogen to reach lower temperatures than necessary with adsorbents. These inert systems have demonstrated the ability to quantitatively trap C₂ to C₈ hydrocarbons (Plass-Dülmer et al., 2002) and C₂ to C₄ carbonyls and methanol (Apel et al., 2003).

1.5 A New Instrument

To provide the German (and wider European) science community with more opportunities to investigate the atmosphere, the German Federal Ministry of Education and Research, the Helmholtz Society, and the Max Planck Society jointly funded the High Altitude, Long Range Research Aircraft (HALO). With a range of ten thousand kilometers and a maximum altitude of fifteen kilometers, HALO provides new opportunities for the European science community. Large suites of instruments can be combined to investigate the atmosphere more thoroughly and with greater coverage than previously possible (DLR, 2009).

In order to take full advantage of this new platform for the measurement of VOCs throughout the atmosphere, a fast GC-MS was constructed for use aboard HALO. The Fast Observation of Trace Organics System (FOTOS) combined a novel cryogenic trapping system with a customized, commercial fast GC. Sample concentration and focusing occurred on inert, resistively-heated, cryogenic traps. Faster GC analysis was achieved by use of MS detection, narrow-bore capillary GC, shorter columns, accelerated temperature programming, and carrier gas flow programming. For safety reasons, however, helium was selected as the carrier gas instead of hydrogen. The entire system was controlled by a custom electronic control system which facilitated parallel cycling, resulting in the fastest possible measurement frequency. Together, these various aspects made FOTOS a flexible, fast GC, capable of measuring a wide range of VOCs with only minor modifications.

This dissertation has three main purposes. Chapter 2 discusses in detail the design and construction of FOTOS. Special consideration for certification for use aboard HALO is presented, as well as a discussion of internal performance and consistency tests. Chapter 3 presents the results of the first field campaign with FOTOS, an intercomparison with the GC-FID system at the Meteorological Observatory at Hohenpeißenberg (MOHp), part of the

German Weather Service and a Global Atmosphere Watch (GAW) Station. Chapter 4 contains first results from a large-scale measurement campaign in the boreal forest at the SMEAR II Station of the University of Helsinki. At the time of writing, the certification process for HALO was not yet completed, so the campaign in Finland is presented to demonstrate the reliability of FOTOS performance and results, and its suitability to airborne, in situ measurements. Chapter 5 outlines future design and scientific directions with FOTOS, and Chap. 6 provides a summary of this work. Two Appendices are included, App. A describes the custom, electronic control system within FOTOS and App. B presents the program specific to FOTOS which runs that control system.

Chapter 2

A New, Fast GC-MS System for in situ, Airborne Detection of VOCs

2.1 Gas Chromatography in Atmospheric Science

At the conclusion of his acceptance lecture for the Nobel Prize in Chemistry in 1952, Archer J. P. Martin (Martin, 1964) mentioned the work he had started with Anthony T. Jones to apply the principle of partition chromatography (for which he was receiving the Nobel Prize) to gas-liquid chromatography. First mentioned by Martin and Synge ten years previously (Martin and Synge, 1941), gas-liquid chromatography, commonly referred to simply as gas chromatography (GC), developed quickly as a powerful analytic technique for separating complex mixtures of volatile compounds. Successive advancements in detection methods, including flame ionization (Harley et al., 1958) and electron capture (Lovelock, 1958), led to increased use of GC.

As early as 1962 (Altshuller and Clemons, 1962), GC techniques have been used for the analysis of ambient air. Since that time, great progress has been made in the field of GC, including the advent of fused-silica capillary columns (Dandeneau and Zerenner, 1979), producing ever more stable, reproducible columns, with a wide variety of stationary phases for the analysis of specific sets of compounds. Sophisticated multi detector systems are now routinely operated in laboratories around the world. Furthermore, GC systems have been placed in many ground based field sites to monitor long term variations in halogenated VOC (e.g. ALGAGE). As stated in Sect. 1.4, the successful reduction of GC analysis times has made possible in situ, GC-MS measurement aboard research aircraft (e.g. Apel et al., 2003).

As the primary focus of this thesis, these collective experiences were utilized in the construction of the Fast Observation of Trace Organics System (FOTOS), a fast GC-MS for in situ, high time resolution measurement of VOCs in ambient air samples, with detection limits on the order of 1 pptv. FOTOS was designed and constructed with a custom three-trap cryogenic sampling and concentrator system, a modified fast GC (Modular Accelerated Column Heater (MACH) system in conjunction with a Low Thermal Mass system controller (LTM-75MS, RVM Scientific, now Agilent)), an Agilent 5973N quadrupole mass spectrometer



Figure 2.1: The High Altitude Long range (HALO) scientific aircraft of the DLR. Photo credit: German Aerospace Center (DLR, 2011).

(MS), and a Zero Air Generator and calibration system (ZAG), as well as the other necessary supporting components (e.g. heated inlet, gas bottle rack, pumps, power distribution, etc.). The entire instrumentation was designed and constructed for use aboard the new High Altitude Long Range Research Aircraft (HALO) shown in Fig. 2.1, for which certain specific constraints (e.g. materials, weight, center of mass) had to be observed.

This chapter has two main objectives: first, to discuss in detail the design and function of FOTOS, including calibration and data processing aspects; and second, demonstrate its performance in terms of speed, efficiency, precision, accuracy, and stability. This will be shown through laboratory tests and selected data from two field campaigns: an intercomparison with the GC systems at the Meteorological Observatory at Hohenpeißenberg (MOHp), and the HUMPPA-COPEC 2010 campaign at the SMEAR II station near Hyytiälä, Finland.

2.2 HALO Specific Modifications

When constructing an instrument designed for use aboard an aircraft, the specific requirements for certification to fly aboard that aircraft must be considered. The certification process for HALO is extensive and obligatory, with specific restrictions on all aspects of construction including, but not limited to: weight (150 kg), center of mass (middle 20 x 20 cm, less than 49 cm above instrument base), size (65 x 55 x 132 cm), power consumption (20 A 28 Vdc, 10 A 230 Vac, 20 A 115 Vdc), mounting strength in every direction (9 g-forces), and using electrical wiring with insulation that burns with low toxic emissions (i.e. excluding commonly used PVC). The amount of space allotted to FOTOS is almost half of that used by Apel et al. for an aircraft GC-MS of similar performance. Additionally, to operate aboard the aircraft, the instrument must be robust, highly automated and require as little maintenance as possible between flights. Furthermore, the system must be able to sample at ambient pressures ranging from 1000 to 150 mbar (corresponding to 0 to 15 km above sea-level).

In order to conform to the size, weight, and strength specifications, custom housing and mounts were constructed for the GC, MS, and other components. The factory mount and

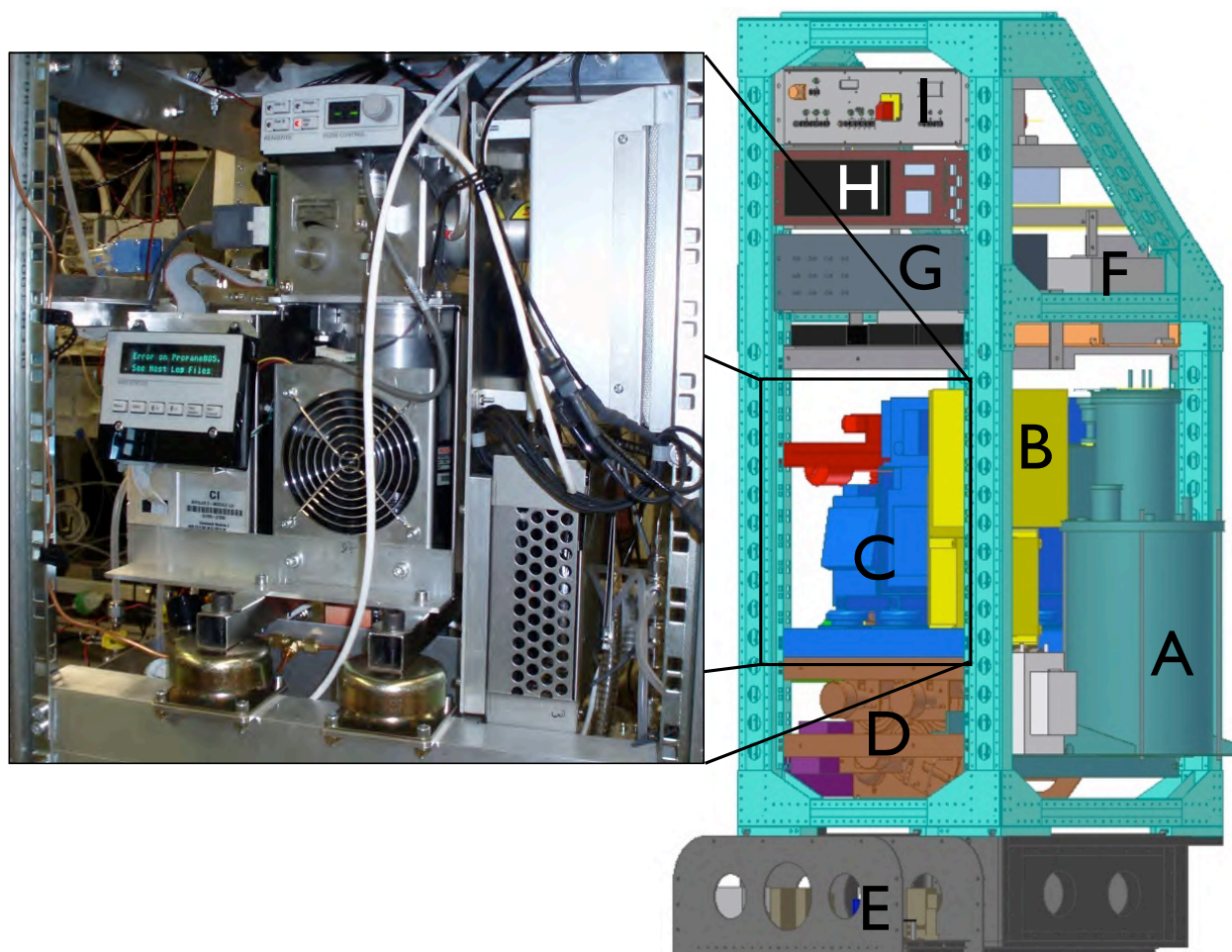


Figure 2.2: Schematic showing the parts of FOTOS mounted within HALO rack: A) the liquid nitrogen dewar and sampling system, B) the GC, C) the MS, D) the gas bottle rack, E) the ZAG in the rack drawer, F) the GC electronics, G) secondary power distribution, H) the V25, and I) primary power distribution.

housing for the MS was replaced entirely with a custom 2 mm stainless steel housing mounted to 10 mm square supports all set on four vibration insulators (Stop Choc, C2075). The MACH column, transfer, and fan modules were mounted to a 4 mm Al plate alongside the LTM heated transfer oven (see detail in Fig. 2.2). The GC was rotated to vertical and the LTM electronics separated and mounted elsewhere to allow the liquid nitrogen dewar and sampling traps, specifically the cryofocusing trap, to be mounted as close as possible to the GC inlet, as displayed in Fig. 2.2. Due to safety concerns, the standard oil backing pump for the MS was replaced with a four-head membrane pump (Pfeiffer MVP 006-4), which also reduces the potential interference from back diffusion of oil residues likely to contain the target analytes. A custom rack for three gas bottles (Helium, calibration, and purge gas) and a Helium purifier (Agilent Big Universal Trap) was constructed and mounted in the bottom of the rack to lower the total center of mass. Due to weight considerations, a custom fiberglass dewar from ILK Dresden was acquired. Although indeed light, the fragility of these glass-fiber dewars has proven to be a considerable drawback.

The automation of FOTOS was greatly aided by a custom electronic control system, the V25 (Max Planck Institute for Chemistry Electronics Department), a fully programmable,

modular control system capable of controlling nearly every aspect of FOTOS, described in more detail in App. A. The V25 for FOTOS was setup to control everything except the GC temperature and MS programming. The GC was controlled by the LTM electronics and on-board software; the MS was controlled by Agilent ChemStation. Both systems communicated with the V25 via a remote Ready/Start signal, which allowed the V25 to have complete control of sample cycling. A series of safety checks were programmed to monitor key system parameters and shut down the system in event of failure. These software interlocks provide the users aboard HALO (who are most likely unfamiliar with the detailed workings of the instrument) with a specific error message should something go wrong. The system was further designed to attempt a restart in the event of most errors, but after a set number of failures to shut off preventing any serious damage to FOTOS or any serious threat to the safety of the aircraft. The complete V25 program specific to FOTOS is presented in App. B.

2.3 Sampling Overview

The FOTOS sampling system consists of three major functional groups working in concert: 1) the sample inlet and calibration system, 2) the cryogenic sampling system, 3) and the GC-MS for sample separation and analysis, as shown schematically in Fig. 2.3 (see also Schematic Parts List in the List of Abbreviations).

Ambient air to be sampled is drawn into the instrument at the point marked “Sample Probe”. Between the sample inlet and cryogenic concentrator, the air sample flows through a

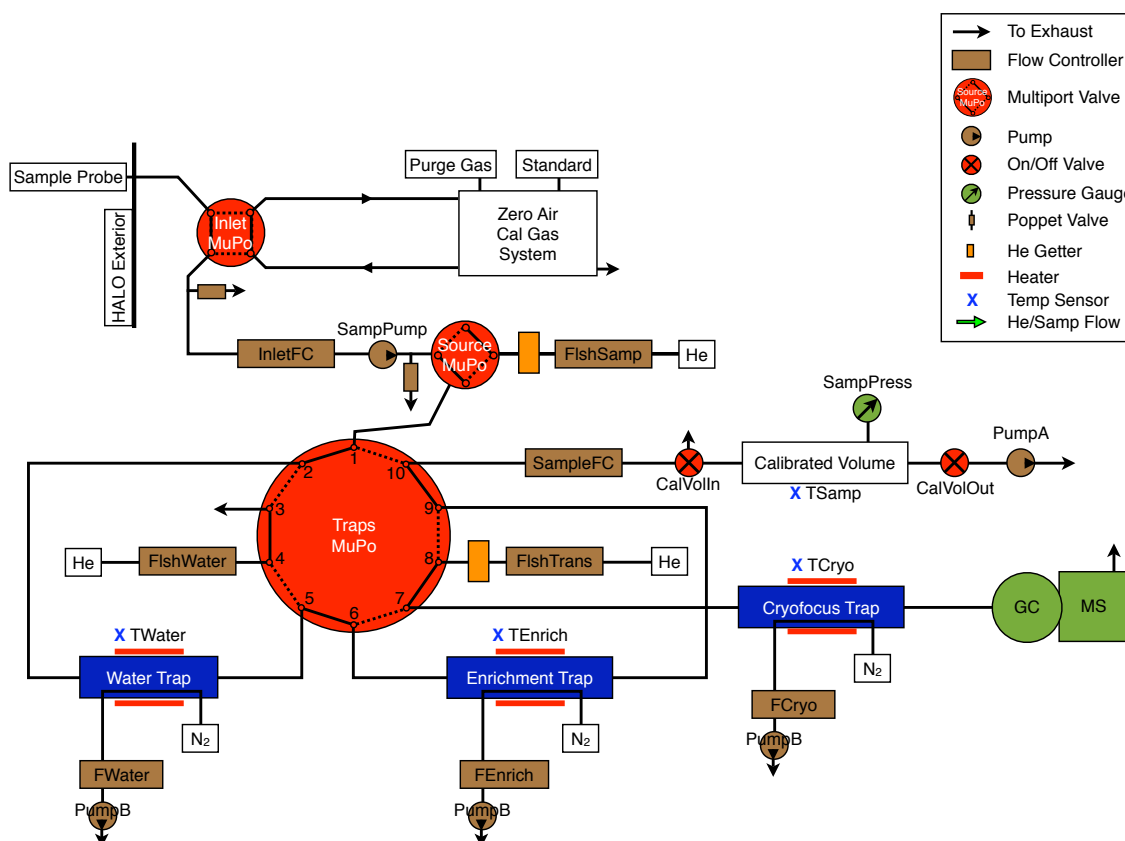


Figure 2.3: Gas flow schematic showing the cryogenic sampling system.

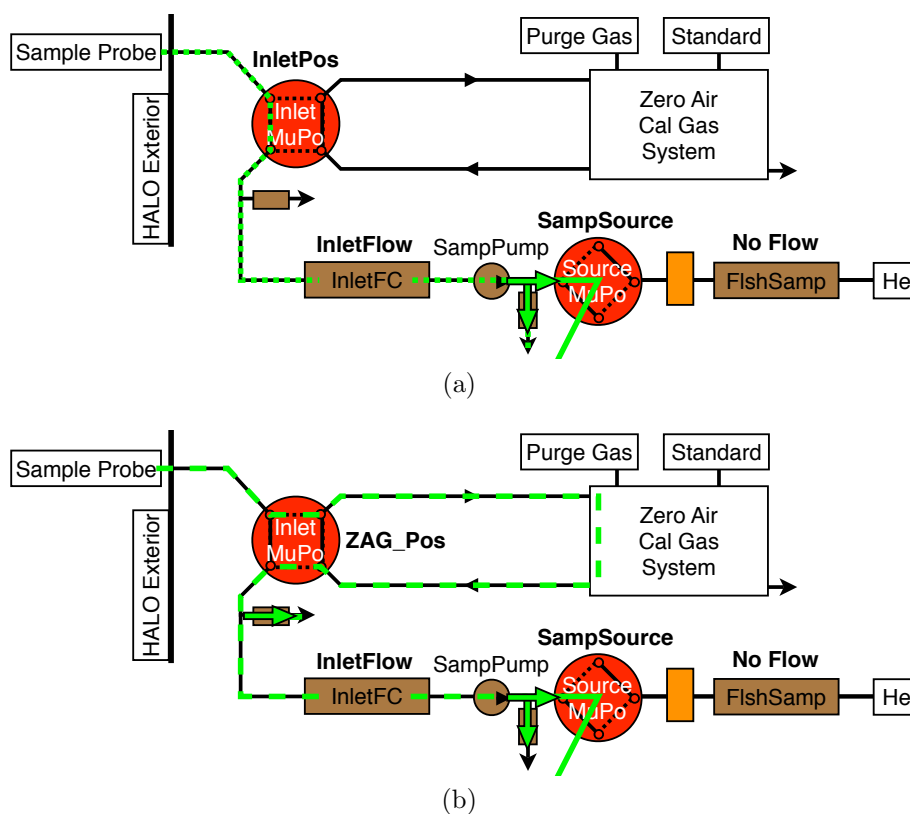


Figure 2.4: Inlet flow schematic for sampling: (a) normally and (b) through the ZAG.

four-port, two-position Vici valve (Inlet MuPo, Vici Valco DVL4MWE2) that determines whether the sample gas passes directly to the sampling system or first through the Zero Air Generator and calibration system (ZAG). During normal sample collection (Fig. 2.4a), sample air is drawn in through the HALO (or other) inlet, the Inlet MuPo valve, and a first mass flow controller (MFC), InletFC, by means of a four-head, membrane pump (SampPump, Pfeiffer MVP 006-4). During zero air or calibration runs (Fig. 2.4b), the sample air is diverted through the ZAG, which produces 5 L/min of zero air, with or without the addition of calibration standard gas. The InletFC is set to 3 L/min (as in normal sample collection), and the excess flow is released out a poppet valve (Swagelok SS-4C-1) at 68.9 mbar (1 psi) of overpressure, which provides the InletFC with sufficient pressure to maintain its flow, while allowing the ZAG complete control of the zero air and standard gas flows and resulting calibration dilution.

The collection of an ambient sample and its injection into the GC is achieved in three main steps: sample drying and collection; cryofocusing; and injection to the GC. The sample is pushed into the cryogenic sampling system by the sampling pump at 68.9 mbar (1 psi) of over pressure, maintained by a poppet valve (Swagelok SS-4C-1). A four-port, multi-position valve (Source MuPo, Vici Valco CSD4MWE) controls whether the gas flowing through the sampling system is sample gas or purified* Helium purge gas and is connected to a ten-port, two-position valve (Traps MuPo, Vici Valco DC10UWE) where the flow is directed through

*He Purge gas is purified by a mini, heated Helium purifier (Vici, HPM) after the MFC (FlshSamp, Bronkhorst 10 sccm He).

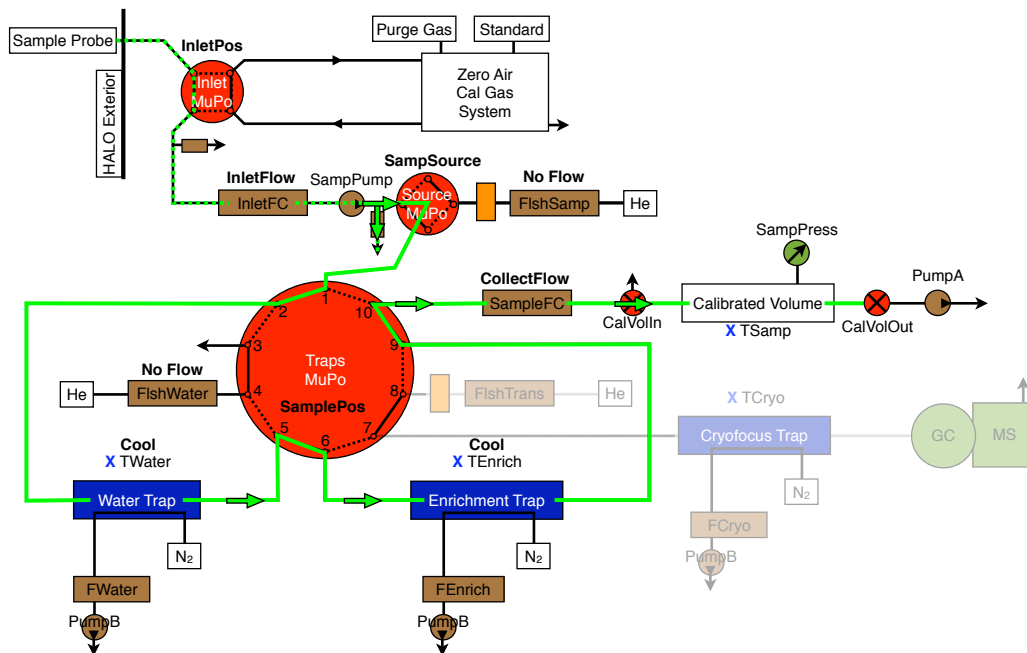


Figure 2.5: Flow schematic for sample drying and enrichment.

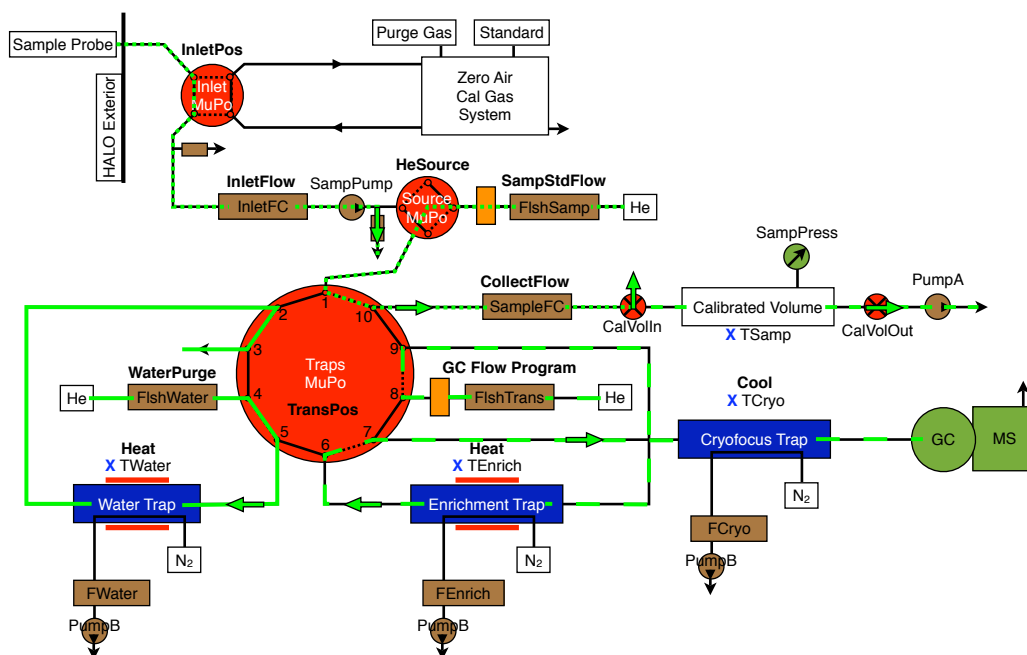


Figure 2.6: Flow schematic for transferring the collected sample from the enrichment trap to the cryofocusing trap.

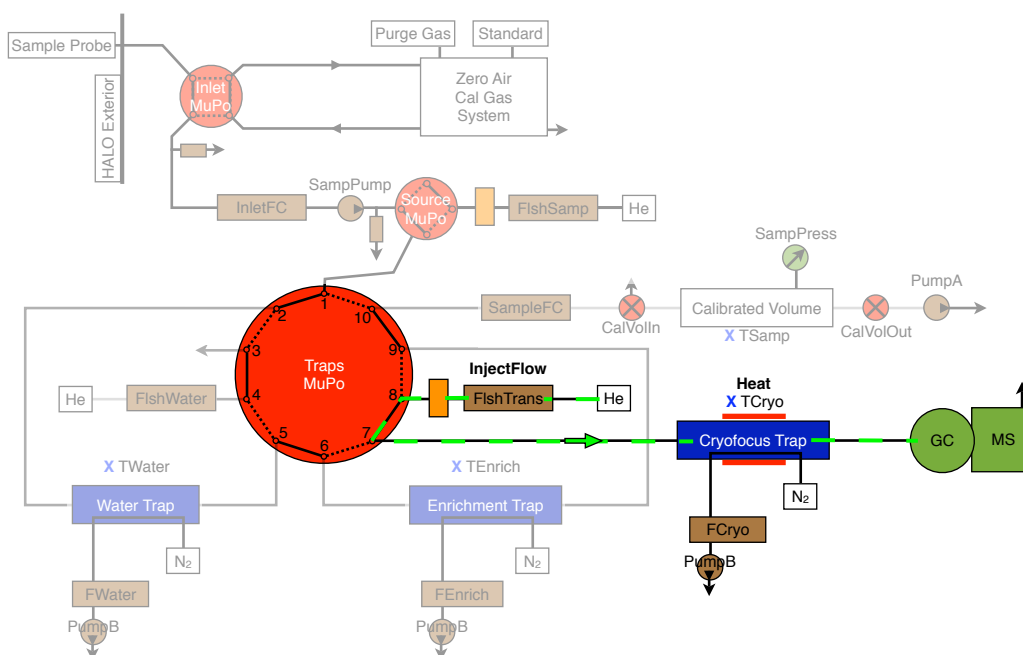


Figure 2.7: Flow schematic for injection of the focused sample to the GC-MS.

the three traps. The sample is dried by a hollow water trap and collected on the enrichment trap, as shown in Fig. 2.5. Typical trapping temperatures are -40°C for the water trap and -135°C for the enrichment trap; however, these traps are capable of cooling down to -130°C and -185°C , respectively. After the full sample has been collected (as determined by the pressure (SampPress) and temperature (TSamp) change in the calibrated volume), the Traps MuPo is switched (see Fig. 2.6), the enrichment trap is purged at $+100^{\circ}\text{C}$, and the sample is recollected on the lower volume cryofocusing trap, typically at -135°C , via Helium flow (again purified by a HPM after the MFC (FlshTrans, Bronkhorst 10 sccm He)) at a rate determined by the GC programming (between 1.5 and 2.0 sccm). During sample transfer, the water trap is purged at $+70^{\circ}\text{C}$ with 50 sccm Helium flow (via FlshWater, Bronkhorst 50 sccm He). After the sample is transferred to the cryofocusing trap, the enrichment and water traps are reset to collect the next sample.

While the next sample is being collected, the V25 waits for the GC to reach 70°C (20°C above the GC program starting temperature) and the cryofocusing trap is then heated to $+100^{\circ}\text{C}$ (6-12 seconds, see Sect. 2.8), injecting the sample (see Fig. 2.7). As soon as the GC is ready (30 seconds later), the GC and MS are triggered starting the temperature and carrier gas flow programs. Due to these independent and overlapping cycles, measurement points are obtained every 5.5 minutes even though the processing of a single sample requires almost twice as much time.

In addition to the normal sampling routines, instruments aboard an aircraft should be capable of purging the sample inlet during taxiing and takeoff to avoid saturation of the

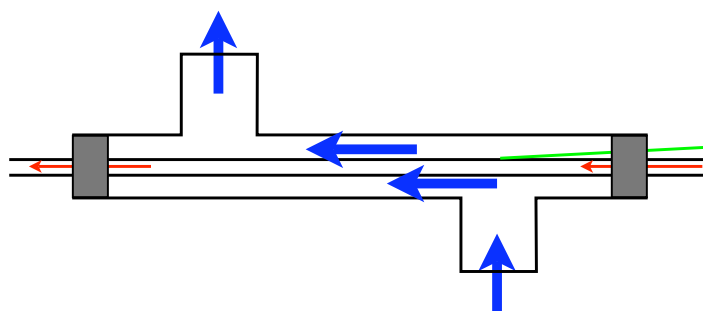


Figure 2.9: Schematic of trap in housing. Blue arrows indicate flow path of cooling nitrogen and red arrows indicate sample flow. The green line represents thermocouple placement.

The construction of these traps was greatly complicated by the relationship between their heating and cooling methods. The basic design required that the heating and temperature measurements occurred within an air-tight housing through which the cooling nitrogen gas flowed (see Fig. 2.9). This housing needed, in turn, to be as short as possible to increase heating and cooling rates. Swagelok unions (mostly Nylon with some stainless steel reducers) with short Teflon tubing pieces were found to provide the construction flexibility and durability required. In order to reduce ice accumulation without compromising cooling efficiency, the traps were well insulated, and Teflon-coated heating wire (KLETTI, KM-HC-PS) was wrapped around the tubing carrying the cold nitrogen gas from the traps to the MFCs. This also helped bring the nitrogen gas into the operating temperature range of the MFCs (0–70 °C). To reduce the length of the transfer lines between the traps, the two multi-position valves connected to the traps (Traps MuPo and Source MuPo) were mounted directly to the dewar holder. This section will focus on the construction of the dewar and traps. Discussion of the performance of these systems (e.g. heating and cooling rates) will be left for Sect. 2.8.

2.4.1 Dewar Construction

The construction of the liquid nitrogen dewar played a critical role in the operation and routine maintenance needs of FOTOS. The dewar, as seen schematically in Fig. 2.10, was fitted with a number of ports and sensors to monitor several properties related to dewar performance and liquid nitrogen usage. The largest opening was the “neck” of the dewar. With an inner diameter of 10.0 cm, the neck extended 20 cm above the top of inner cavity. The inlets for the heat exchange coils were at the top of the neck, preventing liquid nitrogen from being drawn into the coils, which could lead to blockage or other problems. The outlet side of the heat exchange coil was insulated to protect the cooled air from the warmer head space. The cooling nitrogen streams exited the dewar through thin-walled 1/4 inch[†] Teflon tubing sealed with o-rings in a flange (the “hat”) of one of two designs. The first hat consisted of a silicon o-ring between two aluminum plates, separated from external (warm) air by 6 cm of insulation. When the plates were drawn together by a center screw, the o-ring was pressed

[†]As these and following tubing connections were most readily available in US customary units, tubing diameters in these units will be reported here. For reference: 1 inch is 25.4 mm, 1/2 inch is 12.7 mm, 3/8 inch is 9.53 mm, 1/4 inch is 6.35 mm, 1/8 inch is 3.18 mm, and 1/16 inch is 1.59 mm.

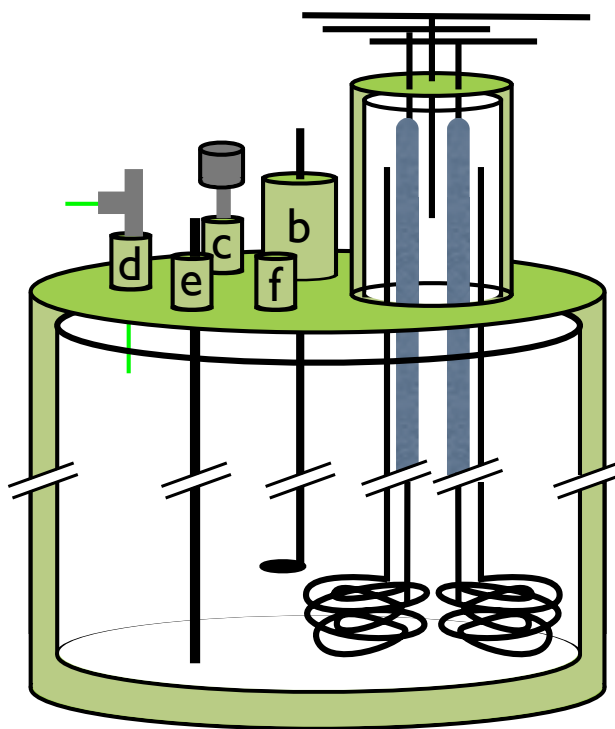


Figure 2.10: Diagram of cryogenic dewar showing various ports. The largest opening (the “neck”) is for the trap cooling nitrogen flows. The additional ports are: b) liquid nitrogen heater; c) filling and safety burst valve; d) fill vent, pressure gauge, thermocouple (green line), and relief poppet; e) liquid nitrogen level gauge; and f) burst valve optional position.

outward against the inner wall of the neck, sealing the opening and securing the hat, with the mounted traps, to the dewar. Following the MOHp campaign (see Chap. 3), a second, simpler hat design made use of a securing flange at the dewar neck. In this case, a glass-fiber plate (Kunststoffe Hertrampf, Hgw 2372.1) was secured to the neck via nuts embedded in a flange around the neck opening. The 1/4 inch tubing was again sealed with o-rings, attached to the underside of this glass plate. The plate was insulated from the cold dewar head space with 6 cm of insulation.

The dewar was equipped with five further ports to accommodate the following: a liquid nitrogen level gauge (CryoVac, 185); a heater (ThermoCOAX, THX 06-80-0185); an emergency burst valve (Type U35n2-03L); a fill port; and a final port for a temperature reading (Omega 5TC-TT-K-30-36), a pressure reading (SensorTechnics, CTE9003AM4-X), a poppet valve (Swagelok SS-4C-10), and a fill vent. These ports were also sealed with small flanges secured to nuts embedded in flanges at the port openings. This was necessary in order to reposition the glass-metal unions away from the vacuum chamber of the dewar, where the differing thermal expansion coefficients resulted in the formation of leaks in previous dewar designs. The pressure gauge and poppet valve were later also moved away from the dewar itself and connected by a 1/4 inch Teflon tube of sufficient length so that the nitrogen gas at the pressure gauge was near ambient temperature. This reduced fluctuations in the pressure reading due to differences in temperature, and prevented the poppet valve from being frozen

open. It was also decided to mount the burst valve on the fill port, further reducing the congestion of the dewar accessory ports.

Shortly before the HUMPPA campaign (see Chap. 4), it was discovered that the fiberglass dewar vacuum had developed a leak. By constant pumping on the vacuum port with a turbo-molecular pump, a vacuum pressure of $1.3\text{--}6.5 \times 10^{-3}$ mbar was achieved, which was sufficient for running 10 hours between dewar fills.

2.4.2 Sample Drying

A purely cryogenic water trap (i.e. entirely based on physical cooling and without additional chemical drying agents) was desired for FOTOS to allow the observation of a wide variety of compounds without concern for losses or artifacts. Significant losses of alcohols, ketones, and aldehydes, in addition to causing terpene rearrangement has been observed in the use of Nafion[®] dryers (Burns et al., 1983). Two designs for the 1/8 inch OD water trap were tried, thin-walled Teflon tubing wrapped in enameled heating wire and stainless steel directly heated. The target length of the “cooled region” (the length from the cold nitrogen flow in and out) was 10.5 cm, and the total length was made as short as possible with that constraint.

The Teflon trap was wrapped transversely with enameled heating wire (0.40 mm OD, Isabellenhütte ISA-CHROM 80), with 5 mm between windings over the length of the trap within the Swagelok housing (12 cm). Thus the cooled region was able to be fully heated during the purge/transfer stage of sampling cycle. Within the trap housing, the heating wire was soldered to the electrical leads to the heater module of the V25. A thermocouple (Omega 5TC-TT-K-30-36) was wrapped under a section of the heating wire such that the tip lay in the middle of the trap length, between two turns of the heater. The thermocouple and heater leads were then sealed by means of short lengths of Teflon tubing in Swagelok reducers, sharing a cross union with the cooling nitrogen exhaust. While providing a chemically inert water trap, this design was extremely difficult to construct, bulky, and difficult to achieve adequate temperature regulation due to poor thermal contact of the heater wire and thermocouple with the Teflon tubing surface.

The alternative stainless steel trap was, in comparison, a much more simple design. The heating was achieved by using copper clamps to connect the heating leads (here a 4x12 AWG wire) directly to the trap, just outside the trap housing. As seen in Fig. 2.11, a thin, sheathed thermocouple (Omega KMQXL-020G-6) was attached to the water trap with thermal epoxy (UHU Plus 300) so that the tip was positioned just opposite the incoming cool nitrogen flow.

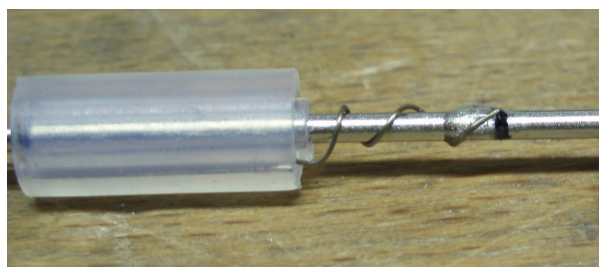


Figure 2.11: Detail of a metal water trap with thermocouple.

The thermocouple was sealed between the two Teflon tubes (1/4 and 3/8 inch) used to seal the trap in the 3/8 inch Swagelok housing. In this configuration, the only tubing connections to the trap housing were those for the trap itself and the cooling nitrogen flow. This greatly simplified the trap configuration and isolation. Although not the recommended method for joining tubing of differing size, this method of stacking tubing was found to be sufficiently air tight, while minimizing the distance from the heater clamps to the cooling flow path. One small complication of direct trap heating was the necessity of electrically isolating the trap from a complete grounding loop. Due to the rigorous construction of the V25, namely that the heater circuit was galvanically isolated (see Sect. A.3.4), it was only necessary to isolate one of the connections between the trap and the Traps MuPo, in this case with a Nylon reducing union (Swagelok NY-200-6-1).

2.4.3 Sample Enrichment

To enable artifact free sample collection, while maintaining the flexibility to trap any compound of interest, the sample enrichment trap was constructed of 1/16 inch OD stainless steel packed with 3 to 5 cm of inert glass wool. Three different designs for heating this trap were investigated: bare tube directly heated, indirectly heated with heater wire, and a wrapped tube directly heated. These three designs were found to be comparable in their heating and cooling rates, but vastly different in their ease of construction and durability. Additionally, variation in the amount of packing material had minimal effects on the heating and cooling rates. The major factor found to affect heating and cooling rates was the length of the cooled and heated regions of the trap. This length was therefore kept as short as possible, which was about 5 cm using 1/4 inch Swagelok unions (NY-400-3, and NY-400-4).

The bare, directly heated trap was initially favored for its ease of construction. Much like the water trap described in Sect. 2.4.2, a thermocouple was attached to the tube using thermal epoxy (UHU Plus 300), and either sealed with a Teflon tube and 1/4 to 1/16 inch reducer (with the thicker thermocouple, Omega 5TC-TT-K-30-36) or between the stacked 1/8 and 1/4 inch tubing used to seal the trap in the housing (for the thinner thermocouple, Omega KMQXL-020G-6), analogous to the water trap in Fig. 2.11. Again the heater leads (this time 2x12 AWG) are connected to the trap with copper clamps just outside the trap housing. Similar to the directly heated water trap, electrical isolation was achieved with a Nylon union (Swagelok NY-100-6) on the downstream side of the trap. While simple in design, this trap resulted in often sporadic temperature readings, with the potential for rapid extreme overheating.

The indirectly heated trap exhibited more stability, but involved a much more difficult construction and greater fragility. Enameled heating wire (0.22 mm OD, Isabellenhütte Alloy 90) was wrapped transversely the length of the trap within the housing in adjacent windings, with thermal epoxy (UHU Plus 300) providing increased thermal contact to the trap. The ends of the heating wire were sealed in stacked Teflon tubing and soldered to 24 AWG wiring outside of the trap housing. The entire length of heater wire outside the housing, including the soldered union, was encased in epoxy to provide a thermal load and

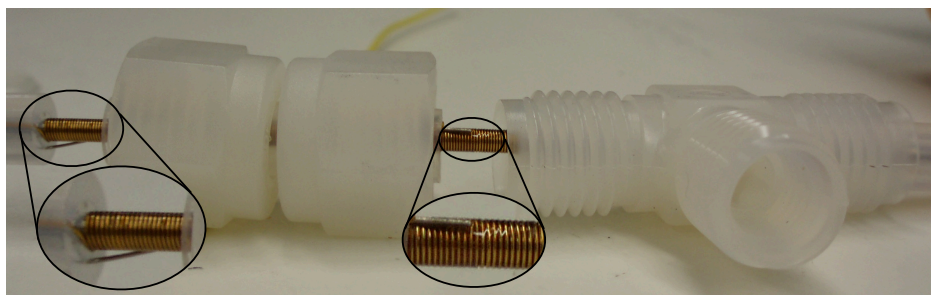


Figure 2.12: Wound trap during curing, showing thermocouple on top of heater wire windings.

prevent the wire ends from melting. A thermocouple (Omega KMQXL-020G-6) was also sealed in the stacked tubing on one end and glued on top of the heater wire windings, as shown in Fig. 2.12. The trap housing had to be partly assembled before wrapping was complete, as the middle tubing could not fit over the ending stacked tubing. The final union, however, was bored through at $1/4$ inch and was thus able to be installed last. The heater wire had to be wound very carefully because two breaks in the enamel could result in an electrical short through the trap, causing cold spots during trap purging. Furthermore, after a month of use, the repeated expansion and contraction of the trap caused breaks in the heating wire, and the trap would no longer heat. However, temperature readings for this trap were much more stable and the potential for extreme overheating was greatly reduced.

The final design of a wrapped, directly heated trap combined elements of both of the previous designs. The trap was wound with the same heating wire and technique as described for the indirectly heated trap. However, the epoxy could be cured without partial assembly of the trap housing. After curing, the end of the heating wire opposite the thermocouple was broken, allowing the stacked tubing to be removed, simplifying housing assembly. Breaks in the enamel were also irrelevant, as the resistance of the stainless steel trap was much lower than that of the heater wire. Furthermore, the stacked tubing could now be cut to be flush with the end nut, minimizing the dead space between the heater clamps and the cooled region. As with the directly heated water trap, this simplified design, as seen Fig. 2.13, aided the total trap configuration and isolation. The major drawback to this design was the fragility of the thermocouple used. This was particularly problematic during transport if the end connectors of the thermocouple were not properly secured to the dewar body.



Figure 2.13: A completed enrichment trap with housing.

2.4.4 Sample Focusing

The third cryogenic trap, the cryofocusing trap, provided a means for reducing the physical dispersion of the collected sample, which produced a more consistent, sharper injection. By reducing the trap dead volume, both the physical and temporal space of the injection were reduced, ultimately resulting in a narrower injection. As the width of the chromatographic peaks was greatly dependent on the width of the injection, cryofocusing greatly improved the subsequent chromatographic performance. Therefore, this trap had a design similar to the enrichment trap, but with a more compact trapping region (e.g. only 2 to 3 cm of glass wool instead of 3 to 5). The most important quality of the cryofocusing trap (aside from being able to trap the sample) was rapid heating to the injection temperature, reducing the temporal dispersion of the whole sample. Therefore small sacrifices in stability for increased speed were acceptable. The designs tested for this trap were identical to those described in Sect. 2.4.3 with the following addition.

The final trap design tested for the cryofocusing trap was a modification of the bare, directly heated trap described for the enrichment trap. In this case, the trap was a thick-walled (0.5 mm ID instead of the usual 1.0 mm ID), 1/16 inch stainless steel tube. Instead of being packed with glass wool, a 0.35 mm OD, 0.25 mm ID, deactivated silica capillary, externally coated in Silicone-Base Heat Sink Compound (Radio Shack, 276-1372), was used. This technique had the additional benefit of reducing the number of unions between the cryofocusing trap and GC. The capillary was run as a continuous piece from the Traps MuPo to the MACH column. For the packed 1/16 inch tube cryofocusing traps, a reducing union at the inlet to the LTM transfer oven was necessary.

Trap Type	Tube OD	Tube ID	Wrapping	Heating	Acceptability*					
					Heating	Cooling	Stability	Construction	Robust	Electronics
Water Trap										
Teflon	1/8 inch	2.2 mm	0.40 mm	Indirect	-	+	-	-	+	+
Metal	1/8 inch	2.0 mm	none	Direct	+	+	+	+	+	0
Enrichment and Cryofocusing Traps										
Direct Wrapped	1/16 inch	1.0 mm	0.22 mm	Direct	+	+	+	0	+	0
Direct Bare	1/16 inch	1.0 mm	none	Direct	+	+	-	+	+	0
Indirect	1/16 inch	1.0 mm	0.22 mm	Indirect	+	+	+	-	-	+
Capillary	1/16 inch	0.5 mm	none	Direct	+	+	0	+	+	0

* Acceptability codes: unacceptable (-), manageable (0), acceptable (+)

Table 2.1: Trap design summary table

2.5 Separation and Detection

The fast cycling of FOTOS was also a function of the speed of GC separation and detection by MS. FOTOS utilized the Modular Accelerated Column Heater (MACH) system in conjunction with a modified LTM-75MS (RVM Scientific, now Agilent). The MACH system consisted of a GC column (20 m x 0.25 mm x 1.0 μm , PLOT- Al_2O_3 "S"), heater, and temperature sensor wrapped together in insulation, resulting in a minimal thermal load to heat and cool. The prototype system purchased was retrofitted with a high-power tubeaxial fan (ebm-papst 6314/2TDHHP), which further reduced GC column cooling times by approximately 50%. It was also found that drilling ventilation holes in the GC mounting plate behind this fan also contributed to a faster cooling rate, while additional holes behind the GC column yielded insignificant improvement. Moreover, tests performed with a more powerful fan (ebm-papst 6318/2TDH4P) produced comparable cooling rates, indicating the limiting factor was the rate of thermal diffusion from the MACH column. An operational drawback to this fan was the considerable sound power generated during operation (79 dB, or about as loud as an electric hand mixer).

To further reduce the instrument idle time as the GC cooled, the sample injection was programmed to occur before the GC was fully cooled. While this reduced the reproducibility of peak retention times, peak integration software advances (see following paragraph) reduced this concern so that the gains in cycling frequency were more relevant. The temperature program (50 °C, 65 °C/min, 170 °C for 60 seconds, 200 °C/min, 190 °C for 58 seconds) and the carrier gas flow program (2.0 sccm for 30 seconds, -0.33 sccm/min, 1.5 sccm, +0.50 sccm/min, 2.0 sccm for 60 seconds), shown in Fig. 2.14, were also optimized for fast GC separation of the NMHCs. Especially difficult to separate with this short column were n-butane and ethyne, as well as the four butene isomers. The atypical reduction in the carrier gas flow improved the resolution of these compound groups.

While MS detection of specific ions generally improves chromatographic resolution, this was unfortunately of little help when measuring the light hydrocarbons. Most hydrocarbons that displayed similar retention times (e.g. iso- and n-butane or the four mono-butenes) had overlapping or nearly identical fragmentation patterns. Optimization of the Select Ion Monitoring (SIM) grouping led to clipping of some peaks as retention times shifted (see Sect. 3.4.5). In this case, the similar fragmentation patterns for the NMHCs were later exploited by including m/z 41 in all ion groups. Although not the most abundant ion for some target compounds, m/z 41 showed a similarly responsive, precise signal for m/z ratios it replaced in the affected SIM groups.

An additional difficulty of faster GC-MS cycling, was an overwhelming increase in the number of chromatograms acquired, which then had to be integrated and analyzed. This aspect of the project was aided greatly by a collaboration with the group of Andreas Engel at the University of Frankfurt, Institute for Atmospheric and Environmental Sciences. The chromatogram peak integration was accomplished with an automated Gaussian curve fitting program (Engel et al., 2010), which was shown to be more reliable than manual baseline peak

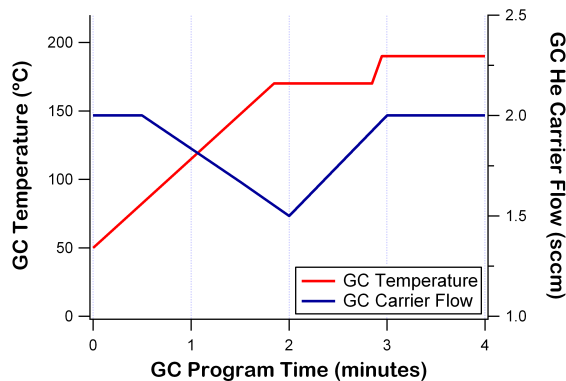


Figure 2.14: Flow and temperature programming of the GC.

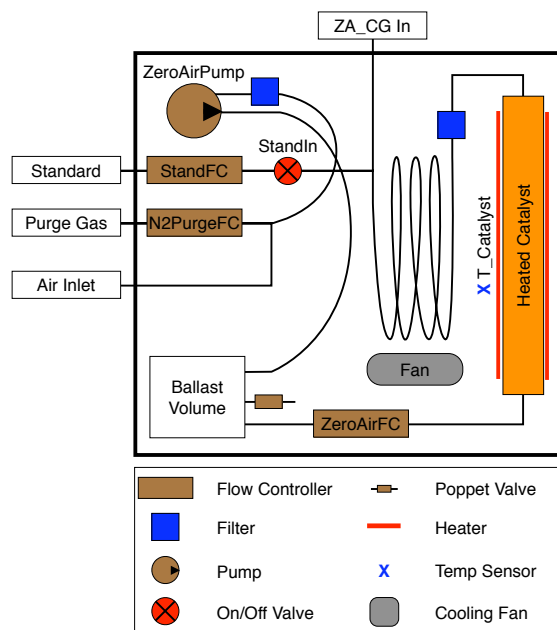


Figure 2.15: Schematic of the Zero Air Generator with calibration and purge gas MFCs.

integration using ChemStation software from Agilent (Laube, 2008). This program, written for execution in IDL Virtual Machine, was also capable of compensating for shifts in peak retention times by calculating an adjusted retention time from the detected peaks of a few marker compounds. In an iterative collaboration, data from FOTOS served as an important test for the robustness of this automated program. Data analysis was further automated with a series of import, quality checking, calibration, and analysis functions written in the data analysis program Igor from WaveMetrics.

2.6 Calibration

Accurate calibration is essential to any trace gas measurement. As stated in Sect. 2.3, as the sample first enters FOTOS, it passes through a four-port, two-position Vici valve, Inlet MuPo, that determines whether the sample gas passes directly to the sampling system or first through the ZAG. This valve was chosen for its large bore size (4.0 mm), which allows for less restricted flow than that of the lighter solenoid valves originally used (Clippard ETO-3-24-V). The ZAG is broadly based on that of Apel et al. (2003) with the addition of a cooling fan (ebm-papst 614F) and solenoid valve (StandIn, Clippard ET-2-24-V) after the calibration gas MFC to further eliminate any possible leakage of calibration gas during zeroing cycles (see Fig. 2.15).

Ideally, the source gas for the ZAG would come from a separate inlet, allowing the sampling line to remain unchanged during zero and calibration runs, and the output of the ZAG is introduced to the sampling line as close as possible to the sampling inlet. Due to constraints aboard HALO, a separate inlet is not possible and the best alternative configuration has been used. Additionally, due to potential saturation of the airplane boundary layer with jet

Compound	Mixing Ratio	Uncertainty	
	[ppbv]	[ppbv]	Percent
ethane	7.55	0.15	2.0
ethene	11.80	0.20	1.7
propane	2.86	0.05	1.7
propene	7.45	0.15	2.0
iso-butane	3.34	0.05	1.5
n-butane	2.88	0.05	1.7
ethyne	9.85	0.20	2.0
trans-2-butene	2.47	0.05	2.0
1-butene	3.70	0.05	1.4
iso-butene	3.17	0.05	1.6
cis-2-butene	2.64	0.05	1.9
iso-pentane	1.32	0.02	1.5
n-pentane	2.94	0.05	1.7
1,3-butadiene	5.90	0.10	1.7
propyne	3.21	0.05	1.6

Table 2.2: Partial composition of NPL standard with uncertainties

fuel hydrocarbons during takeoff, an inlet purge setup with purge gas and MFC (N2PurgeFC; MKS, 500 sccm N₂) was also necessary. For the ground-based HUMPPA campaign described in Chap. 4, the N2PurgeFC and StandIn valve were removed and an additional standard gas MFC (Bronkhorst, 100 sccm Air) installed in order to increase the dynamic calibration range.

For calibration, a gravimetrically prepared standard from National Physics Laboratory, UK (NPL) was acquired (Grenfell et al., 2010). The standard, although ten years old, showed impressive stability, evident from regular measurement and comparison with new standards purchased from NPL. The components of the standard relevant to this work (of the 30 total in the standard), together with their mixing ratios and uncertainties are shown in Tab. 2.2. The stated accuracy for most compounds was equal to or less than 2% uncertainty. This represented up to 30% of the total uncertainty of mixing ratio calculations.

To test the scrubbing efficiency of the ZAG, a comparison with a PTR-MS and its catalyst scrubber (as in Lindinger et al., 1998) was performed. As seen in Fig. 2.16, the output of the ZAG in FOTOS was below the detection limit of the PTR-MS for a wide range of compounds. This was clearly seen when comparing the signal and standard deviation of all signals during the scrubbed air measurements with the corresponding zero signal and standard deviation during the two unscrubbed periods. In the case of m/z 33, for example, the average raw counts (and standard deviations) of the initial zero points, the total scrubbed signal, and the final zero points were 1400 (81), 1336 (77), and 1349 (69), respectively. The difference between the sample and zero points for m/z 33 during scrubbing was 5.43, roughly 1/15 the standard deviation for zero points. This difference was either negative (indicating less VOC in the FOTOS zero air as in the doubly scrubbed air) or less than the corresponding standard deviation for all monitored masses except m/z 45 (acetaldehyde, de Gouw and Warneke,

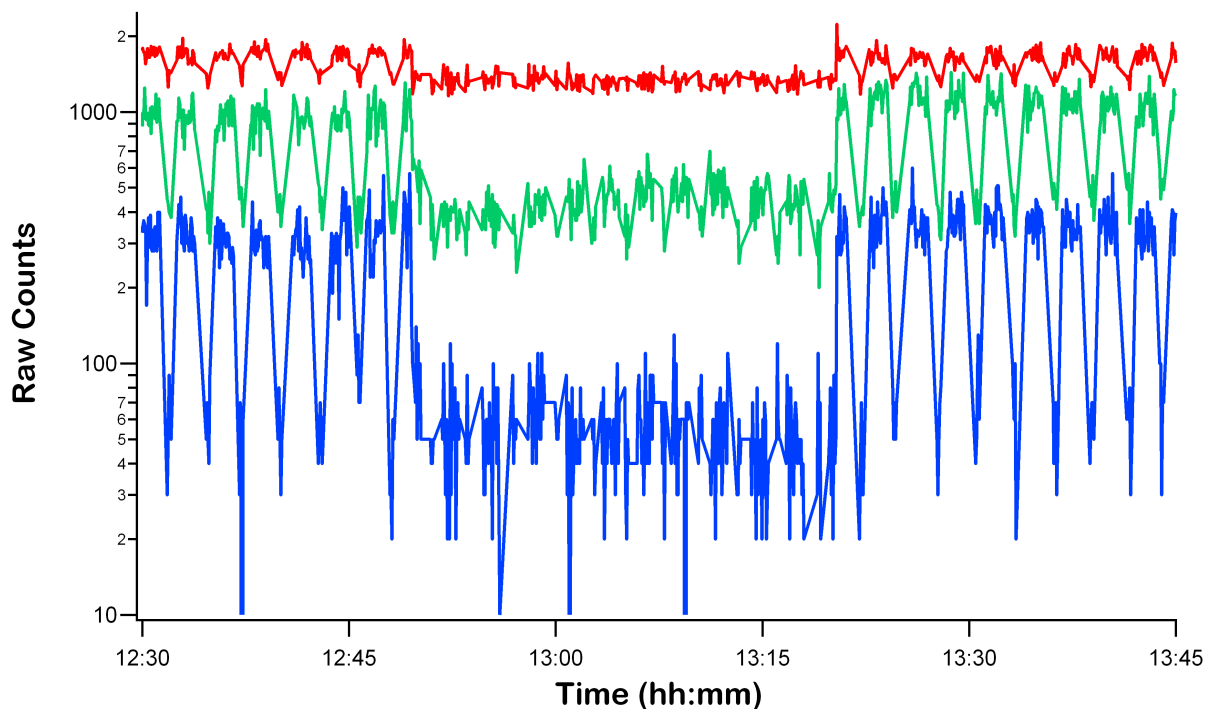


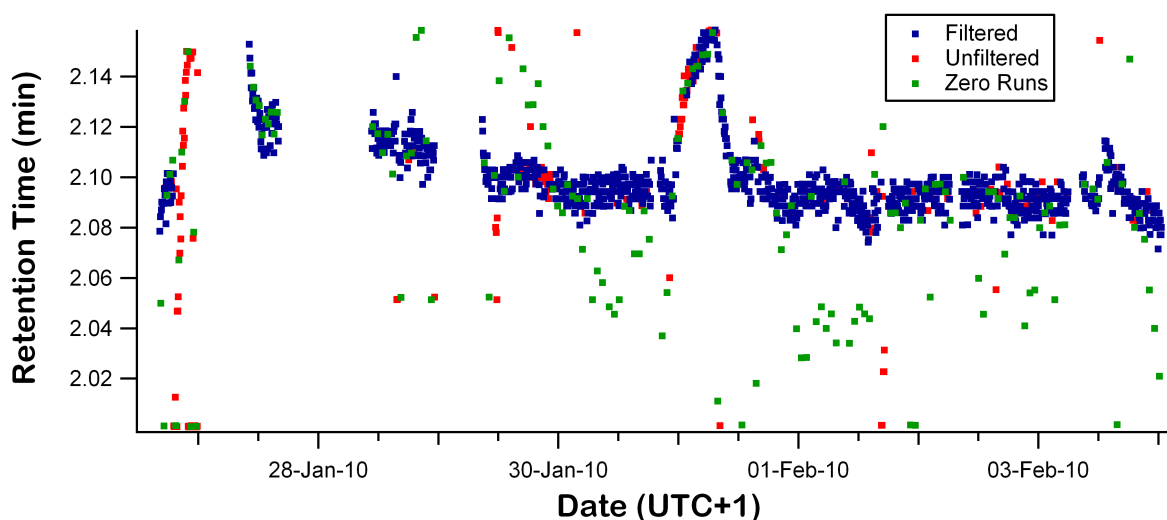
Figure 2.16: PTR-MS signal of air scrubbed by the ZAG, preceded and followed by unscrubbed air. The red line is the signal at m/z 33, green at m/z 45, and blue at m/z 59, typically representing methanol, acetaldehyde, and acetone, respectively.

2007) and 46 (NO_2), where the difference was 2.01 and 7.32 times the zero points standard deviation, respectively. The signal for m/z 46 actually showed significant increase in signal through the ZAG, perhaps due to higher combustion within the ZAG of FOTOS as in that of the PTR-MS. These tests indicated that the ZAG was well suited for determining the instrument background signal levels during the measurement of VOCs at pptv levels.

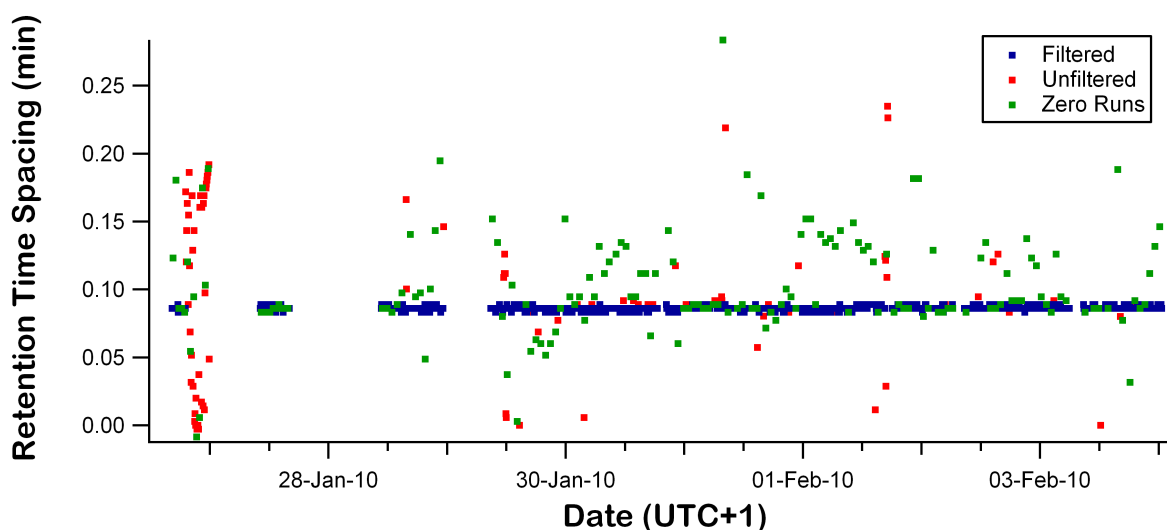
2.7 Data Quality Control Measures

Due to the large number of chromatograms collected (as many as 250 in one day with thirteen peaks each), automated peak integration was necessary to analyze data from FOTOS in a reasonable time frame. As the integration of each individual peak could not be manually verified, certain quality checks were introduced to ensure correct peak identification and resolution. Sets of compounds with similar retention times were grouped and checked for consistent spacing. All peaks with retention time spacing more than three standard deviations from the average for a given data set were iteratively removed until only those points remained which were within three standard deviations of the average of the remaining data points. This filter was applied to all points, sample and calibration, except for zero runs.

In addition to simply looking at retention times, this filter also removed the data points for which the integration routine returned a result of no peak found. As a valid retention time spread required identified peaks in all compounds of a given retention time grouping, this filter may have removed some valid data points. For example, if the iso-butane peak for some reason was not found, then the retention time spread between iso- and n-butane was deemed



(a) Time trace of the retention time of the iso-butane peak. Blue points indicate all data points remaining after the filter. Red points indicate those data points removed by the retention time filter. Green points indicate zero run points, which are not subject to the filter.



(b) Time trace of the difference in retention times between iso-butane and n-butane. Red points, again, indicate those points removed by the filter, and green points show that the outliers of the filtered points are zero runs.

Figure 2.17: Effect of retention time filter on intercomparison data set

invalid, resulting in the removal of both the iso- and n-butane data for that run. However, as the compounds of a given retention time grouping most often had similar sources, a low or undetectable mixing ratio of one compound was accompanied by similarly low mixing ratios of the other compounds. Upon closer examination, it was determined that such detection of one compound and not the others was most often due to a significant retention time shift, leading to improper peak identification, which was the main purpose of this filter.

As an example, the data from the MOHp intercomparison are shown in Fig. 2.17a. Filtering the data in this manner allowed for fluctuations in the retention time and resulted in minimal losses of acceptable data. This data set contained 1166 butane-pair, sample data points before filtering and 1050 after filtering, a reduction of less than 10%.

With an automated analysis routine optimized for locating peaks, proper handling of zero runs (in which there should be no peaks) required additional attention. Depending on the background noise of a particular run, either a spike of noise was integrated, or it was indicated that no peak was found. For the case of a zero run, no peak found was valuable information to be preserved. Additionally, the fitting of noise as signal peaks resulted in inconsistent retention times of the zero run “peaks”. This was clearly seen in the standard deviation of the iso- and n-butane retention time spread for the unfiltered data set. For only the ambient sample runs, the standard deviation of the butane retention time spread was 0.015 minutes, and for only the zero runs, that value was 0.043 minutes. For these reasons, the zero runs were excluded from the retention time filter, and later considered as a whole to determine the background of the sample measurements (see Sect. 2.8.5). Figure 2.17b shows that after filtering, the data set contained a tight band of retention time spreads plus a much more noisy collection of zero runs.

In addition to integration errors, system malfunction also resulted in unreliable measurements. As discussed in App. A, a wide collection of system parameters, such as temperatures, heating parameters, valve positions, and gas flows, were collected in log files, which were thoroughly checked for irregularities in system conditions and performance. For the MOHp intercomparison, these checks revealed several performance irregularities and operator errors, not inconsistent with the first extended use of a new instrument. Most of the performance issues were related to MFC failure, which was later determined to be due to overloading the MFC power supply. Most of these periods of system malfunction were detected and removed by the retention time filter. The most significant undetected period was from 23:15 on the 30th to 07:45 on the 31st (the broad spike in the middle of Fig. 2.17a), when a malfunction in the heating of the enrichment trap was caused by a similar MFC power fluctuation.

These automated data processing and quality control measures were also applied to the HUMPPA data set. After filtering by retention time spacing, the remaining data was checked for apparent inconsistencies in mixing ratio (i.e. outlying points). The instrument logs and chromatograms of suspect data points were controlled, and those points for which obvious operational errors could be identified were removed. As further evidence of the thoroughness of the retention time filter, only seven data points from over 4000 were removed after individual inspection. Some remaining points appeared to be inconsistent (e.g. the high data point at 14:36 UTC on the 23rd of July), but as no evidence of malfunction could be determined from the available data, these points were assumed to represent actual atmospheric events. The brevity of these events suggested influence from the immediate proximity which would be hard to document or trace (i.e. a passing car or delivery truck).

2.8 Performance

The overall performance quality of FOTOS can be effectively summarized by analyzing the speed and collection efficiency of the three cryogenic traps as well as the precision and accuracy of the resulting chromatograms. The performance of the traps was demonstrated through

various laboratory and field testing. The accuracy of the output of FOTOS was determined during an intercomparison with the GC systems at MOHp, which will be discussed further in Chap. 3, and internally through regular calibrations during the HUMPPA campaign, which will be discussed here. Further discussion of the HUMPPA data will be given in Chap. 4. In terms of overall system performance, FOTOS was shown to consistently and accurately measure up to 13 different VOCs with a sampling frequency of approximately 6 minutes (again, see Chap. 3). With the GC cooling fan exchange described in Sect. 2.5, this time was cut to 5.5 minutes. It should be noted that the maximum speed was to some extent dictated by the target compounds. Higher boiling point compounds were inherently more difficult to achieve in short times. Moreover, NMHCs have many common ions limiting the extent to which selected ion monitoring could be used to minimize the run times.

2.8.1 Trapping Speed

Four different designs were thoroughly tested for the enrichment and cryofocusing traps, as described in Sect. 2.4. Figure 2.18 shows the typical temperature cycle of three of these traps: first, a directly heated trap wrapped in wire providing additional thermal load; second, a bare tube directly heated; and third, an indirectly heated trap. Note that the heating rates for all three traps are comparable (11, 12, and 10 seconds from -135 to $+100$ °C), while the cooling rates for wrapped traps differs by a factor of two from the bare trap (25, 9, and 21 seconds from $+100$ to -135 °C). However, the bare trap exhibited erratic temperatures after cooling. An additional 13 seconds were required before the bare trap could be considered ready for sample collection and was followed by continued instability. The indirectly heated and wrapped directly heated traps, meanwhile, both required less than 9 seconds to achieve the same (or even better) stability.

After testing the various trap designs, a final configuration was selected based on speed and stability, namely: a directly heated water trap; a wrapped directly heated enrichment trap; and a bare, thick-walled, directly heated cryofocusing trap. The bare cryofocusing trap exhibited slightly less stable holding temperatures than the enrichment trap, but was also

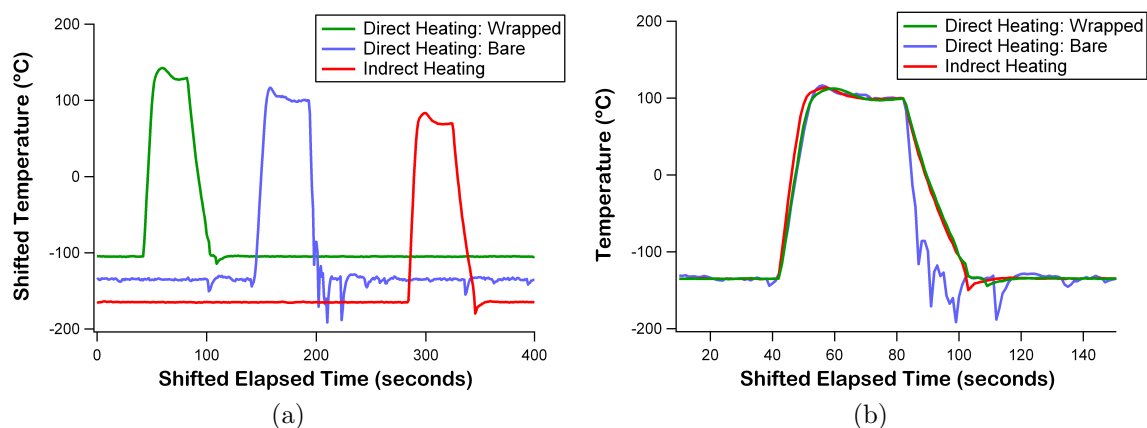


Figure 2.18: Comparison of trap heating and cooling rates during the MOHp intercomparison. Time and temperature axes have been shifted where indicated to facilitate visual comparison.

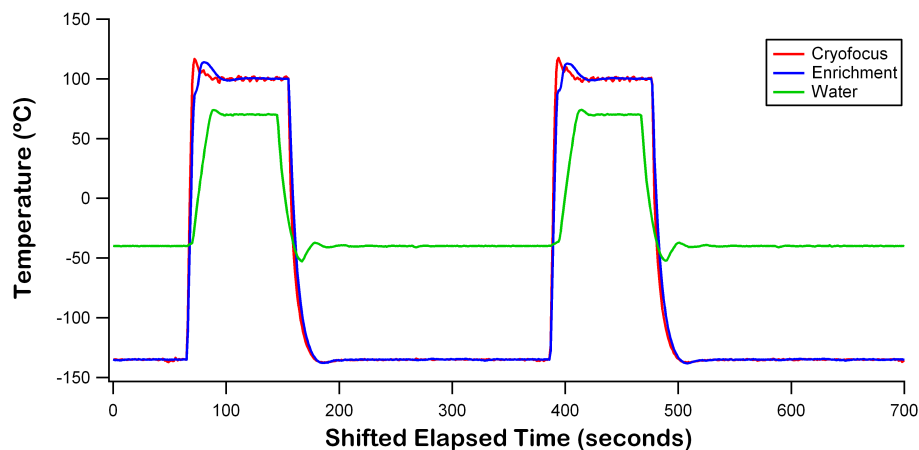


Figure 2.19: Typical trap temperature cycling during the HUMPPA campaign. The time axis has been shifted to facilitate visual comparison.

somewhat faster (see Fig. 2.19), although much of the difference in heating time was likely due to programming differences. In this final configuration, the enrichment and cryofocusing traps were heated from -135 to $+100$ °C in 11.5 and 6.0 seconds, respectively, and were cooled in 24.5 and 23.5 seconds, respectively. In comparison, the water trap was heated from -40 to $+70$ °C in 22.5 seconds and was cooled in 15.0 seconds. These traps cycled consistently and quickly, providing for fast sample processing and sharp injections to the GC.

2.8.2 Trapping Efficiency

Although traps hand-packed with glass wool were convenient and reliable, the trapping efficiency of these traps was found to be highly variable from one trap to the next and difficult to reproduce. However, tests varying the sample trapping temperature indicated that all the C_4 VOCs and higher can be quantitatively trapped with this method, as well as propene. Using an enrichment trap with 3 cm and a cryofocusing tap with 2 cm of tightly-packed glass wool, various temperatures were tested to investigate the trapping efficiency of the 13 compounds identified in Fig. 2.20 and Tab. 2.3. These tests were in many cases conclusive, showing a significant (10–20%) decrease in measured mixing ratio above a certain temperature, with a further 50–60% reduction the next step higher, as seen in Fig. 2.21 for iso- and n-butane. Trapping temperature directly correlated with boiling point and polarity, as expected.

Similar trends indicated that the following compounds were quantitatively trapped at the noted temperatures: propene (-120 °C), iso-butane (-120 °C), n-butane (-110 °C), and iso- and n-pentane (-100 °C). The four butenes, butadiene, and propyne exhibited no clear trend, although this was more likely due to their mixing ratios being near the limit of detection. Propane and ethyne appeared to not be quantitatively sampled under these conditions.

For most of the 13 compounds measured, a sample of 50 mL provided sufficient sample to be quantitatively detected. Notable exceptions were trans- and cis-2-butene (see Tab. 2.3). As these compounds exhibit lower ambient mixing ratios (less than 10 pptv on average), larger samples may be necessary to lower the detection limit for these compounds.

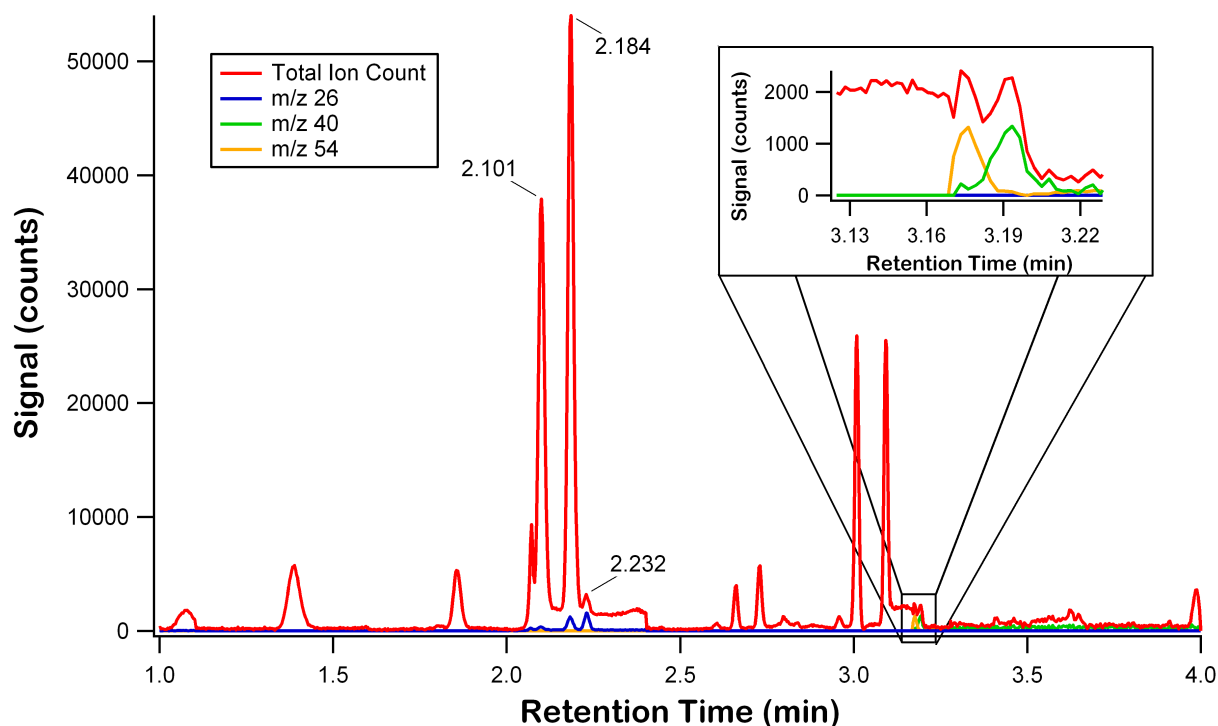


Figure 2.20: A typical chromatogram from the MOHp intercomparison. The sample shown was collected on January 30th, 2010 from 08:00 to 08:02. The detected compounds (and their retention times, in minutes) are listed in Tab. 2.3.

Compound	Mixing Ratio [pptv]	Retention Time [minutes]	Trapping Temp. ^a [°C]	Boiling Point ^b [°C]
ethane				-88.6
ethene				-103.77
propane	259.9	1.390	< -140	-42.1
propene	64.1	1.859	-120	-47.69
iso-butane	229.2	2.101	-120	-11.73
n-butane	368.8	2.184	-110	-0.5
ethyne	33.0	2.232	< -140	-84.7
trans-2-butene	-0.1	2.605		+0.88
1-butene	7.8	2.660		-6.26
iso-butene	2.4	2.731		-6.9
cis-2-butene	-1.6	2.800		+3.71
iso-pentane	97.9	3.007	> -100	+27.88
n-pentane	115.6	3.092	> -100	+36.06
1,3-butadiene	10.0	3.178		-4.41
propyne	15.8	3.194		-23.2

^a Blanks indicate compounds for which the trapping temperature could not be conclusively determined.

^b CRC Handbook of Chemistry and Physics, 91st Edition. It should be noted that these are the boiling points at standard conditions, i.e. 1 bar of vapor pressure. At the significantly reduced partial pressures present in ambient air, the boiling points for these compounds would be depreciated.

Table 2.3: Measured compounds identified in chromatogram of Fig. 2.20, with retention times, trapping temperatures, and standard boiling points for reference.

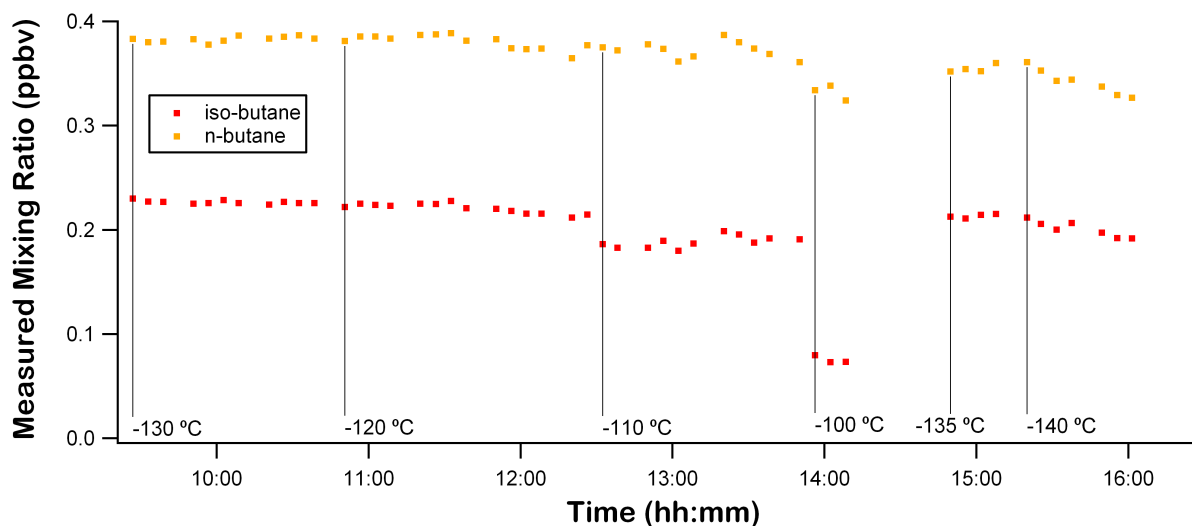


Figure 2.21: A series of butane ambient measurements at trapping temperatures ranging from -140°C to -100°C , as indicated by tags in the figure.

Two compounds not detected were ethane and ethene. Although many attempts were made to trap and detect these compounds, even with trapping temperatures to -150°C and below, it was concluded that this trap construction was inadequate for the quantitative trapping of these low-boiling hydrocarbons. In attempting these low trapping temperatures, irregularities in the chromatograms were observed not seen in similar cryogenic systems, e.g. the GC-FID at MOHp traps at -186°C without difficulty (Plass-Dülmer et al., 2002). A key difference of these two systems was the use of an ozone filter by MOHp. With a boiling point of -111.35°C at standard conditions, trapping of ozone at ambient levels was expected at -150°C . Continued work at these low temperatures would require the use of such a filter, as well as testing for resulting interferences (Helmig, 1997; Pollmann et al., 2005). Fortunately, the long-term plan for this instrument was the measurement of higher-boiling halogenated and oxygenated VOCs. In consideration of this and the significant changes to the system that would be required to trap these compounds, optimization of other aspects of the system remained the focus of this work.

2.8.3 Signal Precision

The stability and precision of FOTOS was determined from repeated measurements of a compressed standard (see Fig. 2.22). The relative standard deviation of the n-butane peak areas was 0.22% for m/z 41 (the smaller of the two peaks), and 0.21% for m/z 43. That this signal was representative of only the current sample and not due to the build up of memory effects was tested and the results displayed in Fig. 2.23. In this test, a zero air run was preceded and followed by ambient air. The ambient air to zero air peak area ratio was 0.016 for m/z 43 and 0.014 for m/z 41. Unfortunately, the zero air signal for some alkenes was rather high. For 1-butene, the signal to zero air peak-area ratio for the same three runs was 0.60. Although less pronounced, similar behavior had been observed in other GC monitoring systems as well (Plass-Dülmer et al., 2002).

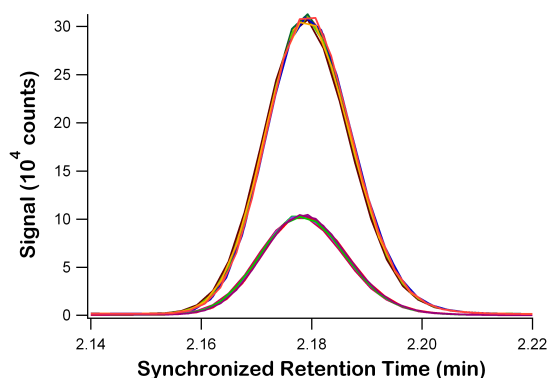


Figure 2.22: Nine successive measurements of n-butane from a standard, m/z 43 above and m/z 41 below.

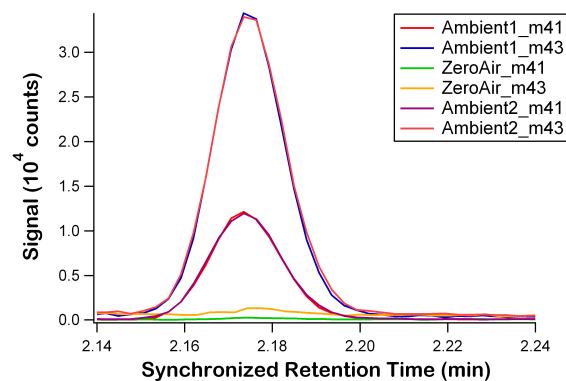


Figure 2.23: The m/z 43 and 41 signals from three consecutive measurements: ambient air, zero air, and ambient air.

2.8.4 Signal Accuracy

During the HUMPPA campaign a series of calibration runs were performed as controls of measurement accuracy. In the case of n-pentane, this resulted in a control range of 4–225 pptv, measured at six different levels, approximately one level every two hours (see Sect. 4.2). All calibration points were treated to the same quality control and calibration routine as the sample data. These “measured” mixing ratios were compared to those calculated from the zero air and standard gas flows recorded by the V25 (“calculated mixing ratios”). The average difference of the measured and calculated mixing ratios for n-pentane for the entire campaign was 0.26 pptv with a standard deviation of 1.4 pptv. This was heavily influenced by a single large discrepancy during the time of the water trap heater repair discussed in Sect. 4.3. With this single point removed, the average difference dropped to 0.18 pptv, with a standard deviation of the 0.87 pptv. As seen in Fig. 2.24, there was a tendency to slightly over-report low mixing ratios and under-report high ones, which was also observed in the mixing ratios errors for iso-pentane.

In the case of iso-pentane, the largest error was observed at the very end of the campaign, due to difficulties of extrapolating calibration factors beyond the final calibration run. The instrument logs show irregularities for the last calibration point, so the interpolated calibration factors for iso-pentane from the 7th of August at 18:15 UTC until the end of the campaign (August 8th at 20:30 UTC) were replaced with the average of the previous four calibration points. The average error and standard deviation for all iso-pentane data points before this correction were 0.27 pptv and 0.95 pptv, respectively, and 0.37 pptv and 0.59 pptv after this correction. The butane isomers were significantly more noisy with no clear outliers. The average difference and standard deviation were 1.0 pptv and 2.2 pptv for n-butane, and 2.0 pptv and 4.2 pptv for iso-butane.

Detection limits were estimated to be three times the standard deviation of the filtered calibration errors. This resulted in detection limits for the HUMPPA campaign of 2.6 pptv for n-pentane, 2.0 pptv for iso-pentane, 6.6 pptv for n-butane, and 12.6 pptv for iso-butane.

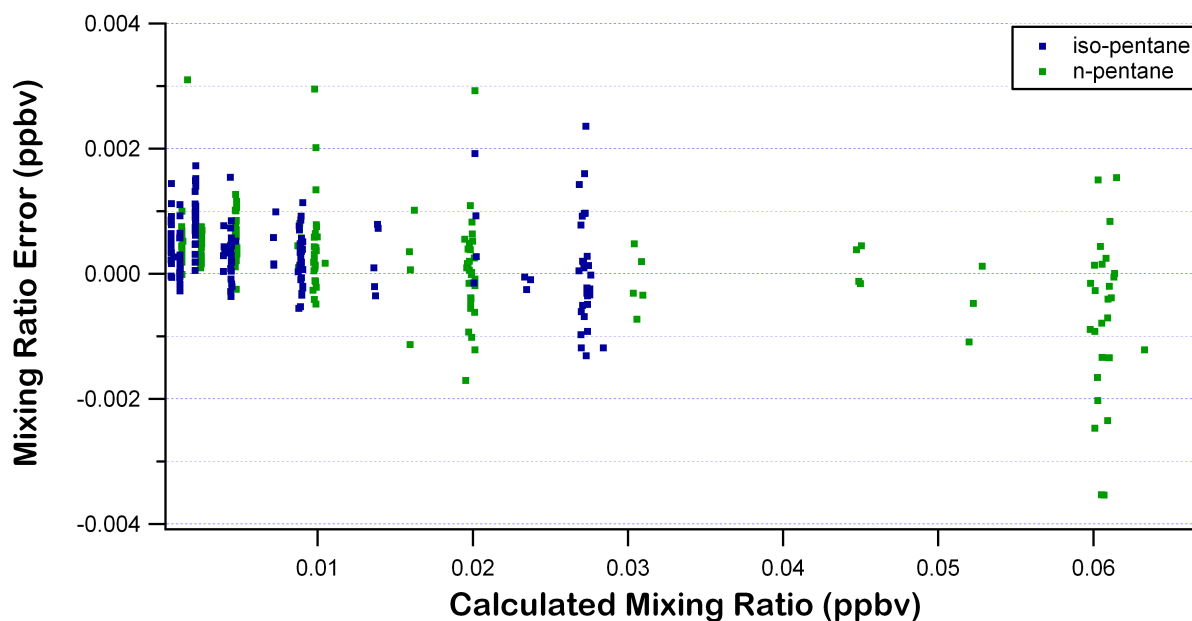


Figure 2.24: Error calculation for n-pentane. The bottom axis shows the calculated mixing ratio from the zero air and standard gas MFCs. The left axis reflects the measured mixing ratio minus this calculated one.

2.8.5 Signal Stability

As a measure of total system stability, the response factors (integrated peak area divided by diluted mixing ratio of calibration runs) for the measured compounds were considered as a function of time, displayed in Fig. 2.25. There was a clear trend of decreasing sensitivity through the first half of the campaign, which leveled off for the last half. The pentanes exhibited higher sensitivity than the butanes, which was reflected in the accuracy observations of Sect. 2.8.4. The filament of the MS ion source burned out on July 19th (right vertical line of Fig. 2.25) and the system was switched to the reserve filament. This resulted, as expected, in a step change of all response factors.

2.9 Conclusions

To facilitate the measurement of trace volatile organic compounds (VOCs) in situ during atmospheric research flights of the High Altitude Long Range (HALO) aircraft, a new gas chromatography mass spectrometry (GC-MS) instrument was developed and assembled according to the specifications provided for aircraft measurements. A cryogenic sample enrichment, focusing, and injection system was designed, constructed, and tested for speed and trapping efficiency. This fast sampling system, together with a customized, fast GC and MS detection facilitated high frequency processing of ambient samples, returning measurements of 13 different C_2 to C_5 hydrocarbons at high precision every 5.5 minutes. This high measurement frequency was achieved by having independent control of each of the three traps (and all other system parts) through the in-house developed, comprehensive, modular control system, V25.

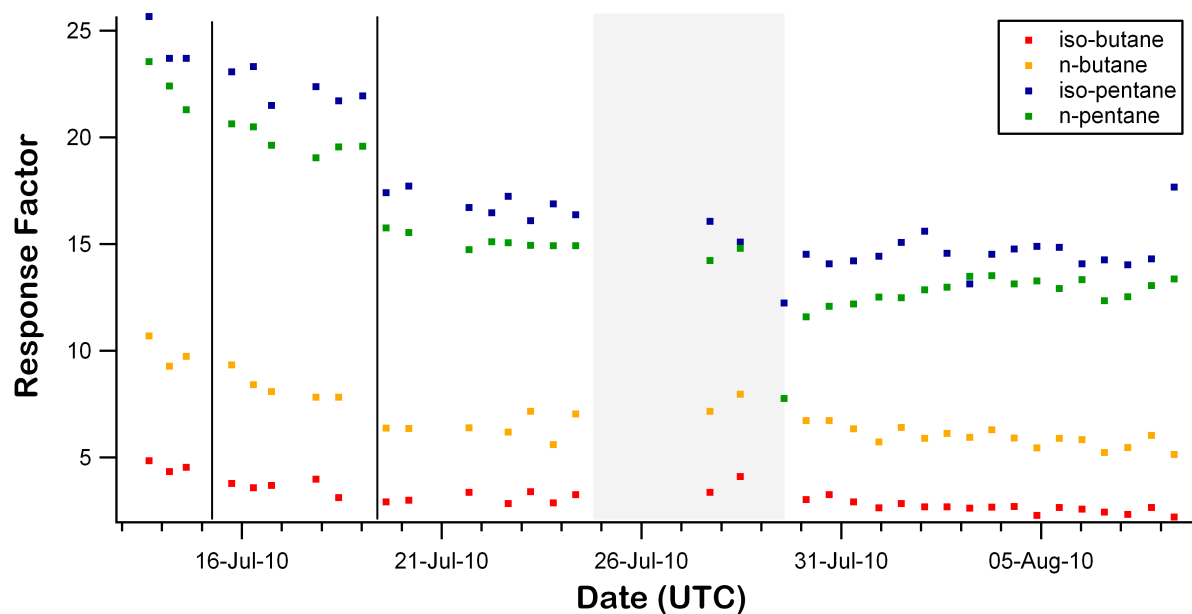


Figure 2.25: Time trace of the pentane and butane response factors (integrated peak area divided by diluted mixing ratio) from the HUMPPA data set. Vertical lines indicate the timing of MS tunes. The gray area corresponds to the period of water trap heater failure discussed in Sect. 4.3.

A variety of different cryogenic trap designs were constructed and tested. It was determined that the best configuration consisted of a 1/8 inch OD, hollow, stainless-steel, directly-heated water trap; a 1/16 inch OD, 1.0 mm ID, glass wool packed, wrapped stainless-steel, directly-heated enrichment trap; and a 1/16 in OD, 0.5 mm ID, bare stainless-steel, directly-heated cryofocusing trap containing a deactivated, silica capillary on which the sample was focused and union-free injected onto the GC column. This configuration provided for fast and stable temperature cycling leading to reproducible trapping, but was unable to trap the highly volatile species ethane and ethene.

As a whole, the Fast Observation of Trace Organics System (FOTOS) was proven to be highly precise, with the standard deviation of repeated standard measurements reaching below a quarter of a percent. Memory effects from one run to another were also shown to be below 2%, except in the cases of certain alkenes. Detection limits were determined to be as low as 2.0 pptv. With such results, it was determined that FOTOS was capable of providing high frequency, precise, sensitive, accurate measurements during research flights of the HALO aircraft. Such a system would also produce valuable data on other platforms and in ground-based measurement campaigns.

Chapter 3

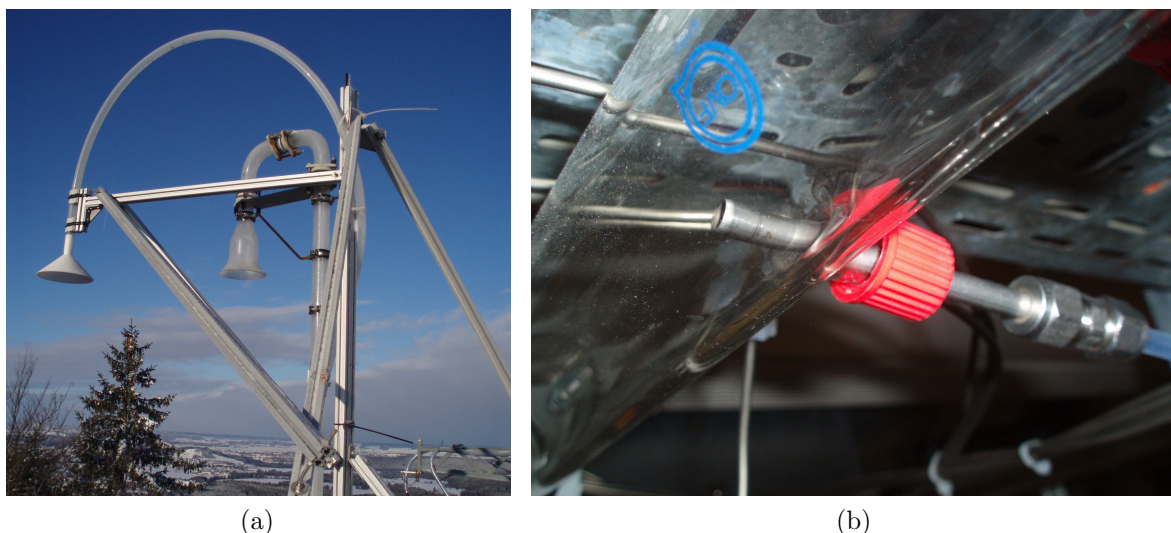
An intercomparison at the WMO-GAW Global Station Hohenpeißenberg

3.1 Measurement Standards

Precision and accuracy are the chief concerns of any analytical scientist. In the field of atmospheric monitoring, this is even more so, as long term measurements only have value if the measurement techniques are consistently precise and accurate. To this end, the World Meteorological Organization (WMO) Global Atmospheric Watch (GAW) network has developed strict guidelines for the quality of measurements at certified stations. These Data Quality Objectives (DQO) include accuracies of 10% for alkanes, 20% for alkenes, and 10% for alkynes above 100 pptv. For all compounds below 100 pptv, an accuracy of 50% is deemed acceptable (Rappenglück et al., 2006).

Therefore, when considering how or where to test the accuracy of measurements by FOTOS, the Meteorological Observatory at Hohenpeißenberg (MOHp) is a prime candidate. Atop Hohen Peißenberg, 980 meters above sea-level, MOHp is the oldest mountaintop weather observatory in the world and, since January 1st, 1999, a GAW Global station. Among the many measurements performed regularly, more than 40 hydrocarbons have been measured twice daily for the past 15 years. In intercomparisons with other GC systems, those at MOHp have demonstrated superb accuracy and precision (Plass-Dülmer et al., 2002), making it an excellent choice for testing the quality of a new instrument.

This chapter will describe the results of an informal intercomparison between FOTOS and the GC-FID system at MOHp. The accuracy of the measurement of 13 C₂ to C₅ hydrocarbons will be presented followed by discussion of possible sources of deviation. A brief mention of the advantage of higher time resolution measurements will be followed by discussion of improvements to FOTOS initiated following this campaign.



(a)

(b)

Figure 3.1: (a) The glass inlet (rear center) for the GC-FID sampling line at MOHp. (b) The connection for FOTOS to the sampling line.

3.2 Sampling and Comparison Setup

From January 26th to February 4th, 2010, FOTOS measured from the sample line of the GC systems (one with an FID, one with an MS) at the Meteorological Observatory at Hohenpeißenberg (MOHp). The sample line was a 4 cm ID glass tube with an air flow of $1 \text{ m}^3/\text{min}$ from the roof of the observatory (10 meters above ground, approximately the top of the surrounding canopy). The inlet was an unfiltered glass funnel, as seen in Fig. 3.1a. The GC-FID system used at MOHp was connected to the sample line ten meters from the inlet and was configured as described by Plass-Dülmer et al. (2002), with the following alterations: the Nafion dryer was replaced by a moisture trap at -40°C and an ozone filter, $\text{Na}_2\text{S}_2\text{O}_3$ on a PTFE coated, glass fiber filter, replaced ozone removal by heated stainless steel. The reported times of these data points were the midpoints of the 15 minute sample collection.

The sampling line for FOTOS was connected to the main glass line by a 1/4 inch stainless steel tube inserted through a Teflon o-ring sealed port to the middle of the sample stream (see Fig. 3.1b) three meters downstream of the MOHp GC inlets. FOTOS was configured as described previously (see Chap. 2) with the following trap configuration: a bare, directly-heated enrichment trap with 3 cm of tightly packed glass wool in the trapping region; a wrapped, indirectly-heated cryofocusing trap with 2 cm of tightly packed glass wool; and a Teflon, indirectly-heated, unpacked water trap (see Sect. 2.4). On February 1st, the indirect heater for the cryofocusing trap failed, at which point the trap was left in place, but switched to direct heating (i.e. now a wound, directly-heated trap). During this campaign, the GC cooling fan had not yet been updated as mentioned in Sect. 2.5.

From January 26th to February 4th, both instruments sampled at their respective maximum sampling rates, 70 minutes for the MOHp system and 6 minutes for FOTOS. During this intensive period, the MOHp system performed no calibration or zeroing runs, having previously demonstrated the need for only biweekly calibrations (Plass-Dülmer et al.,

2002). From January 26th to 29th, FOTOS performed alternating zeroing and calibration runs every third measurement, and starting January 29th, this frequency was raised to every fifth measurement. Calibrations were cycled between three different mixing ratios. It was then determined that the calibration scheme, being optimized for upper tropospheric mixing ratios (as would be seen in a flight campaign), was poorly covering the sample range. To correct this, the calibration gas was sampled 14 times without dilution on February 2nd. These points, together with a higher concentration calibration curve measured after the campaign, provided a sufficient range for determining calibration factors for all compounds measured. The data set was subjected to the quality control measures outlined in Sect. 2.7.

3.3 Characteristic Results

During the course of the intercomparison, thirteen different hydrocarbons were regularly detected (see Fig. 2.20 and Tab. 2.3). The time series for n-butane showed typical features seen in many compounds (see Fig. 3.2). The first two days exhibited significantly elevated mixing ratios, with all points in excess of 850 pptv, during a pollution event from Munich (approximately 56 km to the Northeast). The concentrations for many hydrocarbons during this period were among the highest recorded in the previous 15 years of monitoring at

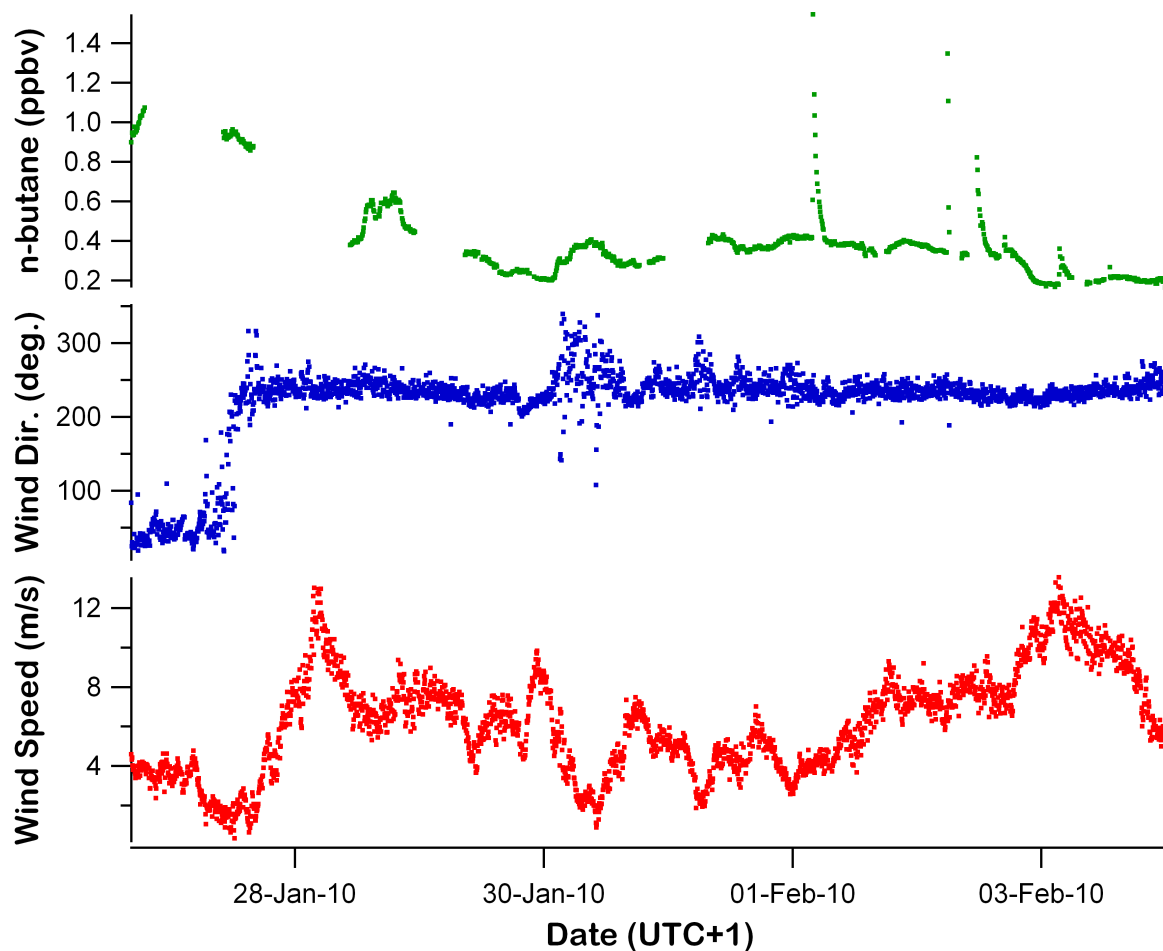


Figure 3.2: Time trace of n-butane measured at m/z 41 with wind direction in degrees and wind speed in m/s.

MOHp (C. Plass-Dülmer, personal communication, 10 Feb 2010). An additional peak of high concentration (above 600 pptv) was also observed during the second half of January 28th. Mixing ratios declined through midnight on the 30th, then another broad peak occurred during the morning of the 30th, as the wind speed dropped and wind direction became more variable. The period of January 31st through February 2nd was characterized by fairly steady mixing ratios with constant winds from the southwest. During this period, several strong spikes followed by smooth exponential decay were observed. Zero runs and calibrations during this period appeared normal, however these peaks were not seen in the MOHp GC data. On the evening of February 2nd, the mixing ratios dropped to the lowest level of the comparison as wind speed increased. A small peak in mixing ratios was observed on the morning of the 3rd during a short period of especially high winds, which were some of the strongest of the measurement period. Although the measurement period of this intercomparison was somewhat brief (only ten days), a wide variety of atmospheric and chemical conditions were observed, providing a basis data set for a comprehensive comparison.

3.4 Signal Agreement

The mixing ratios determined by FOTOS and those measured by the GC systems at MOHp showed remarkably good agreement, as discussed in the following subsections and summarized in Tab. 3.1. In order to directly compare measurements, the data from FOTOS had to be reduced to the time scale of the MOHp data. This was accomplished by averaging those data points from FOTOS whose midpoint was within the given MOHp sample time. These averages were then divided by the MOHp values, resulting in an “agreement ratio” that would be unity for perfect agreement. As the measurements by FOTOS and MOHp were not technically of the same sample, it could be argued that the DQO in this case could be relaxed. This should be evident when comparing the agreement ratio with the standard deviation of the FOTOS points averaged for comparison. It was expected that differences in sampling would be most evident for those sample periods with the highest variability. However, as no significant correlation of these two values was found, this discrepancy was ignored.

A clear trend of agreement as a function time in some compounds was seen, especially those of higher mixing ratios (e.g. n-pentane, see Fig. 3.3), which was due to the calibration being based on a single point during the comparison (measured directly from the bottle and marked in Fig. 3.3, see also Sect. 3.2), instead of at regular intervals.

In the following subsections, a case by case comparison of the compounds measured by FOTOS is presented. The agreement ratios as described above are presented as a function of mixing ratio measured by the MOHp GC-FID, on a logarithmic scale for clarity. Values acceptable by the GAW DQO were highlighted with a white background, and unacceptable values in gray. For example, in Fig. 3.4, if the measurement from FOTOS perfectly matched that of MOHp, then all data points would lie on the thick line level with 1.0 on the left axis. Those measurements that satisfy the GAW DQO would be within the white space at the top of the graph. That all the points had an agreement ratio less than one indicated that

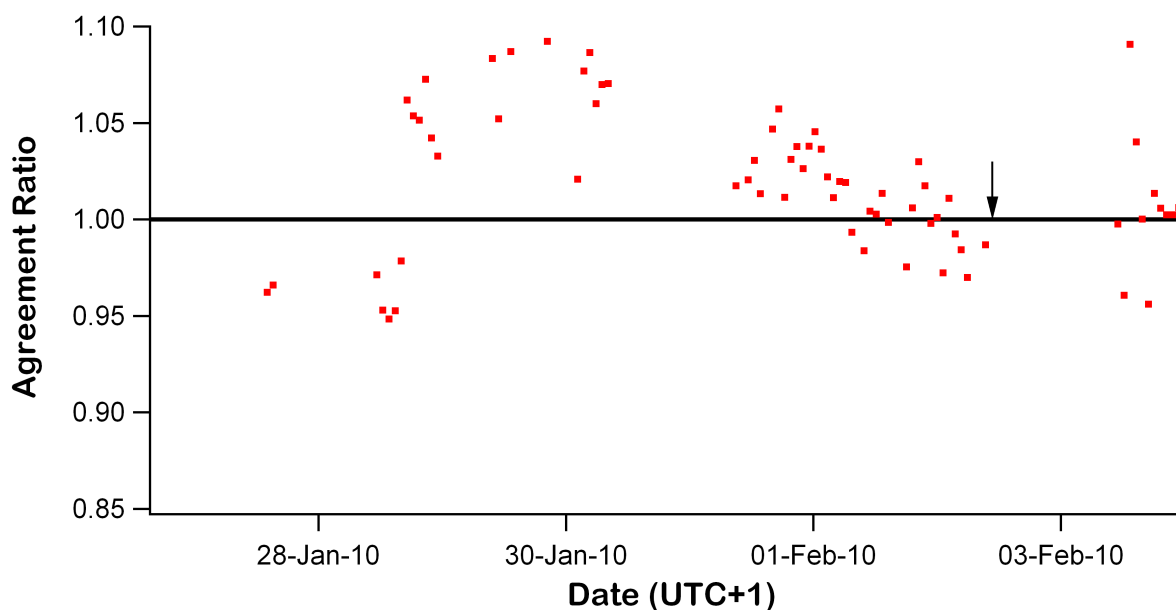


Figure 3.3: Time trace of the ratio of n-pentane measured by FOTOS with that measured by MOHp. The black arrow indicates the time of the FOTOS calibration.

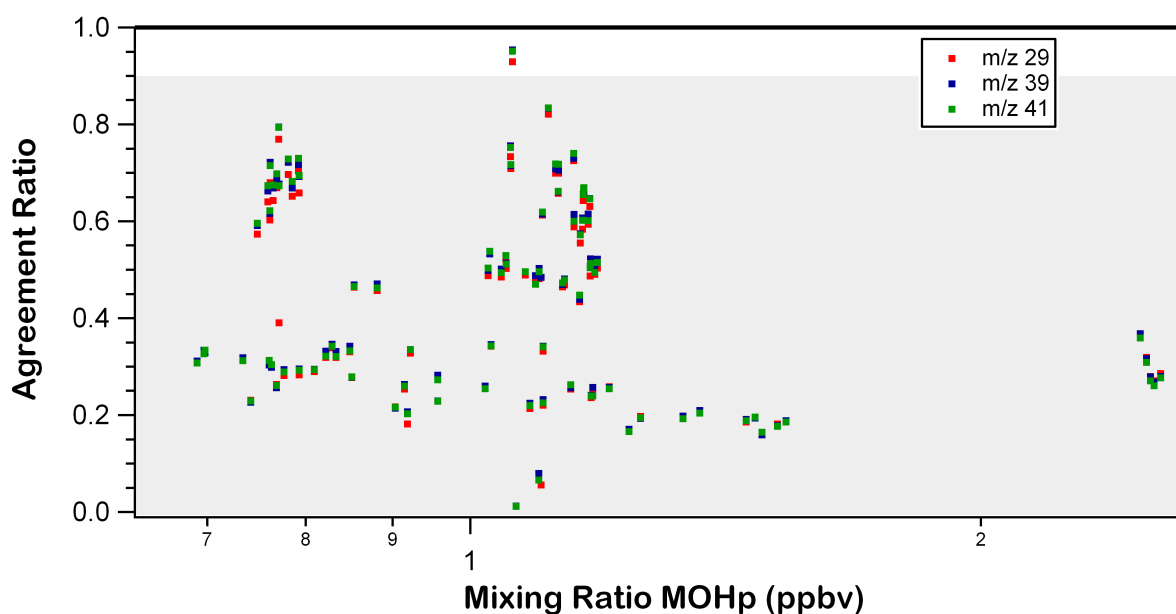


Figure 3.4: The ratio of propane measured by FOTOS with that measured by MOHp as a function of mixing ratio. A single high point at a mixing ratio of 1.102 ppbv with an agreement ratio of 3.44 in the m/z 41 signal was excluded for presentation clarity.

FOTOS measured a lower mixing ratio than the MOHp GC-FID. Agreement ratios greater than one would signify over-estimation of the mixing ratio by FOTOS.

3.4.1 Propane and Propene

Propane and propene were the lowest boiling alkane and alkene considered for this intercomparison. As such, evidence of breakthrough was most likely to be seen here. This was clearly the case for propane (see Fig. 3.4). Except for a single, outlying high point measured only at m/z 41 (excluded from the graph), all the measurements of propane were significantly lower

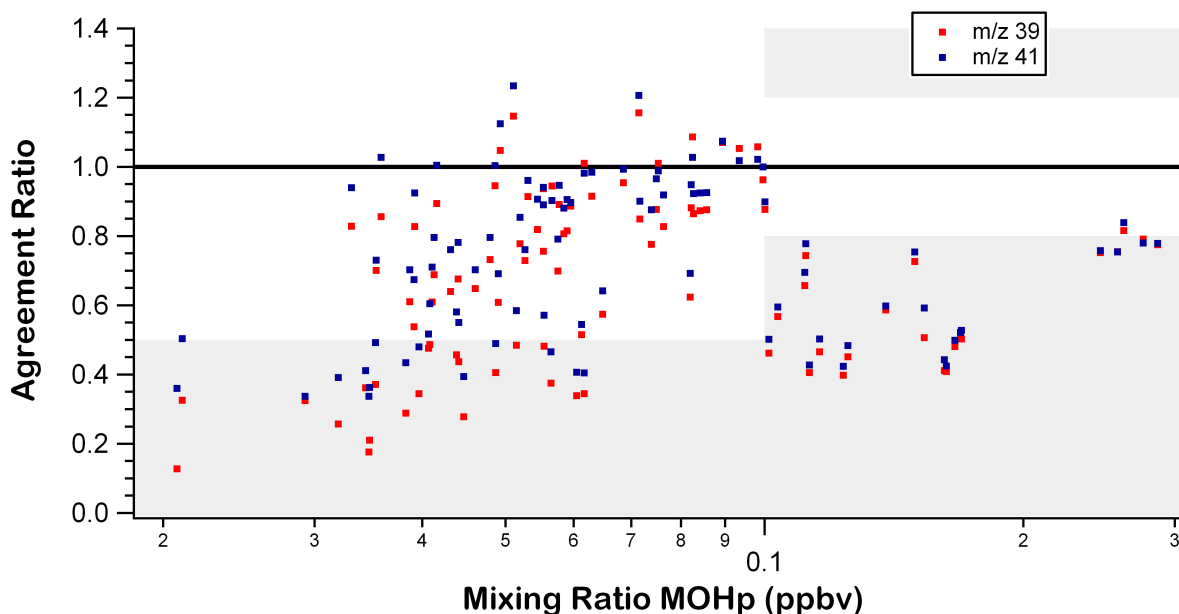


Figure 3.5: The ratio of propene measured by FOTOS with that measured by MOHp as a function of mixing ratio.

than the values obtained by the MOHp systems. Propene, however, approached quantitative trapping by FOTOS, with values being reported above and below the MOHp measurements (see Fig. 3.5). For propane and to a lesser degree propene, the measurements from each of the different ion fragments of a particular compound showed good agreement as well. For propane, 93.3% and 98.7% of m/z 29 and 94.9% and 99.1% of m/z 41 values were within 5% and 10% of the m/z 39 values, respectively. This was an important point for compound identification, and also illustrated the stability of the measurement.

3.4.2 Butanes

The agreement between FOTOS and MOHp for iso- and n-butane was very good for m/z 41, but showed interference in the m/z 43 signal. This was seen as a m/z 43 peak in the chromatograms that normally preceded the iso-butane peak, but often encroached on this peak. As this interference peak was often not to be seen, meaning it was either co-eluting with iso-butane or before the ion group which included m/z 43, use of this ion for quantization was less accurate (see Figs. 3.6 and 3.7). For both butane isomers, several high outliers were evident, which related to the spikes mentioned in Sect. 3.3.

3.4.3 Ethyne

The lowest boiling of all hydrocarbons measured, ethyne (or acetylene) showed similar evidence of breakthrough as was seen in propane (see Fig. 3.8). An additional difficulty for this measurement was the resolution of the ethyne and n-butane separation. As these compounds had similar retention times, slight changes in the system often resulted in co-elution. Specifically, changes in ambient humidity were found to induce these effects. While co-elution reduced the number of ethyne data points, it did not affect the n-butane

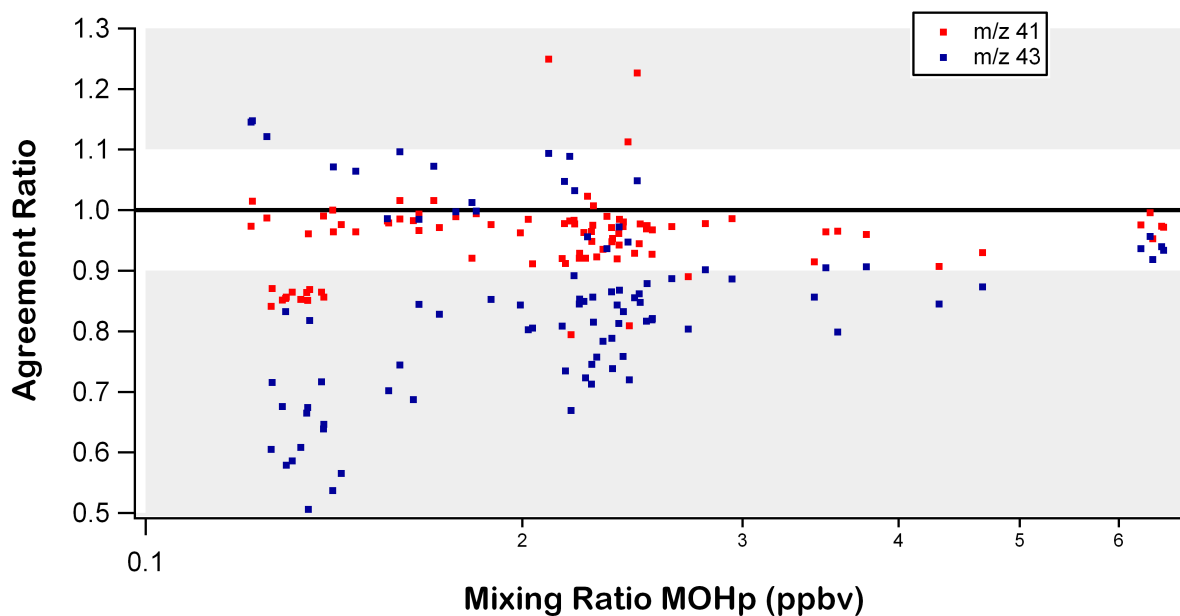


Figure 3.6: The ratio of iso-butane measured by FOTOS with that measured by MOHp as a function of mixing ratio.

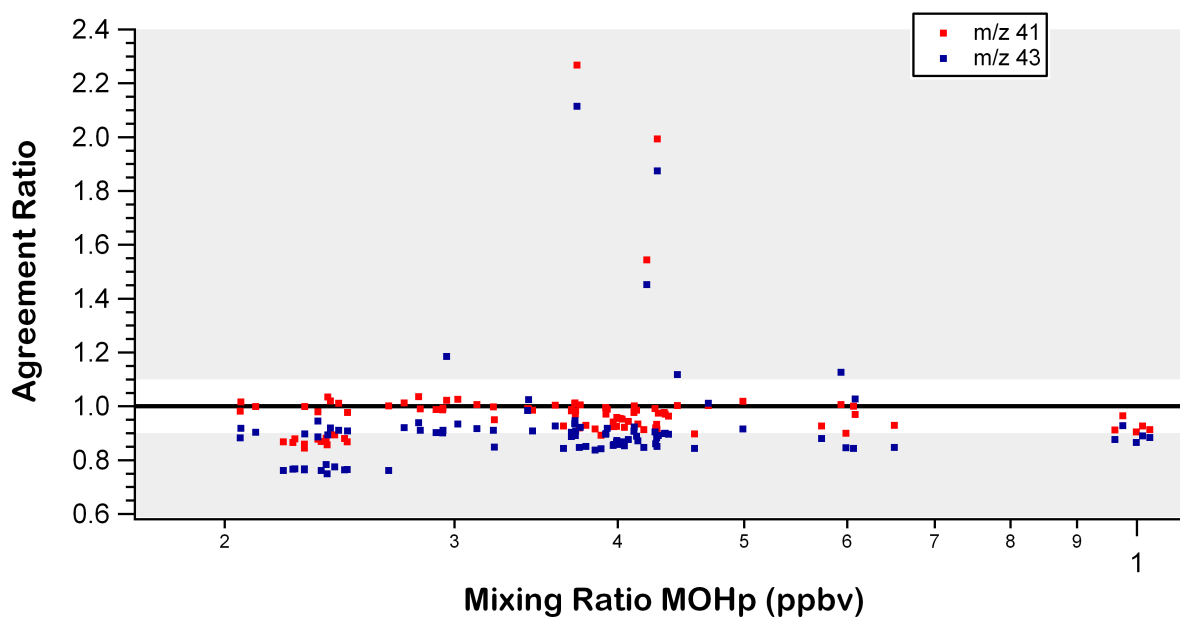


Figure 3.7: The ratio of n-butane measured by FOTOS with that measured by MOHp as a function of mixing ratio.

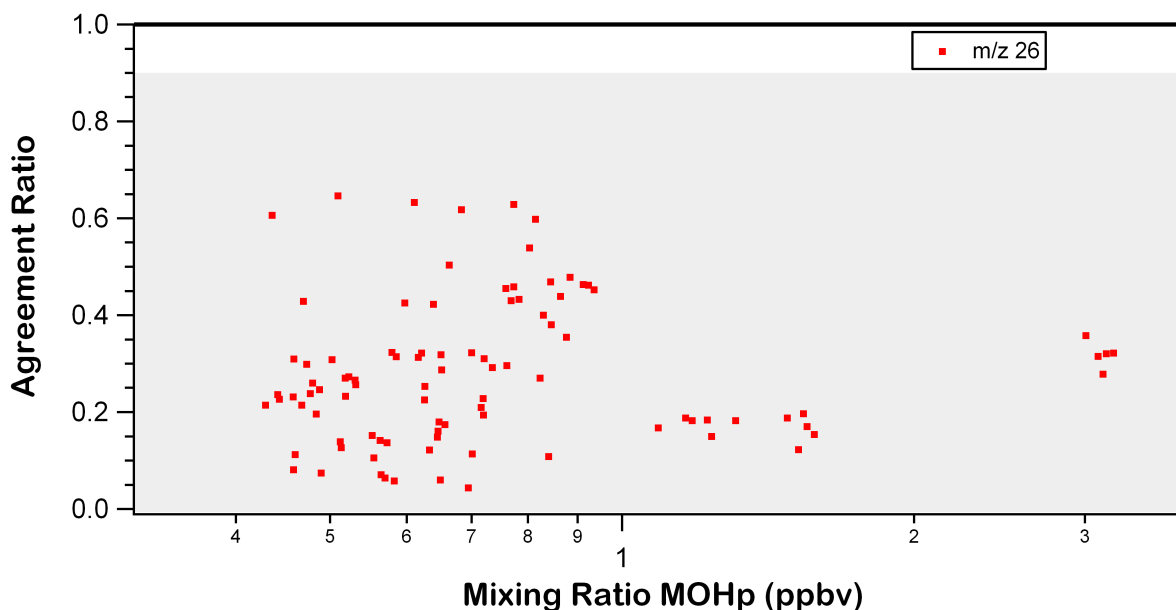


Figure 3.8: The ratio of ethyne measured by FOTOS with that measured by MOHp as a function of mixing ratio.

measurement at m/z 41, as the heaviest, isotopic-substituted, ethyne fragment possible was at m/z 28.

3.4.4 Butenes

The four isomers of butene, namely *trans*-2-, *iso*-, 1-, and *cis*-2-butene, exhibited regular retention time spacing and similar mixing ratio trends. For all butene isomers, m/z 39 showed the most noise, especially for *cis*-2-butene, and m/z 41 and 56 exhibited relatively similar behavior. In the case of *iso*-butene (see Fig. 3.9), 70.0% and 93.2% of m/z 56 values were within 5% and 10% of the m/z 41 values above 4 pptv. For all butene isomers (see Fig. 3.10), it was clear that the disagreement of the two systems decreased at higher concentrations. The values for *iso*- and 1-butene were both above and below the MOHp values, which indicated quantitative trapping. However, *trans*- and *cis*-2-butene were consistently under-reported by FOTOS, most likely due to mixing ratios which approached the detection limit.

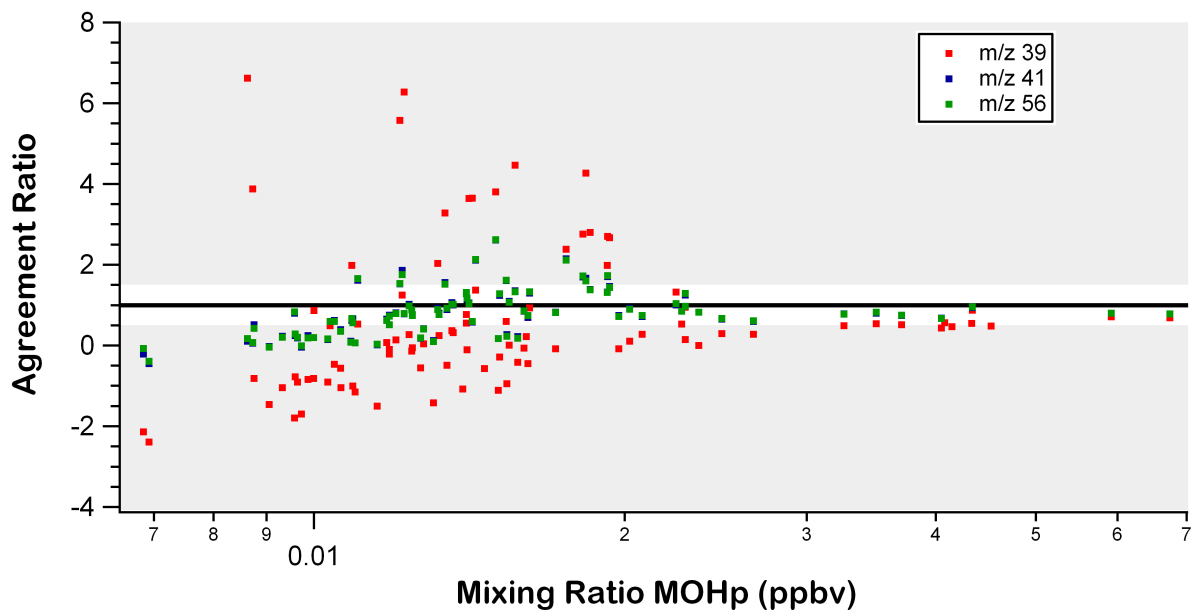


Figure 3.9: The ratio of iso-butene measured by FOTOS with that measured by MOHp as a function of mixing ratio.

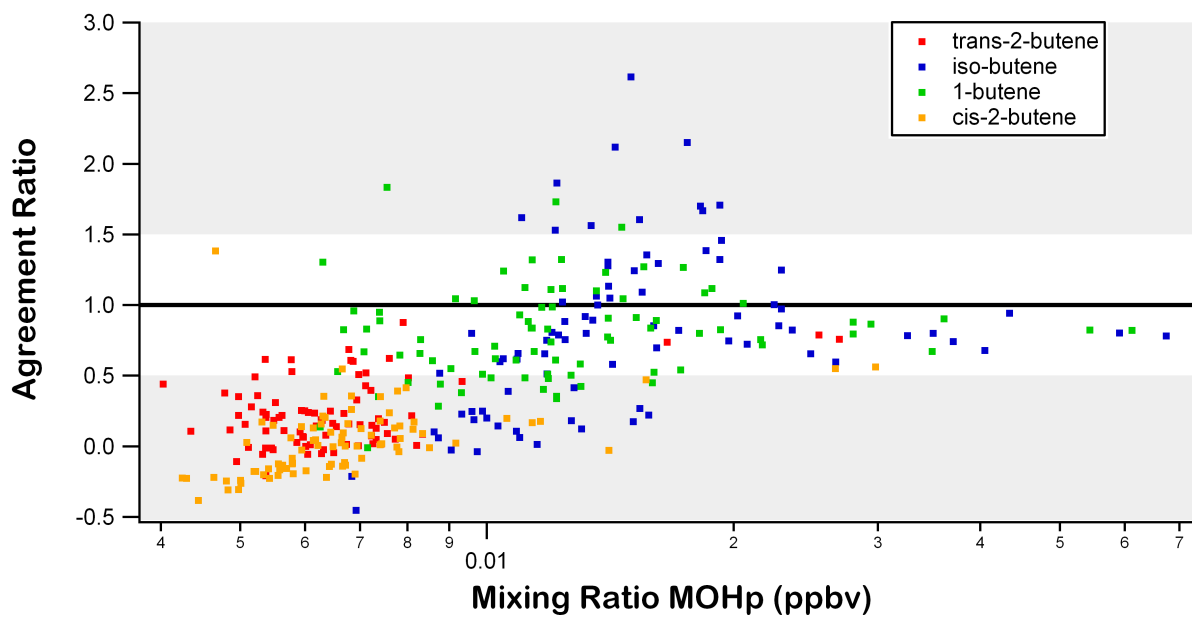


Figure 3.10: The ratio of the four butene isomers measured by FOTOS with that measured by MOHp as a function of mixing ratio.

3.4.5 Pentanes

Of particular concern was the poor agreement observed for iso-pentane, seen in Fig. 3.11. The source of this disagreement was mostly due to poor selection of the ion group timing of the MS Select Ion Monitoring (SIM) programming. This exemplified how important the specific method development was to the overall system. As seen in Fig. 3.12, underestimation by FOTOS was strongly dependent on the retention time of the iso-pentane peak. At a retention time of 3.0 minutes, the ion group switched from m/z 39, 41 and 56 for butenes detection to m/z 43 and 57 for pentanes detection. This switch regularly occurred during

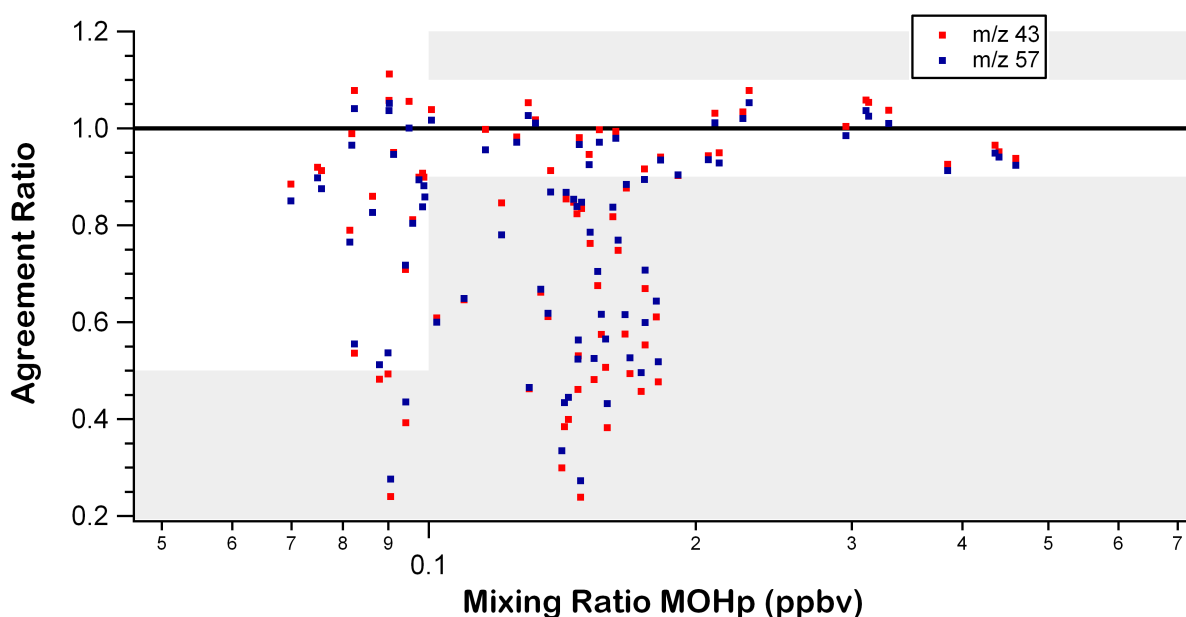


Figure 3.11: The ratio of iso-pentane measured by FOTOS with that measured by MOHp as a function of mixing ratio.

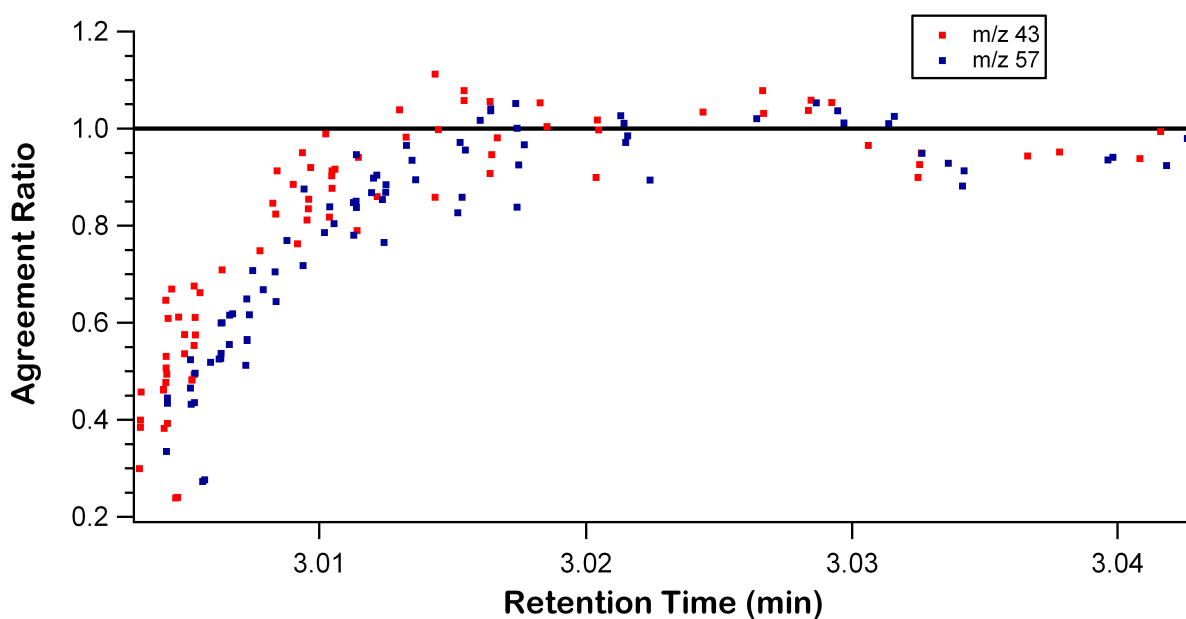


Figure 3.12: The ratio of iso-pentane measured by FOTOS with that measured by MOHp as a function of retention time of the FOTOS peak.

the rise of the iso-pentane peak. While the total ion count for this peak looked normal (due to the high occurrence of m/z 41 in iso-pentane), the signal for any one m/z was clipped, resulting in an underestimation of the mixing ratio. All points with a retention time greater than 3.015 minutes fell within the GAW DQO. The problem of signal clipping was resolved in later measurements (e.g. the HUMPPA campaign, see Chap. 4) by including m/z 41 in all ion groups. For the pentanes, the signal at m/z 57 (which was largely used for identity verification) was later dropped to maintain the highest possible detection frequency in the MS. The retention time for n-pentane was well within the ion window, and this compound exhibited exceptional agreement with the MOHp systems, with all of the m/z 43 values meeting the GAW DQO (see Fig. 3.13).

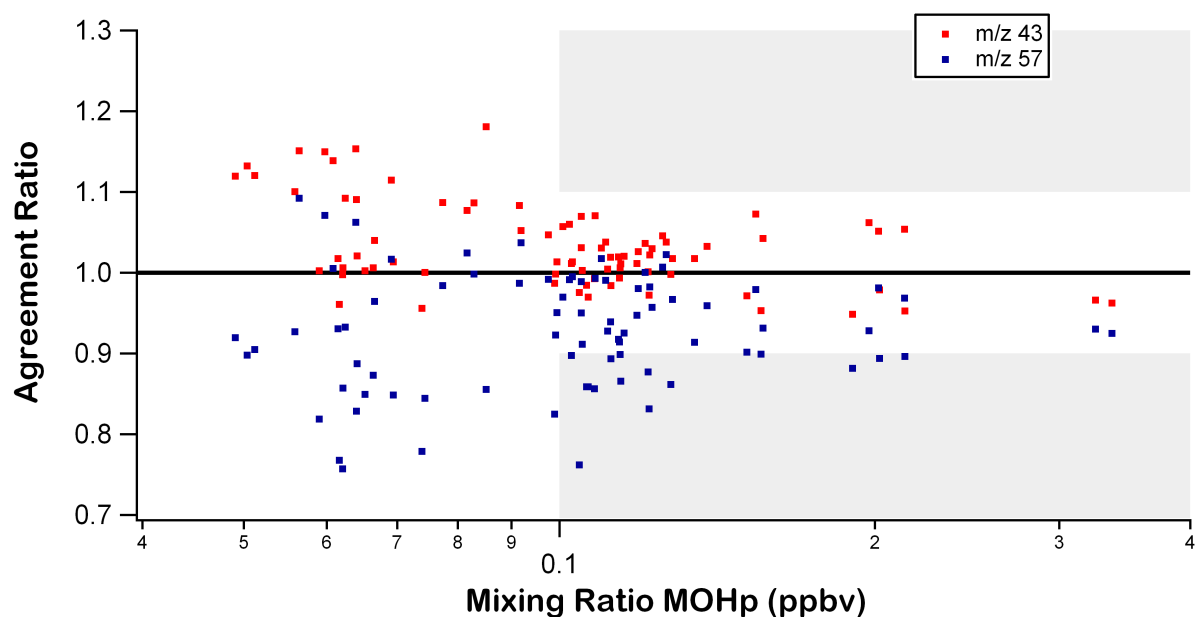


Figure 3.13: The ratio of n-pentane measured by FOTOS with that measured by MOHp as a function of mixing ratio.

3.4.6 Butadiene and Propyne

Agreement for the two doubly unsaturated hydrocarbons, 1,3-butadiene and propyne, was nearly always acceptable, despite their low ambient concentrations (see Fig. 3.14). As with iso-pentane, the butadiene signal suffered from clipping by ion group timing, as seen in Fig. 3.15. Butadiene was monitored at m/z 39 and 54, but excessive interference made it impossible to use m/z 39 for quantization. Other than the few outlying low points, propyne (monitored only at m/z 40) showed a small, consistent under-estimation of less than 20%

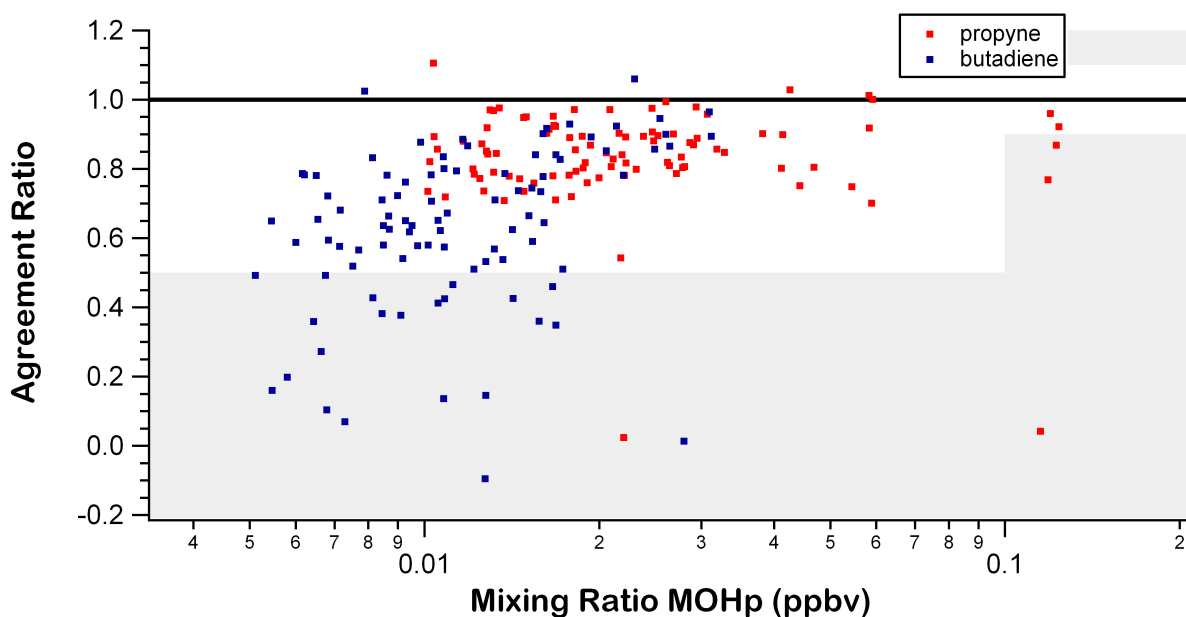


Figure 3.14: The ratio of butadiene and propyne measured by FOTOS with that measured by MOHp as a function of mixing ratio.

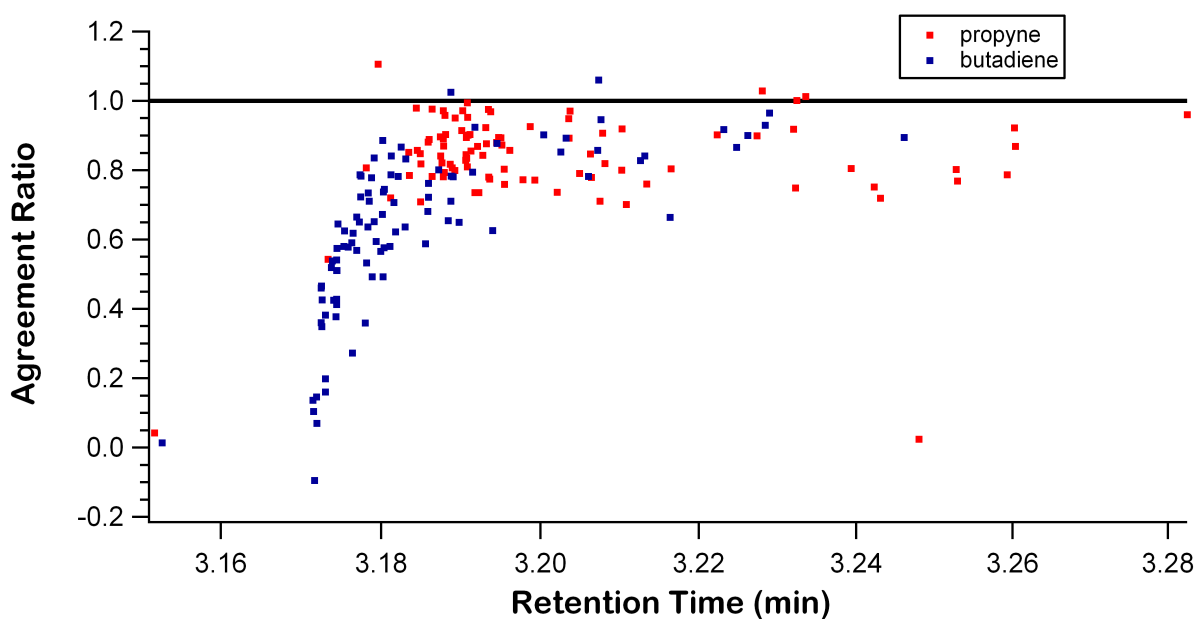


Figure 3.15: The ratio of butadiene and propyne measured by FOTOS with that measured by MOHp as a function of retention time of the FOTOS peak.

on average. The low points for propyne did not appear to correlate to retention time, and therefore reflect the quality of this measurement.

3.4.7 Agreement Summary

The results of the intercomparison were summarized in Tab. 3.1 . The average mixing ratio measured by MOHp, the average and standard deviation of the agreement ratio, and the percent of data points within the GAW DQO were calculated for each m/z ratio monitored for each compound. The m/z selected for future quantization were highlighted, with the compounds analyzed for the HUMPPA campaign in yellow.

Compound	Mixing Ratio Average [†] [pptv]	Agreement Ratio		DQO [%]	m/z
		Average	σ		
propane	1100.2	0.419	0.199	1.1	29
propane	1100.2	0.436	0.202	1.1	39
propane	1100.2	0.466	0.371	1.1	41
propene	80.8	0.669	0.248	55.9	39
propene	80.8	0.732	0.229	63.4	41
iso-butane	234.4	0.955	0.068	80.2	41
iso-butane	234.4	0.844	0.145	28.6	43
n-butane	394.4	0.989	0.190	81.3	41
n-butane	394.4	0.918	0.189	36.3	43
ethyne	851.6	0.280	0.148	0.0	26
trans-2-butene	6.9	-0.096	0.954	6.6	39
trans-2-butene	6.9	0.227	0.232	15.5	41
trans-2-butene	6.9	0.217	0.238	14.3	56
1-butene	15.0	0.706	0.338	67.7	39
1-butene	14.1	0.800	0.331	78.6	41
1-butene	14.1	0.801	0.327	77.4	56
iso-butene	17.8	0.593	1.772	19.6	39
iso-butene	16.8	0.814	0.573	60.7	41
iso-butene	16.8	0.813	0.568	59.5	56
cis-2-butene	7.4	0.031	3.040	6.5	39
cis-2-butene	7.3	0.039	0.258	4.8	41
cis-2-butene	7.3	0.009	0.351	10.7	56
iso-pentane*	219.9	0.994	0.058	100.0	43
iso-pentane*	197.2	0.967	0.063	100.0	57
n-pentane	110.5	1.033	0.053	100.0	43
n-pentane	110.5	0.927	0.071	81.3	57
1,3-butadiene*	15.3	0.822	0.119	100.0	54
propyne	28.1	0.836	0.149	95.7	40

[†] From MOHp GC-FID measurement.

* The values for iso-pentane and butadiene are from those points with a retention time greater than 3.015 and 3.185, respectively, see Sect. 3.4.5 and Sect. 3.4.6.

Table 3.1: Agreement between mixing ratios measured by FOTOS and by MOHp GC-FID.

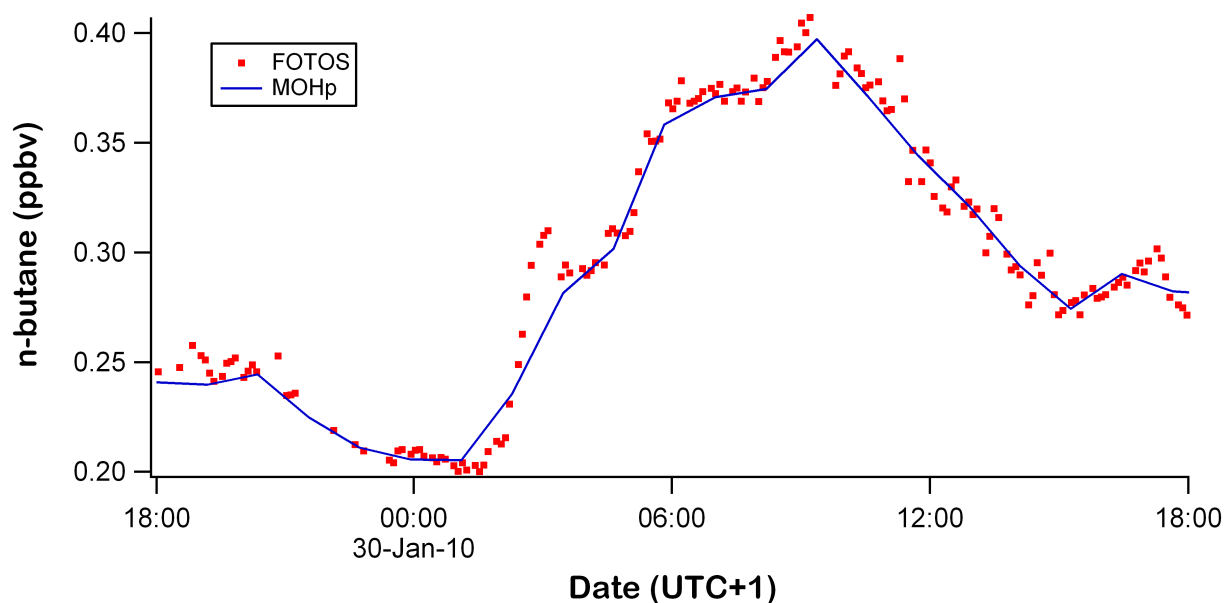


Figure 3.16: A detail of the n-butane time trace measured by FOTOS and MOHp, indicating the additional features detected by the higher time resolution measurements of FOTOS.

3.5 Advantages of Higher Resolution

In addition to signal accuracy comparisons, the intercomparison of FOTOS with the MOHp GC-FID nicely illustrated the benefits of the higher time resolution capabilities of this new instrument. A case study is presented in Fig. 3.16, with the linear interpolation of the MOHp data set represented by the blue line and the FOTOS measurements in red. Both instruments measured similar trends, but significant details were missing from the lower resolution data. The FOTOS data spiked near 03:00, which was dramatically reduced in the MOHp data. Also, the small peak just before 18:00 was significantly under-represented in the MOHp data. The increased resolution was not only a function of sampling frequency, but also the duration of the sampling time. The MOHp GC-FID system had a sampling time of 15 minutes compared to less than two minutes for FOTOS. This further averaged out features of the low resolution signal. This one day provided a nice case study that hydrocarbon mixing ratios did indeed fluctuate on time scales that could not be accurately represented with the typical, one-hour measurement resolution of traditional GC instruments, but were captured by higher frequency measurements. This increase in time resolution coupled with high accuracy and low detection limits (less than 10 pptv) represented a significant improvement.

3.6 Envisioned Improvements Following Comparison

Several points for improvement were made clear during this first field use of the new FOTOS instrument. Most clear and easiest to resolve was the issue of signal clipping by SIM group timing. Although the causes of retention time instability have not yet been thoroughly examined, signal clipping can be avoided in the future by better selection of the ions for monitoring and the timing of ion group changes. One advantage of monitoring NMHC with MS was that nearly all compounds of interest have a m/z 41 fragment. In future

measurements intensives, the ion groups were altered to all contain this m/z ratio. While not always the most abundant fragment, this fragment yielded a large enough signal to meet the accuracy, reproducibility, and sensitivity requirements of this system. This approach effectively eliminated the problem of signal clipping observed in this intercomparison.

It was further observed that the calibration routine could be further optimized. As this was the first field test for this instrument, the necessary frequency of calibrations and zero runs was still under development. Observations of the stability of the detector response factor indicated that continuous calibration within the ambient range would facilitate more accurate measurements. A larger dynamic calibration range was achieved with a larger standard mass flow controller in the zero air and calibration gas system. Extending the dynamic calibration range to above 200 pptv for most compounds was easily achieved without consuming excessive amounts of standard gas. Based on the experience of this campaign, alternating zero air and calibration runs once an hour would provide sufficient data for accurate data processing. A related issue worth investigating was the relatively high background signal for the alkenes, which could be a factor in the higher limits of detection for these compounds.

Another area for improvement was the trapping efficiency for the low-boiling hydrocarbons and the detection limit for the butene isomers. Supporting the observations in Sect. 2.8.2, propane and ethyne showed evidence of breakthrough, and ethane and ethene were absent from the FOTOS chromatograms. This was most likely due to either insufficient trapping surface area, dwell time in the trap, or temperature. There exist various options for increasing the trapping surface area, for example using more glass wool, or micrometer-sized glass beads. Sample dwell time could be optimized by adjusting sample flow rates and pressure. In order to achieve lower trapping temperatures, an ozone filter needs to be installed and tested (see Sect. 2.8.2), as well as increased trap housing insulation and better heating of the cold air between the trap and mass flow controller. As for increasing the detection limit of the butene isomers, a larger sample size and better handling of zero runs should be considered. However, increasing the sample size could have other adverse effects on the total cycle, and should be considered carefully.

Finally, the large signal spikes measured by FOTOS but not by MOHp (see Sect. 3.3) should be addressed. The smooth exponential decay of these peaks suggested a concentration and re-emission from within the instrument or sampling line. As FOTOS sampled downstream of the MOHp GC from the same line, contamination from the sample line seemed unlikely. A more likely possibility was the water trap from FOTOS. Difficulties in the regulation of the water trap temperature at the beginning of this campaign led to a partial abandonment of this trap. Low ambient water levels allowed operation of FOTOS during this time without effective water trapping. The trap temperature fluctuated quite broadly and could have given rise to these large peaks. Due to time constraints, this issue could not be directly addressed, but has not been observed since.

3.7 Conclusion

During a two-week intercomparison, 13 NMHC were measured by FOTOS and the GC-FID of the German Weather Service monitoring station at MOHp. Conditions sampled included a significant pollution event from Munich, sampling from remote southern Germany and western Austria, and periods of more local influence, which provided a wide range of conditions for comparison. During the measurement intensive, both instruments ran at their respective maximum sampling frequency, 6 minutes for FOTOS and 70 minutes for the MOHp GC-FID. Multiple m/z ratios were monitored for most compounds and showed significant agreement. However, larger background and interference at some m/z ratios usually indicated one m/z that was preferable for quantitation. The signals for iso-pentane and 1,3-butadiene showed clipping due to poorly selected timing of the MS SIM group changes. These bad data points were then easily filtered by the retention time of the peak, and only those points were retained that clearly fell within the respective SIM group. Data points from the two data sets with overlapping sample times were compared within the GAW DQO outlined in Rappenglück et al. (2006). Agreement for the C_4 and higher alkanes was exceptional, where over 80% of the butane isomer data points, and 100% of the pentane isomer data points after filtering satisfied the DQO. High agreement was also observed for 1,3-butadiene (100%) and propyne (96%), with lower but satisfactory agreement for the higher concentration alkenes: propene (63%) and 1- and iso-butene (79% and 61%). Propane and ethyne were determined to not be quantitatively trapped by FOTOS, and trans- and cis-2-butene were mostly below their respective detection limits for the duration of the campaign. The higher time resolution of the FOTOS instrument yielded a more feature-rich data set than the traditional GC-FID, which indicated that the higher resolution measurements produces not only more data, but also more information. Although several deficiencies of the FOTOS instrument were observed, many were easily remedied, and the performance of this new instrument was extremely satisfactory. This intercomparison demonstrated that sensitive, accurate, fast measurement of NMHC can be realized with the new FOTOS instrument under field conditions.

Chapter 4

Measurements of Anthropogenic Hydrocarbons in the Boreal Forest

4.1 The Boreal Forest

The extensive boreal forest has a significant impact on the chemistry and physics of Earth's atmosphere. A major feature of the northern latitudes (50 to 65 °N), the boreal forest ecosystem covers 15×10^6 square kilometers, a significant portion of the Earth's total land area (8%) and more than a quarter of all forests (27%) (FAO, 2010). The boreal forest contains 10% of the total carbon in the terrestrial ecosystem and has no parallel in the Southern Hemisphere due to the absence of landmass in the corresponding southern latitudes.

The vegetation of the boreal forest consists of mainly wind pollinated pine and spruce trees with low biodiversity in comparison to other forested areas such as tropical forests. These coniferous trees are known to emit significant quantities of reactive organic trace gases (e.g. monoterpenes) to the atmosphere as a function of temperature and to a lesser extent light (Rinne et al., 2009, and references therein). Rapid atmospheric oxidation of these biogenic trace gases, followed by gas to particle conversion, has been shown to sustain particle concentrations of 1000–2000 particles/cm³ in the climatically relevant size range of 40–100 nm (Tunved et al., 2006; Kulmala et al., 2004). Previous studies from boreal forest sites have indicated that 12–50% of aerosol mass and 50% of cloud condensation nuclei (CCN) originates from forest sources (Tunved et al., 2008; Sihto et al., 2010) and that particle formation over the Finnish boreal forest causes a local radiative perturbation of between -5 and -14 Wm^{-2} (global mean -0.03 to -1.1 Wm^{-2}) (Kurten et al., 2003). It has been suggested that these cooling effects can offset the snow-vegetation albedo effect of the forest (Spracklen et al., 2008).

In the future, the Earth is predicted to warm, and boreal regions more than any other: 2 – 10 °C by 2100 (IPCC, 2007). In order to predict the future impact of the boreal forest on the atmosphere, and thereby to improve assessment of potential climatic feedbacks (e.g. Carslaw et al., 2010), extensive, high quality, and comprehensive data sets must be generated for detailed analysis. In this regard summertime assessments are particularly useful.

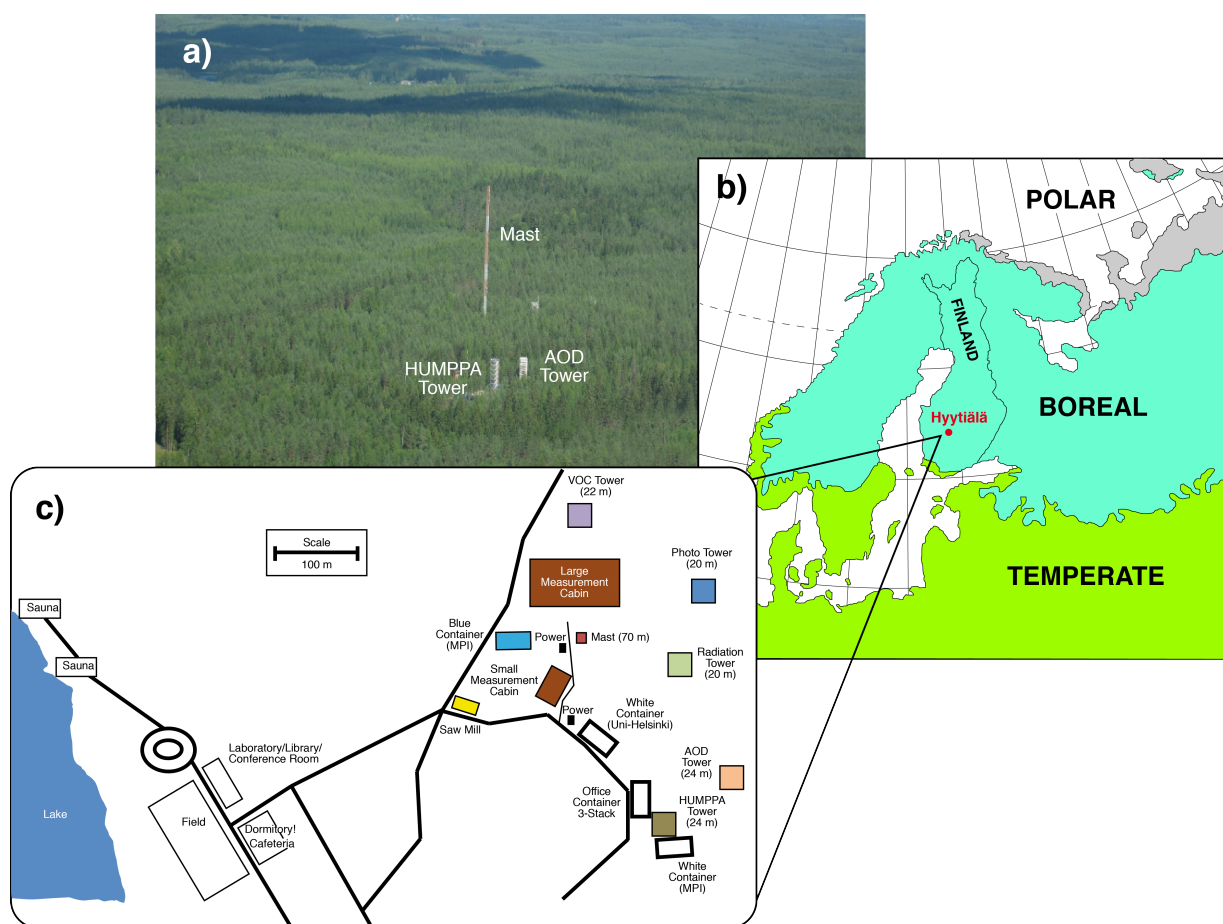


Figure 4.1: This figure is a composite of a) an aerial view taken during the campaign of the Hyytiälä site looking northwest, b) a map of the bioclimatically defined boreal region of Europe, and c) a local map of the site showing locations of instruments and towers.

This chapter presents and discusses results of the FOTOS instrument during the 2010 boreal forest field measurement intensive Hyytiälä United Measurement of Photochemistry and Particles in Air - Comprehensive Organic Particle and Environmental Chemistry (HUMPPA-COPEC 2010). The measurements took place from July 12th to August 12th, 2010, at the boreal forest field station SMEAR II near Hyytiälä, Finland ($61^{\circ} 51' N$, $24^{\circ} 17' E$; elevation 181m asl, see Fig. 4.1). To date, most intensive measurement campaigns performed at this station have been made in spring or autumn, to coincide with periods of most frequent particle nucleation events. In contrast, HUMPPA-COPEC 2010 was focused on characterizing summertime conditions when emission fluxes of volatile organic compounds (VOC), OH initiated photochemistry, and particle growth rates reach their seasonal maximum. In the course of the campaign, an international consortium quantified a comprehensive suite of gas and aerosol phase species. This was the largest campaign staged in the 100 year history of the Hyytiälä station. Further details of measurements, goals, and major events/observations of the HUMPPA-COPEC 2010 campaign have been described elsewhere (Williams et al., 2011).

The relatively sparse human population within the boreal forest region results in lower anthropogenic emissions than at the northern temperate latitudes. However, emissions from

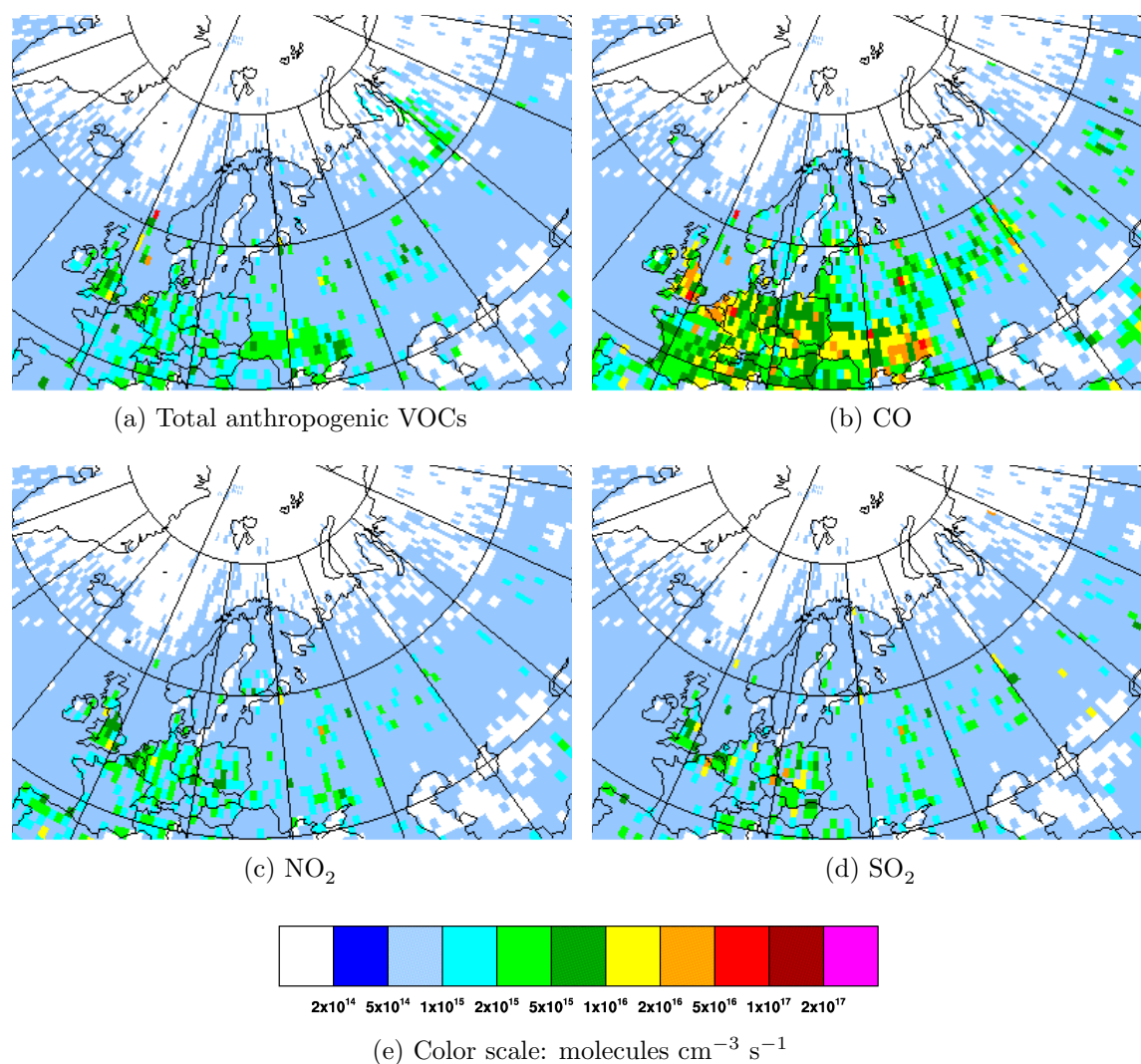


Figure 4.2: Emission source maps from the EDGAR Fast Track 2000 inventory for: (a) total anthropogenic VOCs, (b) CO, (c) NO₂ (as proxy for NO_x), and (d) SO₂. The color scale for all maps is given in (e).

the temperate region do accumulate in the arctic region, most noticeably in the springtime appearance of the “arctic haze” (Barrie, 1986). Due to zonal asymmetries of the polar front, northern Eurasia emissions are believed to be the major source of the pollutants contributing to the arctic haze (Law and Stohl, 2007). Therefore, even in the remote boreal forest where biogenic emissions are dominant, the measurement of anthropogenic NMHCs would yield insight into important regional atmospheric phenomenon.

The significance of anthropogenic emissions in the boreal forest region can be seen in a few of the emission source maps from the Emissions Database for Global Atmospheric Research (EDGAR) version 3.2 Fast Track 2000 inventory (Olivier et al., 2005) presented in Fig. 4.2. Large emission sources in this region and several of the smaller urban areas located closer the site are presented in Tab. 4.1. To compliment the suite of measurements planned for this campaign, it was decided to use FOTOS for the measurement of light NMHCs. This provided valuable additional information about anthropogenic influences and insights into air mass age during HUMPPA-COPEC 2010.

Urban Center	Latitude	Longitude	Population	Distance ^b [km]
Oslo, Norway	59° 57' N	10° 45' E	1.4 mil. ^a	760
Stockholm, Sweden	59° 21' N	18° 04' E	2.1 mil. ^a	440
St. Petersburg, Russia	59° 57' N	30° 19' E	4.8 mil.	390
Helsinki, Finland	60° 10' N	24° 56' E	1.3 mil. ^a	180
Tampere, Finland	61° 30' N	23° 46' E	340,000 ^a	46
Jämsä, Finland	61° 52' N	25° 11' E	22,706	46
Ruovesi, Finland	61° 59' N	24° 04' E	5,036	20
Orivesi, Finland	61° 41' N	24° 22' E	9,618	19
Juupajoki, Finland	61° 48' N	24° 22' E	2,096	6.5

^a Metropolitan area population

^b Distance from city center to measurement site

Table 4.1: Anthropogenic emission sources near SMEAR II station

4.2 Sampling Setup

During the HUMPPA campaign, FOTOS was located in a custom converted container, Blue Container (MPI), and sampled from a line attached to the main sampling mast of the SMEAR II station, as labeled in Fig. 4.1. The sampling line consisted of 30 meters of 1/2 inch (12.7 mm OD, 9.5 mm ID) PFA tubing, wrapped in opaque insulation and heated to 40 °C. The flow through the main line was 12–15 L/min* with 3 L/min diverted to FOTOS during sampling cycles. The inlet was mounted at 16.8 meters above the base of the mast and 1–2 meters above the canopy, level with one of the tiers of SMEAR instruments (see Fig. 4.3a). The sample inlet was filtered by a PTFE filter (Sartorius, 5 µm pore) and protected from rain by a plastic funnel (identical to that seen in Fig. 4.3b). The filters were replaced twice during the campaign, on July 20th and August 2nd. Although no significant reduction in flow was measured before and after filter changes (less than 10%), visible particulate accumulation was observed.

For this measurement intensive, FOTOS was configured as described previously (see Chap. 2) with the following trap configuration: a wrapped, directly-heated enrichment trap (stainless steel, 1/16 inch (1.6 mm) OD, 1.0 mm ID) with 4 cm of loosely packed glass wool in the trapping region; a bare, directly-heated cryofocusing trap (stainless steel, 1/16 inch (1.6 mm) OD, 0.5 mm ID) trapping on 5 cm of a deactivated silica capillary (0.35 mm OD, 0.25 mm ID), which ran unbroken from the Traps MuPo to the MACH GC column; and a directly-heated, unpacked water trap (stainless steel, 1/8 inch (3.2 mm) OD, 1.6 mm ID) (see Sect. 2.4). Trapping and purging temperatures were –40 °C and +70 °C, respectively, for the water trap and –135 °C and +100 °C, respectively, for the enrichment and cryofocusing traps. Trapping efficiency tests similar to those described in Sect. 2.8.2 indicated quantitative trapping for the C₄ and C₅ alkanes with this setup. Before this campaign, the GC cooling fan

*This corresponded to a residence time of 8.5 to 10.5 seconds. As the sampling was an integration of about 1.5 minutes, the dwell time was considered to be insignificant, and sample times reported are simply the midpoint of the sampling period.



Figure 4.3: Sampling inlets during the HUMPPA campaign: (a) showing inlet height for FOTOS with respect to canopy (the inlet was level with the long horizontal bar shown) and (b) showing the methane inlet with filter and rain shield from below.

was updated to a high-power tubeaxial fan, as mentioned in Sect. 2.5, which in part enabled the 5.5 minute cycle time realized for the whole of the sampling intensive.

Zero runs were performed once every two hours and one of seven calibration levels were performed once in the hour between zero runs. Zero runs and calibrations were performed as described in Sect. 2.6, with a larger calibration range for this campaign (4–225 pptv for n-pentane) than the intercomparison at MOHp (4–10 pptv for n-pentane), eliminating the need for off-line calibrations (see Sect. 3.2). This was achieved by coupling a 100 sccm mass flow controller (MFC) to the existing 5 sccm MFC (both from Bronkhorst). For construction reasons, the solenoid valve, StandIn, after the original MFC (see Sect. 2.6) was removed. It was later decided to use only one calibration level for the actual conversion from signal to mixing ratios, and the others as accuracy controls (see Sect. 2.8.4). The data set was subjected to the quality control measures outlined in Sect. 2.7.

To compliment the non-methane hydrocarbon measurements from FOTOS, a GC-FID (Thermo Electron Corporation, Model 55C Hydrocarbon Analyzer) was operated during the campaign for the measurement of methane. This instrument measured from a height of 4 meters above the base of the SMEAR mast through 20 meters of 1/4 inch tubing (PFA, 6.4 mm OD, 4.4 mm ID) at a flow of 1.1 L/min. The sample air was filtered and the sample line heated and insulated (see Fig. 4.3b) as described for the FOTOS sampling line above. Twice daily calibrations were made with a methane standard (Air Liquide) calibrated to have a concentration of 2.0065 ± 0.0050 ppmv by a set of seven NOAA standards on the NOAA 2004 scale (Dlugokencky, 2005).

4.3 Data Coverage

For the majority of the campaign, FOTOS functioned well, providing good data coverage far exceeding typical sampling frequency that would have been achieved by flask sampling.

However, some periods of data loss did occur and were due to both instrument malfunction and environmental difficulties. Large storms resulted in power outages on July 14th and 22nd, as well as a major outage from the evening of August 8th until midday on the 9th. Due to user error, the V25 logs for the period of 03:30 until 11:50 UTC on the 17th of July were lost. The run types (i.e. ambient or calibration runs) of chromatograms measured during this period were determined from the run sequence and peak areas. Regardless of the loss of log data, these data were judged to be reliable, only with a slightly larger uncertainty (e.g. collected sample size had to be estimated, but only introducing an error estimated to be less than 0.2%). The filament of the MS ion source burned out on July 19th and the system was switched to the reserve filament. This resulted, as expected, in a step change of all calibration factors. Finally, in the period from the evening of the 24th until midday on the 29th of July (roughly the gray area of Fig. 4.4), the heater module for the water trap failed and was removed, repaired, and reinstalled (see Sect. A.5). The measurements collected during this time are therefore of lower quality. While this data displays some interesting information, concrete conclusions from this period should be reached only with caution. In total, from the morning of the 12th of July until the evening of the 8th of August, over 5200 chromatograms were collected, covering a range of more than ten resolved hydrocarbons. For n-pentane, this resulted in over 4000 ambient measurements, for a total data coverage of 67.6%, with 91.4% coverage from the installation of the repaired water trap heater until the major power outage on August 8th.

4.4 Results Characterization

The duration of the HUMPPA-COPEC 2010 campaign can be characterized by generally low saturated hydrocarbon levels (n-pentane ranged from 4.5–390.5 pptv, with an average value of 41.5 pptv and a median of 32.6 pptv), with frequent peaks ranging from 1 to 12 hours wide. The trends seen in n-pentane (Fig. 4.4) were typical of those seen in the other saturated hydrocarbons. Three periods of biomass-burning plumes from Russia were confirmed by measurements of acetonitrile (Williams et al., 2011), a specific tracer for biomass burning (Lobert et al., 1990). These periods were on July 26th and 29th, and August 7th–8th. Unfortunately, the first two plumes correlated with the period of water trap heater failure (see Sect. 4.3). The first half of the campaign was characterized by low variability, with several well-formed, well-resolved peaks observed on a low background. The second half of the campaign was much more variable, with frequent, small, short peaks on top of larger features. There were several periods of low alkane levels throughout the campaign, most notably from the morning of the 23rd of July until or after the water trap failed on the evening of the 24th. Low alkane levels were also seen from midday on the 16th until evening on the 17th of July. Other periods of low NMHCs were also seen (e.g. on July 19th and midday on the 3rd and 6th of August), but of much shorter duration.

An additional relevant value to consider is the ratio of n- to iso-pentane. This ratio is a function of the emission source and the aging or mixing of the air since emission. The

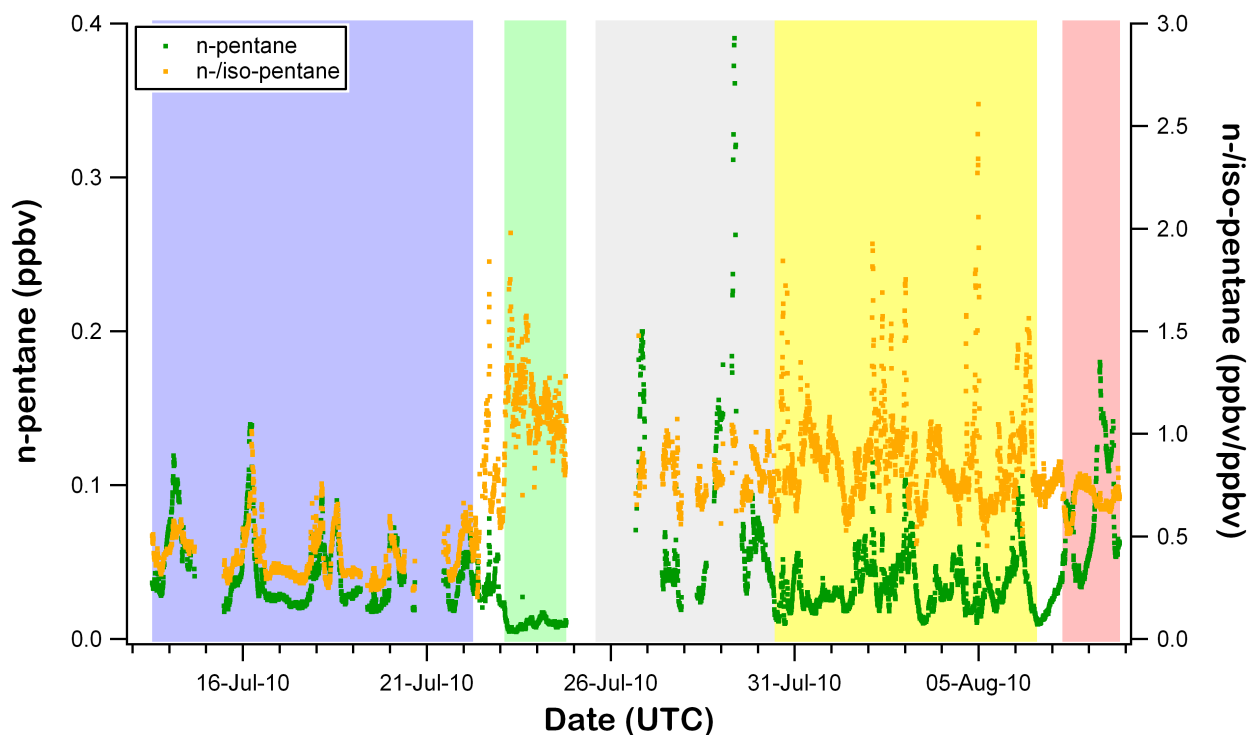


Figure 4.4: Time series of n-pentane for the duration of HUMPPA-COPEC 2010 with the ratio of n- to iso-pentane. Colored regions indicate periods of interest as defined in Sect. 4.4.

reaction rates (at 298 K) of n- and iso-pentane with OH are comparable (3.80 and 3.6×10^{-12} $\text{cm}^3 \text{ molecule}^{-1} \text{ s}^{-1}$, respectively, Atkinson, 2003) but the reaction rates with NO_3 differ by a factor of 2 (0.87 and 1.62×10^{-16} $\text{cm}^3 \text{ molecule}^{-1} \text{ s}^{-1}$, respectively, Atkinson, 1997). The two main sources for the pentane isomers (traffic and biomass burning) have significantly different emission ratios: 0.22 – 0.76 for traffic (Penkett et al., 2007; Warneke et al., 2007; Baker et al., 2008; Bon et al., 2011) and 1.72 – 2.31 for extratropical forest burning (Andreae and Merlet, 2001). However, burning of savannas and grasslands (emission ratio: 0.45) and agricultural residues (1.39) (Andreae and Merlet, 2001), would lower the overall observed emission ratio from a heterogeneous wildfire. Thus, only careful analysis of this ratio can provide insight into emission source and air mass aging.

As seen in Fig. 4.4, the pentane isomer ratio also showed many features, the most striking of which was the significant background shift from the first half to the second half of the campaign. This shift was initiated by a major cold front which crossed the site on the morning of the 23rd, and the new air mass was almost exclusively from the remote north. These features in n-pentane and the ratio of pentane isomers led to the division of the campaign into four broad categories (with dates and regions highlighted in Fig. 4.4): low variability (July 13th to 22nd, blue region), low alkane mixing ratios (July 23rd and 24th, green region), high variability (July 30th to August 6th, yellow region), and biomass burning plumes (July 25th to 30th, gray region, and August 7th and 8th, red region). These periods and corresponding properties of the pentane mixing ratio and isomer ratio have been summarized in Tab. 4.2.

	Date & Time		n-Pentane Mixing Ratio [ppbv]				Pentane Isomer Ratio Average	$\sigma[\delta(\text{n-Pentane})]^b$
	Begin [UTC]	End [UTC]	Average	Median	Maximum	Minimum		
Low Variability	13.07. 12:51	22.07. 06:22	0.0418	0.0341	0.1394	0.0175	0.399	0.00228
Low Alkanes	23.07. 02:36	24.07. 19:08	0.0098	0.0095	0.0272	0.0046	1.141	0.00157
High Variability	30.07. 11:08	06.08. 14:19	0.0342	0.0301	0.1148	0.0099	0.879	0.00279
Biomass Burning 1	25.07. 14:10 ^a	30.07. 11:03	0.0745	0.0533	0.3905	0.0163	0.796	0.00737
Biomass Burning 2	07.08. 06:40	08.08. 20:15	0.0795	0.0668	0.1798	0.0336	0.681	0.00364
Entire Campaign	13.07. 12:51	08.08. 20:15	0.0415	0.0326	0.3905	0.0046	0.720	0.00332

^a The beginning of the first biomass burning period was determined solely from measurements of acetonitrile.

^b The standard deviation of the first derivative of the mixing ratio of n-pentane, in ppbv per cycle time (5.5 minutes). The standard deviation of a value ($\sigma[x]$) represents only the sum magnitude of fluctuations from the average, but not the rate of fluctuation. The first derivative of a value ($\delta(x)$) provides information on the rate of change of a value. Thus standard deviation of the first derivative ($\sigma[\delta(x)]$) would indicate the sum magnitude of fluctuations in the rate of change of a value. Thus a signal with low-frequency fluctuations would have a low $\sigma[\delta(x)]$, and a signal with high-frequency fluctuations would have a high $\sigma[\delta(x)]$. This temporal variability has been abbreviated in the text as simply “variability”.

Table 4.2: Characteristic grouping and associated values for the HUMPPA-COPEC 2010 campaign.

4.5 Specific Periods of Interest

Within the broad characterizations of the previous section, several specific time periods of the alkane traces deserved closer inspection. These included contrasting periods of urban pollution, periods of low alkane mixing ratios, and the three biomass burning events mentioned previously. This further comparison revealed differences in features which appeared similar, but contained enlightening differences. This more detailed inspection revealed the variety of anthropogenic influence seen at this remote boreal forest site, which any lone tracer might not have revealed.

4.5.1 Urban Pollution

The first periods of urban pollution were the first two peaks seen in the NMHC data, namely on the 14th and 16th of July, shown in Fig. 4.5. These two peaks were clearly formed, 18–24 hours wide, with relatively low baseline on either side. The back trajectories (Draxler and Rolph, 2011) for these peaks, shown in Fig. 4.6, indicated that both peaks had significant influence from the European mainland. There were however, subtle differences: the air mass from the first peak had passed recently over St. Petersburg, with a cohesive ensemble of back trajectories; the trajectory ensemble of the second peak indicated much more mixing and was more restricted to lower altitudes. In many respects, these two peaks were representative of the other periods of urban plumes seen in the low variability period of the campaign. The peaks in alkane concentration were broad (base width of 6–24 hours) with periods of flat, baseline signal on either side. The pentane isomer ratio tended to peak with the pentane concentration, and returned to a lower background level between pollution events.

In contrast to the broad peaks of the low variability period, peaks in the alkane mixing ratios of the high variability period were much narrower. This was exemplified by a series of narrow peaks on the 2nd and 3rd of August. Although underlying broader features similar to earlier peaks were discernible, there was much more fine detail to these features. Many of these well defined peaks were only a few hours wide. The back trajectories for various times within this region (Fig. 4.8) showed little qualitative difference. These features illustrated the wealth of information contained within this data set, as well as the advantage of high time-resolution measurements. With traditional GC measurements, which integrate over longer sampling periods, many of these features would have been poorly represented at best, and possibly missed altogether. This was demonstrated by the red line and crosses in Fig. 4.7, which shows the interpolation of a single measurement point per hour. Flask sampling, typically performed no faster than every four hours (Williams et al., 2007a), would have completely missed these structures.

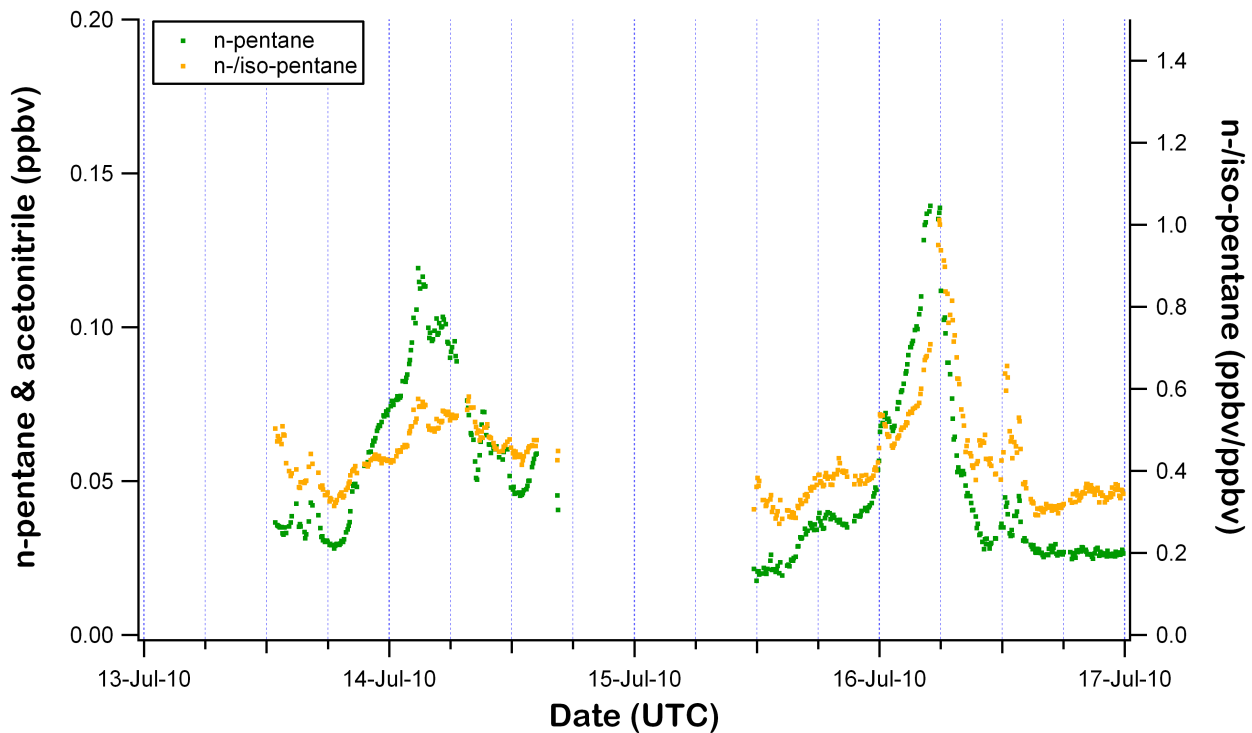


Figure 4.5: Detail of first two urban pollution plumes on the 14th and 16th of July, showing n-pentane with the ratio of n- to iso-pentane.

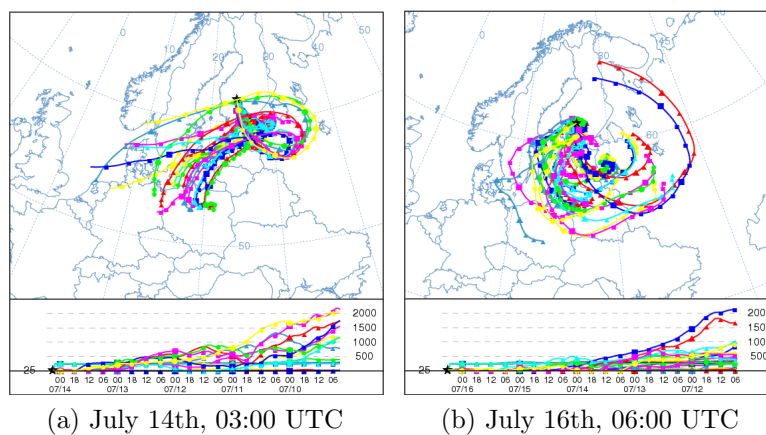


Figure 4.6: Back trajectories for the urban pollution plumes on July 14th and 16th

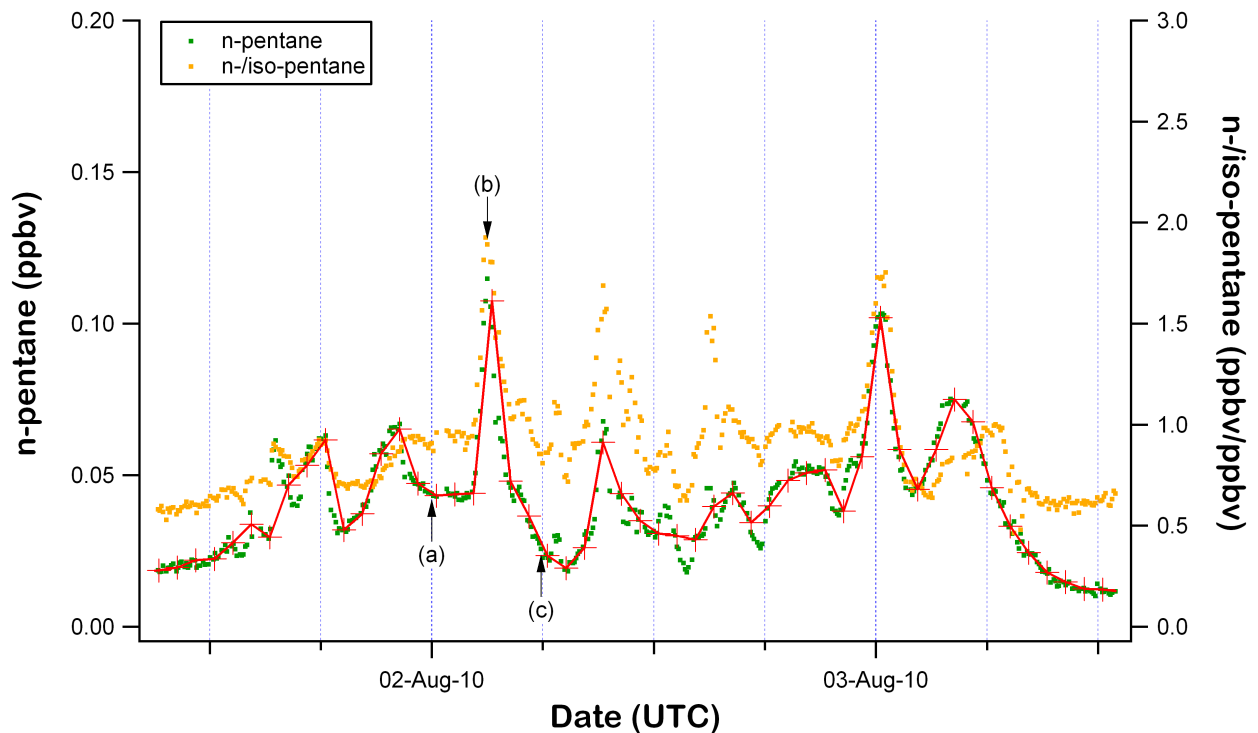


Figure 4.7: Detail of narrow pollution peaks on August 2nd and 3rd, showing n-pentane with the ratio of n- to iso-pentane. The red line is the interpolation of hourly samples (the red crosses) as a demonstration of the features that would be captured with a traditional GC. The lettered arrows indicate the timing of the back trajectories shown in Fig. 4.8.

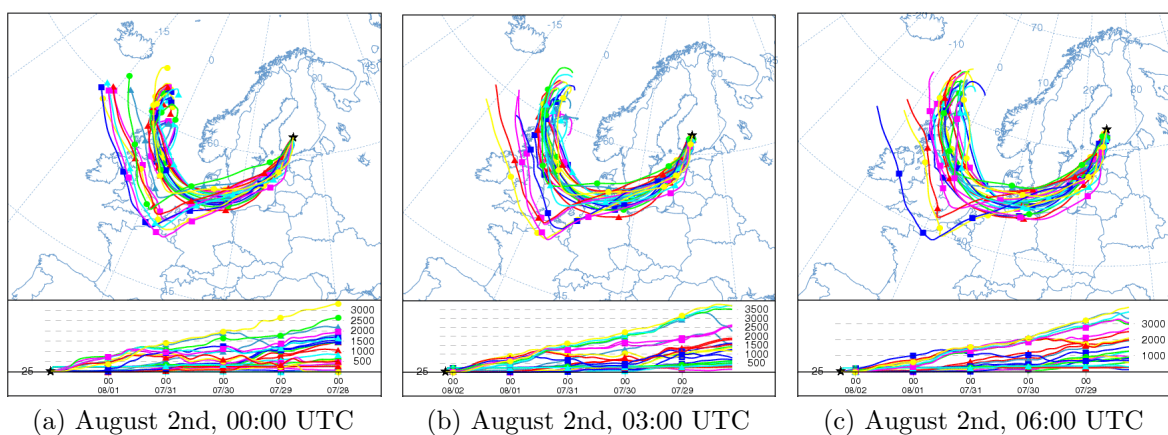


Figure 4.8: Back trajectories for narrow pollution peaks on August 2nd and 3rd

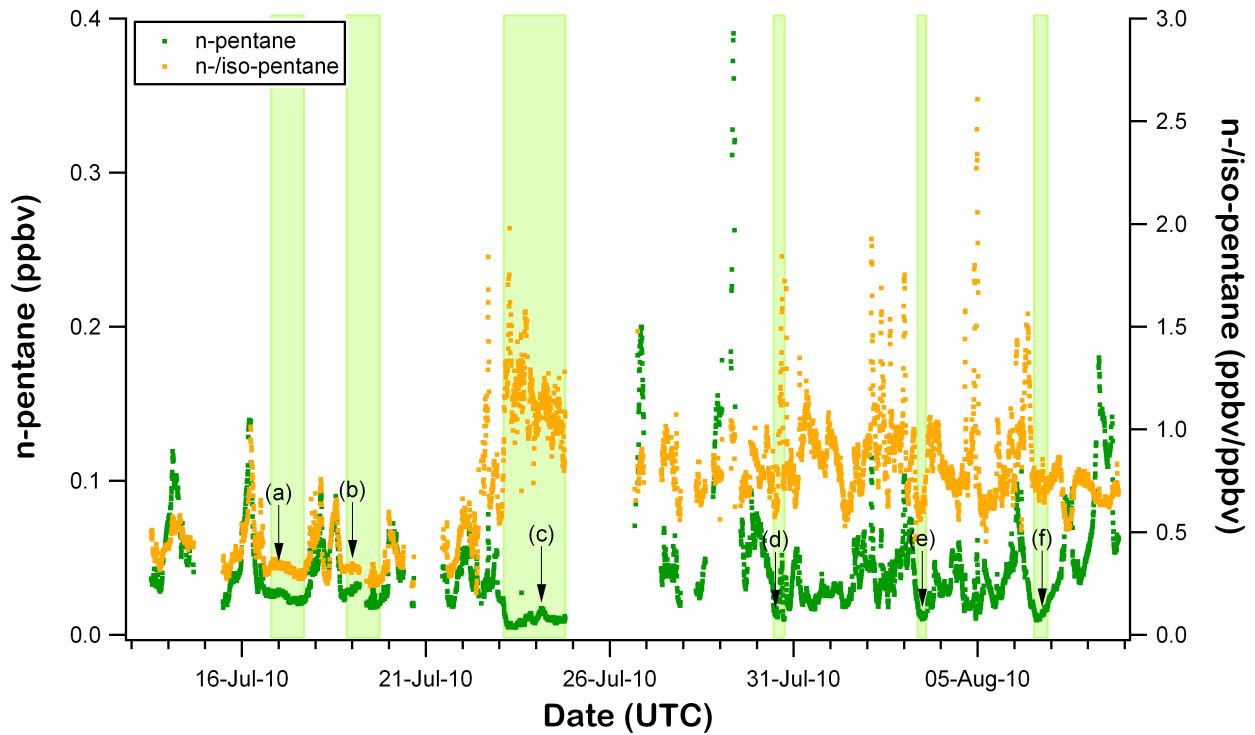


Figure 4.9: Time series of n-pentane for the duration of HUMPPA-COPEC 2010 with the ratio of n- to iso-pentane. Highlighted regions indicate periods of low alkane levels. The lettered arrows indicate the timing of the back trajectories shown in Fig. 4.10.

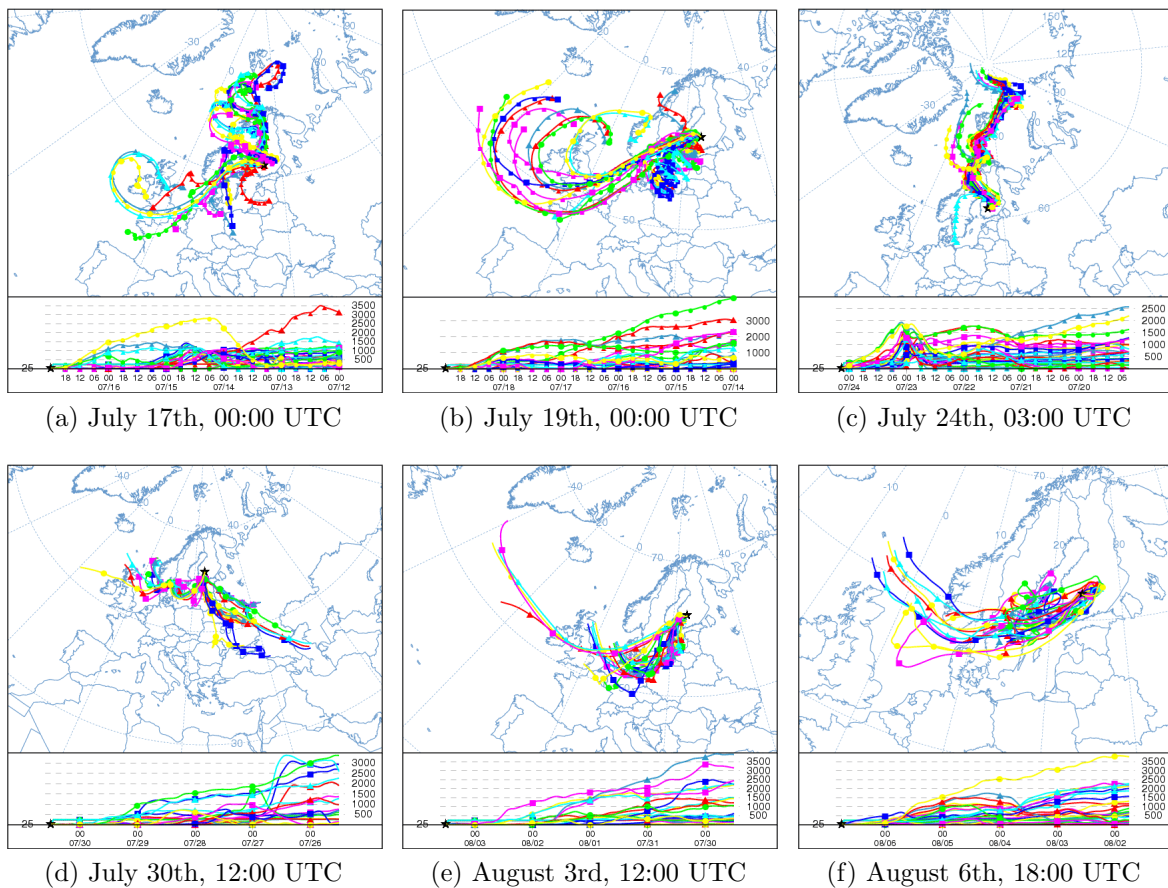


Figure 4.10: Back trajectories for periods of low alkanes

4.5.2 Low Alkane Levels

Among the periods of low alkane levels during the whole of this campaign, six periods, highlighted in Fig. 4.9, were analyzed in further detail. Low alkane levels did not always correspond to low levels in all VOCs, and the identification of these periods can be useful in characterizing conditions representative of the boreal forest. Periods of low alkanes included many times when the wind was coming from the north. The most prominent period was the extremely low pentane mixing ratios and high pentane isomer ratio observed from the morning of the 23rd until the evening of the 24th of July (Fig. 4.9 points c). Similar periods of low alkane mixing ratios and high isomer ratios, but of much shorter duration, were seen on July 30th, August 3rd, and August 6th (Fig. 4.9 points d, e, and f). Longer periods of low alkane levels, but with a low isomer ratio, were seen on July 16th and 17th and again on July 18th and 19th (Fig. 4.9 points a and b).

The back trajectories for these periods revealed a variety of sources for these air masses. On July 17th, the air had come in a large part from the north, but with significant contribution from northern European mainland and Great Britain, although partially from higher altitudes. Several back trajectories for the 19th also descended recently from higher altitudes. On this day, northern Atlantic air was mixing with air which had been contained within the Baltic Sea region for several days. July 19th was a Monday, and this air would represent local weekend emissions and well-mixed distant emissions.

Starting early on the 23rd, a cold front moved over the measurement site, and persisted until the evening of the 24th. Temperatures fell to the lowest of the campaign, with highs for these two days approaching 18 °C and nightly lows below 12 °C, compared to a high of 26 °C and a low of 16 °C the day and night before. The high winds (2.38–3.85 m/s) associated with the cold front passing persisted most of the 23rd, then finally died down in the evening. Winds stayed low through the first half of the 24th (1.29–2.22 m/s), then increased towards the evening (2.01–2.63 m/s) as rain began to fall. Interestingly, during this period of fairly homogeneous northern air, there were still indications of anthropogenic input, suggested by the small peak labeled as point c in Fig. 4.9. In a separate event, a single outlying high point in n-butane (27.2 pptv) with a corresponding low point in the pentane isomer ratio (0.700) was observed at 14:30 UTC on the 23rd. This point was well outside the surrounding measurements (three hour averages excluding this point were 8.0 pptv of n-pentane and an isomer ratio of 1.255), and could not be linked to any system malfunction or irregularity. This point could be explained by a small, transient, local source with a low pentane isomer emission ratio mixing with the low-background, high-ratio air mass. The emission of a car passing upwind of the site would fit this description.

The remaining three short periods of low alkanes appeared similar, but with distinctly different back trajectories. July 30th was the end of a major biomass burning plume from Russia. At this trough in n-pentane, air from eastern Europe was mixing with air which again had minimal land contact while passing over the North and Baltic Seas. The air mass present at the site on midday August 3rd, a Tuesday, was heavily influenced by northern continental

Europe, but the past five days consisted mostly of weekend emissions. The air mass measured on the evening of August 6th was mostly constrained to the sparsely populated Scandinavian region for the five days previous.

It should be noted that among the many periods of low alkane levels observed in this campaign, only July 23rd and 24th represented truly polar air. This observation could provide some insight into why this period also experienced the only particle nucleation event of this measurement intensive.

4.5.3 Biomass Burning

The final periods of interest were the biomass burning plumes from the Russian wildfires. From mid-July to mid-August, wildfires burned 5.8–5.9 million hectares of forested and non-forested land, which caused damage estimated at 12 billion rubles (306 million Euros or 437 million USD). Wildfires in the peat bogs of Russia occur annually, however, the summer of 2010 was worse than normal, due in part to the most intense heat wave Russia had experienced for 130 years (GFMC, 2010). As data from FOTOS was sporadic during the first two plumes, only the plume from the end of the campaign was more closely analyzed. As seen in Fig. 4.11, two peaks in n-pentane and acetonitrile were seen in the last days of the campaign. That the peaks of these two compounds were not correlated indicated that even in the biomass burning events, other sources of anthropogenic pollution were affecting the site. The back trajectories also indicated possible influence from St. Petersburg (Fig. 4.12). The second n-pentane peak was most likely a combination of these two sources. The n-pentane mixing ratio began to rise in the early hours of August 8th peaking shortly after 06:00 UTC as acetonitrile began to rise, and then shortly after 15:00 UTC both signals peak together. The pentane isomer ratio fell during both events, reaching a minimum of 0.513 on the 7th and 0.619 on the 8th. In comparison, the maximum of the isomer ratio during the St. Petersburg pollution event on July 14th was 0.581. This would imply that either the pentane sources during these biomass burning plumes were still predominately from the major metropolitan area of St. Petersburg, or that the isomer ratio of pentanes from these fires after aging about five days within this plume matched this urban source. A large portion of these fires involved peat bogs, which have not been as well characterized, and these measurements may indicate the value of such a characterization. However, the superposition of burning and city plumes precluded more definitive statements regarding source characterization with this data.

4.6 Comparison with other Tracers

Within this campaign, it appeared that pentane mixing and isomer ratios were impacted both by anthropogenic vehicular emissions from nearby cities and from biomass burning advected from a region 600–700 km distant. As discussed in Sect. 1.2, the pentane isomers come predominately from traffic pollution, with the exception of biomass burning, which was extremely relevant for this campaign. The pentanes have short atmospheric lifetimes, on the order of three days, in comparison with other anthropogenic tracers measured at the site (e.g. CO at 1 month or SO₂ at 5 days). This difference allows the comparison of these

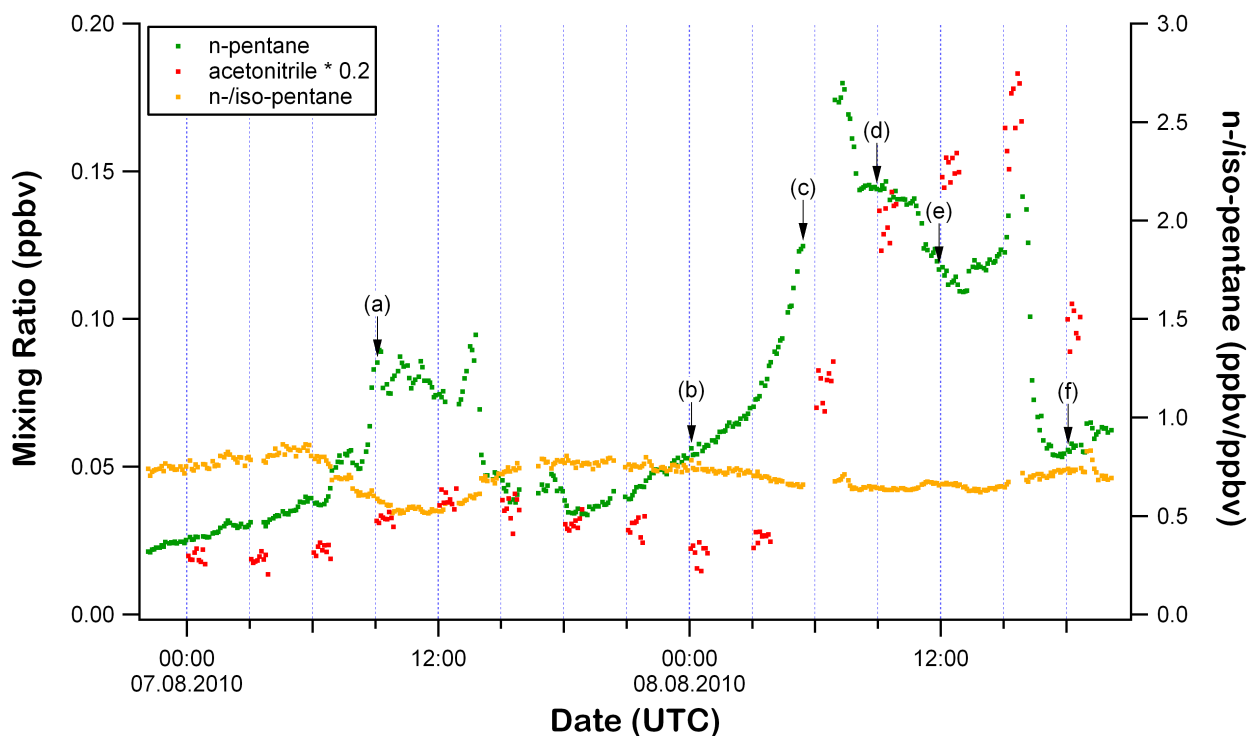


Figure 4.11: Detail of biomass burning plume on August 8th, showing n-pentane with the ratio of n- to iso-pentane. Acetonitrile was assumed from the measurement of m/z 42 with a SMEAR II PTR-MS at 16.8 meters above the base of the mast.

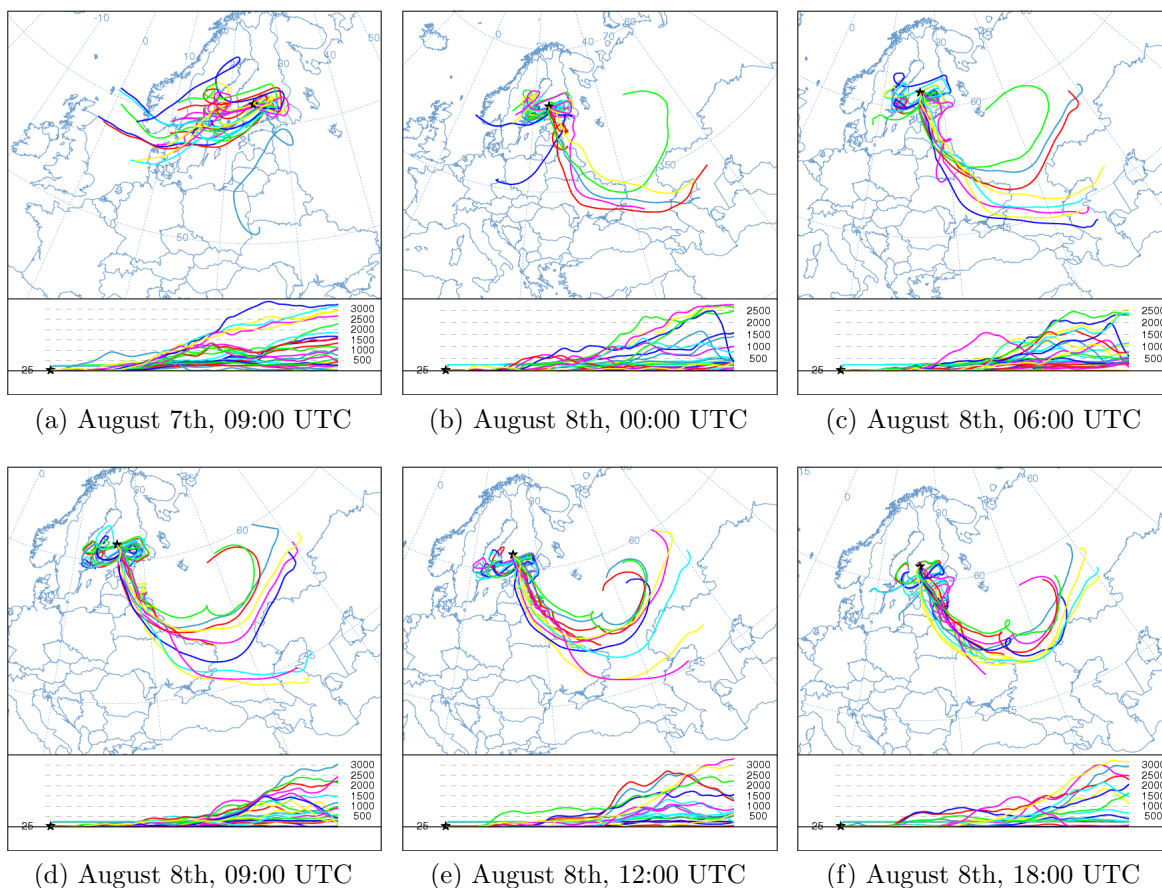


Figure 4.12: Back trajectories for biomass burning plume on August 7th and 8th.

anthropogenic source gases to reveal indications of the distance of pollution sources from the measurement site, provided emission ratios are known and constant. In this section, mixing ratios for n-pentane will be compared to the methane measurements mentioned in Sect. 4.2; CO, and NO_x measured atop the HUMPPA tower by the Horst Fischer group at the MPI for Chemistry; as well as SO₂ at 16.8 meters above the base of the SMEAR II mast and malonic acid measured at the base of the HUMPPA tower by the University of Helsinki.

4.6.1 Methane

The significant change in pentane isomer ratio was correlated to a change in methane mixing ratio as well. As seen in Fig. 4.13a, the lower band, representing the lower isomer ratios from beginning of campaign, contains the majority of the lower mixing ratio methane, and the upper band the majority of the higher methane seen. The average methane mixing ratios (and standard deviation) for the contrasting periods of low and high variability as defined in Sect. 4.4 were 1.751 (0.017) and 1.773 (0.018) ppmv, respectively. This provided independent confirmation of these two regimes via a separate instrument. The only other parameter found to segment the pentane isomer ratio as clearly as methane was time (Fig. 4.13b), which identified the lower band as early in the campaign, followed by the group at low mixing ratios, and finally the higher isomer ratios seen through the end of the campaign.

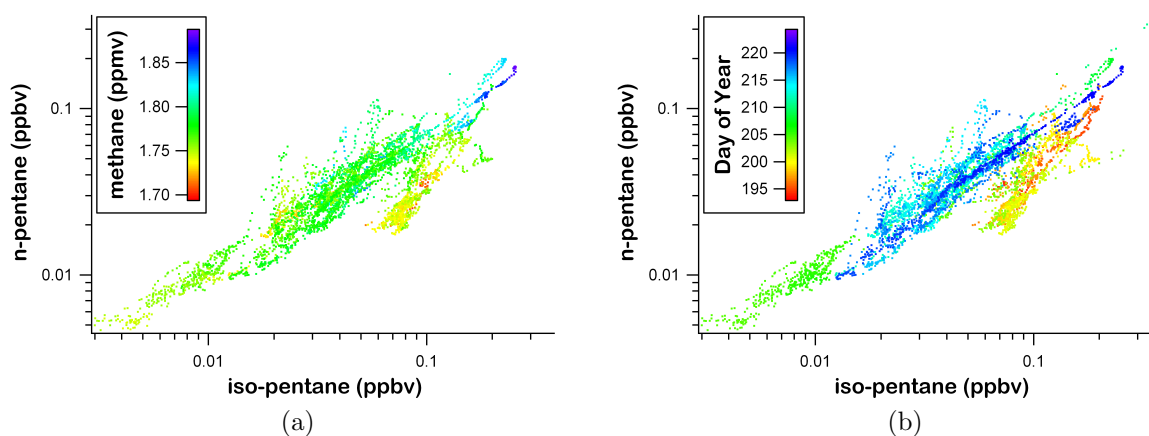


Figure 4.13: Correlation of the pentane isomers showing segregation of (a) methane values and (b) in time.

4.6.2 CO

Carbon monoxide (CO) is commonly used as a tracer of anthropogenic emissions. Unlike pentane, CO can be either emitted directly or formed through photochemistry. With a lifetime of about a month, CO provides a tracer for more distant anthropogenic influence. Analyzing the ratio of n-pentane to CO would therefore give an indication of the age of the pollution observed. The pentane will react more rapidly and the ratio should fall proportionally to oxidant concentration and time since emission (assuming a constant emission ratio). As seen in Fig. 4.14, the correlation between n-pentane and CO was quite good, but there were definite discrepancies, e.g. July 14th, 20th, and 31st, and August 6th. The histogram of this

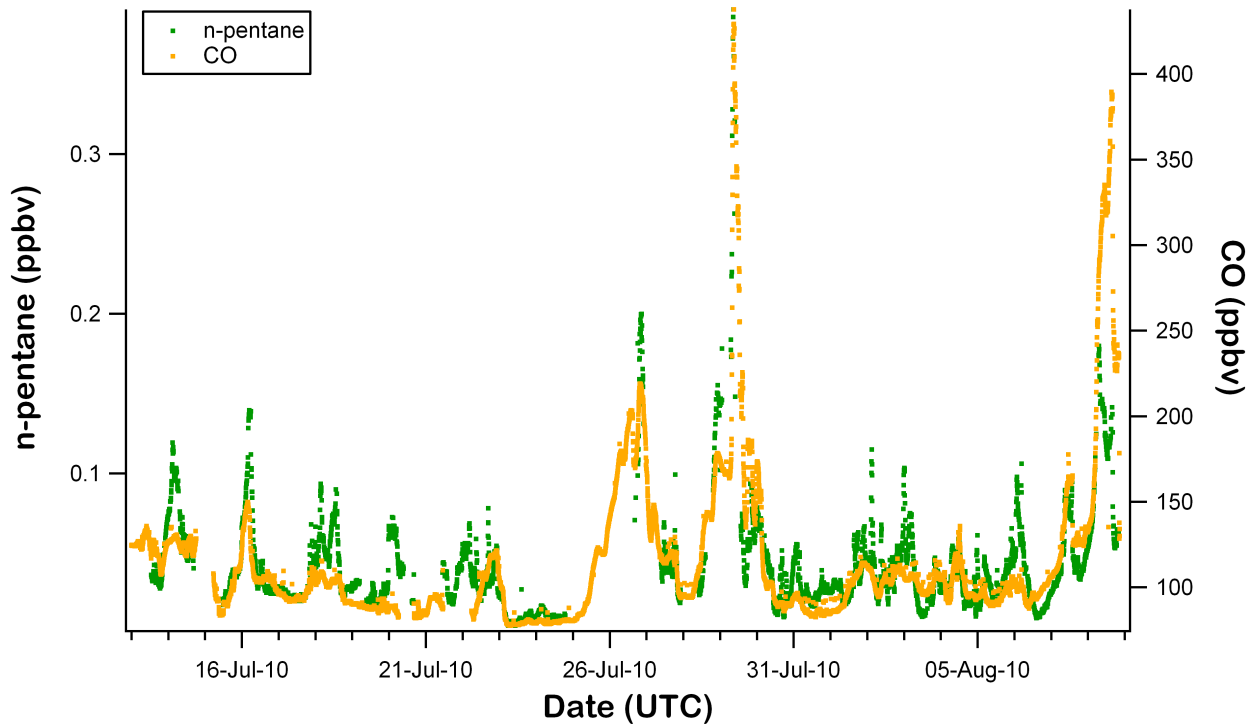


Figure 4.14: Time series of n-pentane for the duration of HUMPPA-COPEC 2010 with CO mixing ratios measured at the HUMPPA Tower.

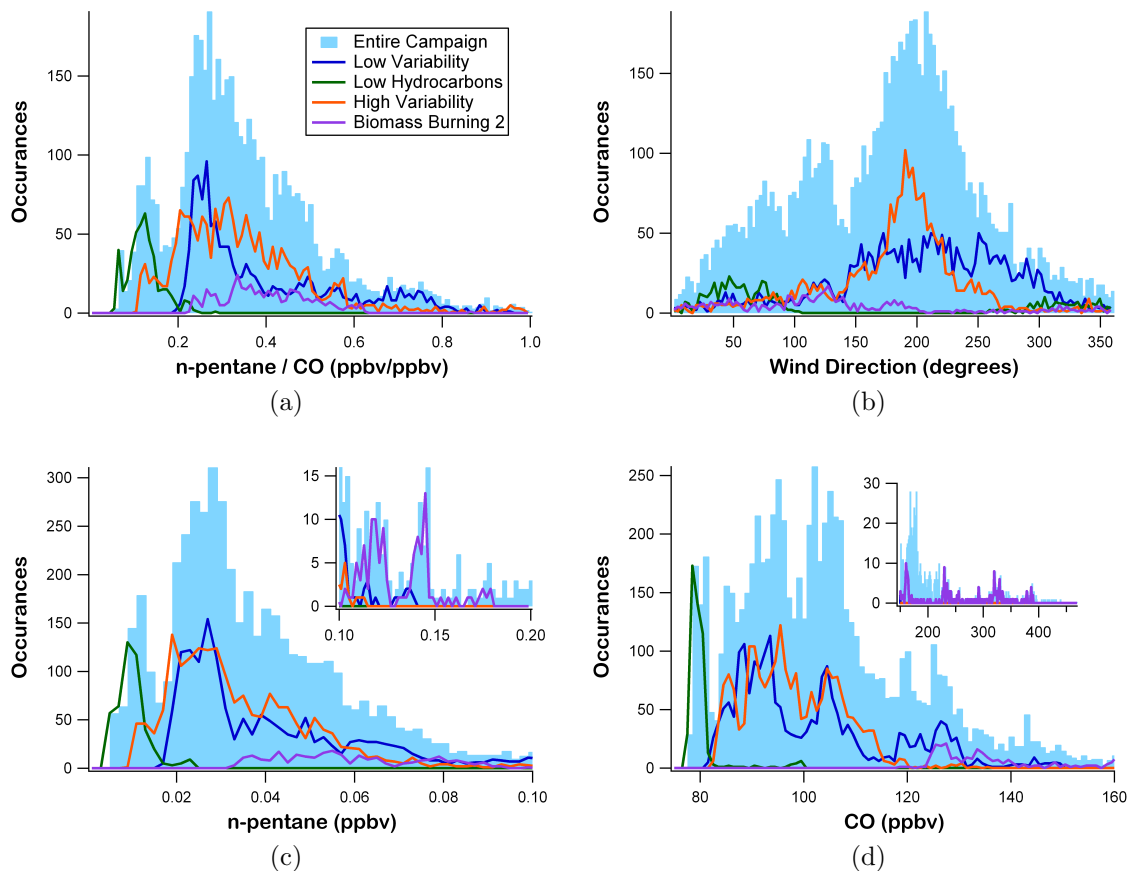


Figure 4.15: Histograms of (a) the n-pentane to CO ratio; (b) wind direction; and the mixing ratios of (c) n-pentane and (d) CO for the entire campaign and by the grouping defined in Sect. 4.4, excluding the first biomass burning period due to lack of pentane data.

ratio was tri-modal, as seen in Fig. 4.15, suggesting several distinct sources. Analysis based on the characteristic grouping of Sect. 4.4 revealed that the mode at lower ratios was almost entirely due to the period of low alkane mixing ratios. Furthermore, the distribution for the low variability period was more narrow than that of the high variability period, with the opposite being true for wind direction (Fig. 4.15b). This difference was not clearly seen in either individual mixing ratio (Fig. 4.15c and Fig. 4.15d). The periods of low n-pentane to CO ratio seen during the high variability period corresponded to the brief periods of low alkane levels identified in Sect. 4.5.2, which were often air masses that had not recently been in contact with an emission source. These observations showed the ability of the ratio of n-pentane to CO to identify aged pollution, better than either value alone can do so.

4.6.3 SO₂

Although SO₂ is considered an anthropogenic tracer, correlation between n-pentane and SO₂ was only cursory (see Fig. 4.16). While 45% of global anthropogenic NMHC emissions result from fossil fuel usage and production, 52% of global SO₂ emissions stem from power generation and the industrial sector (Olivier et al., 2005). Since these sources are not necessarily co-located it was reasonable that they vary independently. The large peak in SO₂ on the evening of July 13th actually preceded the n-pentane peak. Similarly, the n-pentane peak on the 16th was followed by a small peak in SO₂. During both of these events, when SO₂ was at a maximum, n-pentane actually appeared to be decreasing. While there were some correlating events, many cases were clearly seen where increases in one compound occurred independent of the other. These data indicated that the regional sources of these two anthropogenic trace gases were likely near one another, as supported by the EDGAR emission inventory (see Fig. 4.2), but distinctly separated, a conclusion that exceeded the current resolution of this inventory.

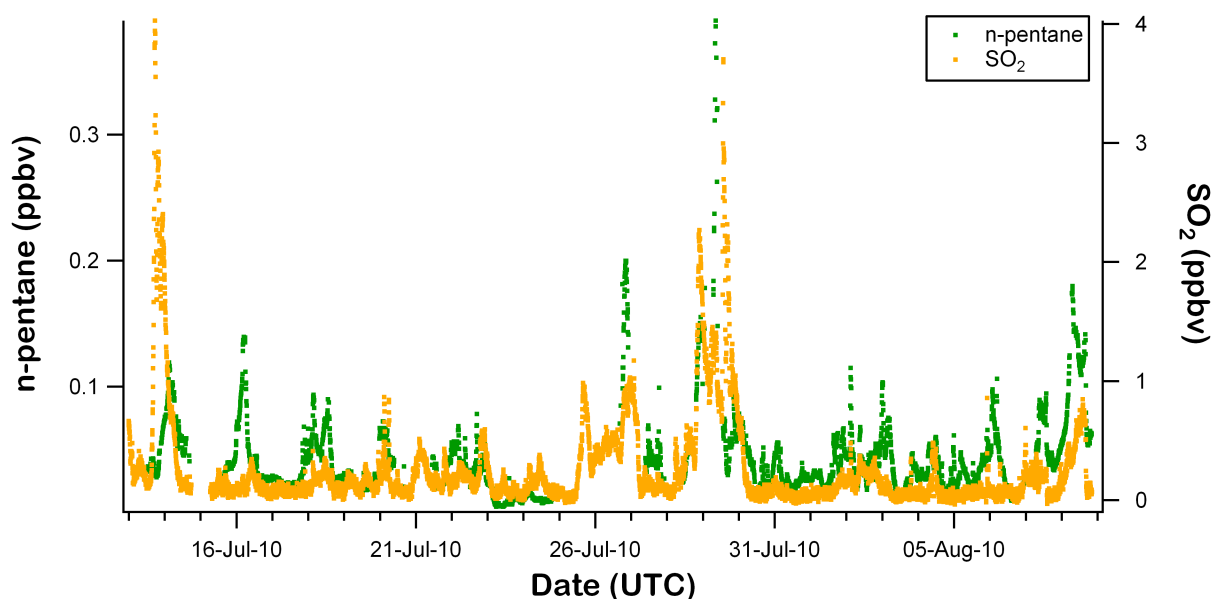


Figure 4.16: Time series of n-pentane for the duration of HUMPPA-COPEC 2010 with SO₂ mixing ratios measured at the SMEAR II Mast.

4.6.4 NO_x

Like the pentane isomers, NO_x (the sum of NO and NO_2) has a significant global source from combustion, with 44–58% of all anthropogenic emissions coming from the transportation sector (Butler et al., 2008). With this shared source, a strong correlation between pentane and NO_x was expected and observed (see Fig. 4.17). However, soil emissions also have been shown to be a significant factor. This natural emission is strongly temperature and moisture dependent (see Ludwig et al., 2001, and references therein). By comparing the median diel cycle of these two compounds, a clear correlation was seen (see Fig. 4.18). This close correlation of NO_x with the anthropogenically emitted pentane strongly suggested that the source of NO_x at this remote, forest site was mostly from transport of traffic emissions and that soil emissions were rather small in comparison.

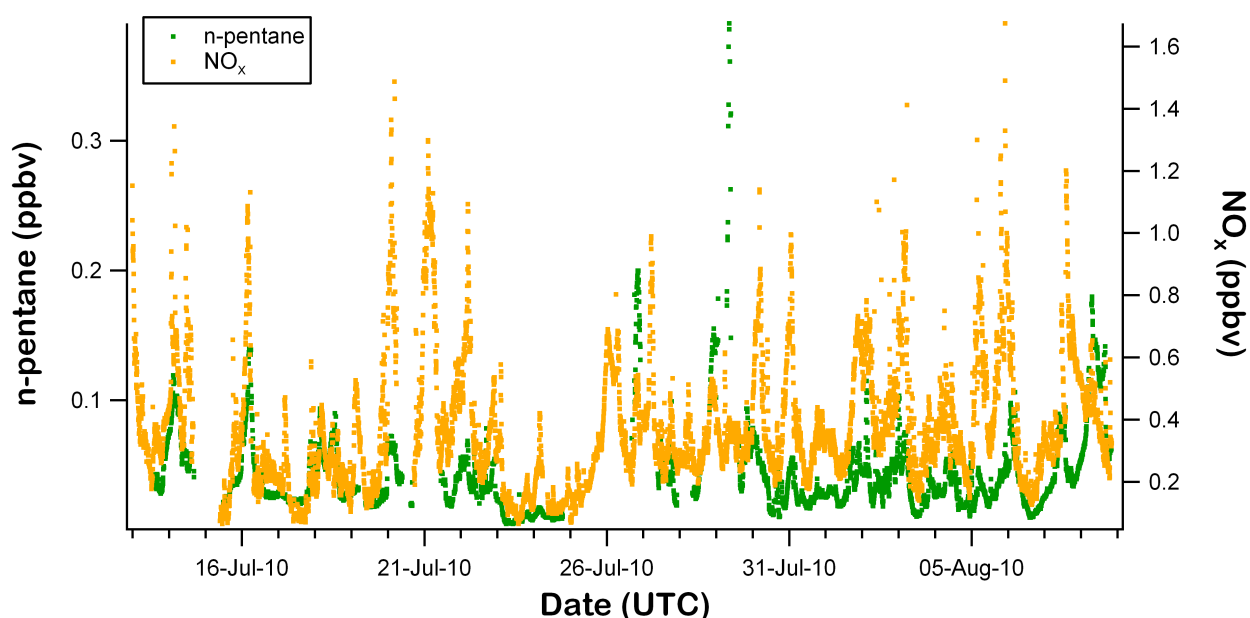


Figure 4.17: Time series of n-pentane for the duration of HUMPPA-COPEC 2010 with NO_x mixing ratios measured at the HUMPPA Tower.

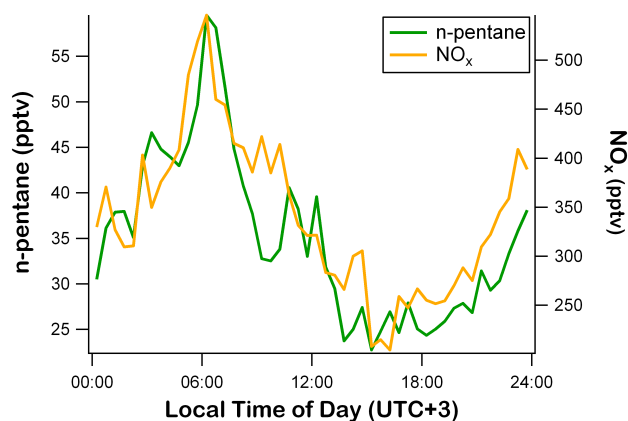


Figure 4.18: Median diel cycle for n-pentane for the duration of HUMPPA-COPEC 2010 with NO_x diel cycle measured at the HUMPPA Tower.

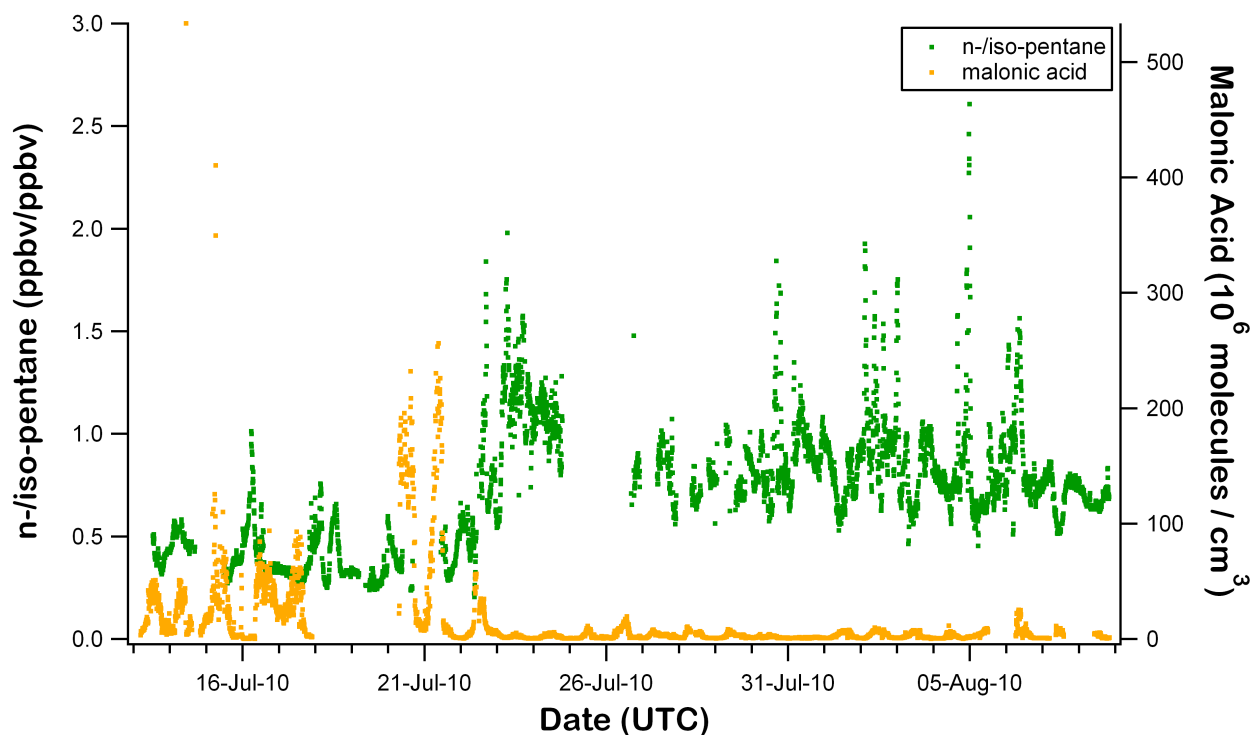


Figure 4.19: Time series of n-pentane for the duration of HUMPPA-COPEC 2010 with malonic acid concentration measured near the base of the HUMPPA Tower.

4.6.5 Malonic Acid

For completeness, n-pentane was compared to malonic acid, a dicarboxylic acid with a predominantly photochemical source in summer months (Kundu et al., 2010). This provided a clear contrast to pentane, an exclusively primary emission. As such a generally poor correlation was expected and observed (0.0018) for these species. However, comparison of malonic acid and the pentane isomer ratio, which is dependent on air mass age, was more enlightening. As seen in Fig. 4.19, malonic acid (measured on-line by chemical ionization mass spectrometry (CIMS)) demonstrated high variability for the first nine days of the campaign, followed by subdued daily peaks from July 22nd until the end of the campaign. This trend was anti-correlated to the pentane isomer ratio. Moreover, malonic acid had a strong diel cycle, which reached its minimum at night. The night with the highest malonic acid concentrations, July 17th, was also the night with the lowest pentane isomer ratio. The correlation of malonic acid with the pentane isomer ratio was 0.17, significantly higher than with n-pentane, but still lower than expected.

4.7 Air Mass Aging

One of the goals of this work was to be able to assess air mass aging with the pentane isomer ratio and by comparison with other anthropogenic and secondary tracers. Upon closer inspection, this proved difficult with this data set. As discussed in Sect. 4.4, due to the similar OH reaction rates and differing NO_3 reaction rates for n- and iso-pentane, higher isomer ratios would be expected as an air mass ages in the presence of both oxidants. Other

	n-Pentane [ppbv]	Pentane Isomer Ratio	Malonic Acid [10^6 molecules cm^{-3}]	NO_x / PAN [ppbv/ppbv]
Low Variability	0.0418	0.399	38.58	1.66
Low Alkanes	0.0098	1.141	1.95	1.19
High Variability	0.0342	0.879	2.86	1.81
Biomass Burning 1	0.0745	0.796	2.90	1.24
Biomass Burning 2	0.0795	0.681	4.12	2.13
Entire Campaign	0.0415	0.720	10.95	1.60

Table 4.3: Aging comparison according to the characteristic grouping

trends that should indicate air mass aging would be a decreasing ratio of NO_x to PAN or NO_y (the sum of NO_x , PAN, and HNO_3), or a decreasing ratio of pentane to CO. Furthermore, the growth of photochemistry products, such as malonic acid or PAN, would also indicate an aged air mass. Of these possible indicators of age, malonic acid concentration and the ratio of NO_x to PAN most clearly indicated that for the first part of the campaign, the low variability period, the site was dominated by more aged air, and that after the cold front passed on July 23rd, significantly newer air was observed (see Tab. 4.3). This was in apparent contradiction to the pentane isomer ratio, which nominally indicated the opposite.

In light of these observations and those of Sect. 4.5.2, the behavior of the pentane isomer ratio during summer in the boreal region should be re-evaluated. That periods of low alkane mixing ratios were observed with both high and low isomer ratios indicated either different regional emission ratios or varying degrees of oxidation. These measurements were made at a high latitude during the summer with nearly 18 hours of daylight. The few hours of darkness together with high levels of reactive, biogenic VOCs prohibited the build up appreciable levels of NO_3 , a highly photo-labile and reactive radical. Because the reaction rate of n-pentane with OH is slightly faster than that of iso-pentane, the typical expectation of increasing pentane isomer ratio with age would be reversed in this regime free of NO_3 . This reversed trend in the isomer ratio would also be observed in air masses with a large Cl exposure, as n-pentane reacts 28% faster with Cl than iso-pentane (25.0 compared to $19.6 \times 10^{-11} \text{ cm}^3 \text{ molecules}^{-1} \text{ s}^{-1}$, Hooshiyar and Niki, 1995). However, differentiation by OH or Cl, even after extended periods of exposure, would be rather small, so that implication of differing regional emission ratios can not be disregarded. Furthermore, the poor correlation between the pentane isomer ratio and other indicators of air mass age indicated that other factors influenced the observed isomer ratio, and that use of this ratio as a measure of air mass age would require deconvolution of these other factors.

In addition to estimating aging, pentane isomer ratios have been used to estimate the concentration of NO_3 (Penkett et al., 2007), which is difficult to measure directly. However, this method assumed a constant emission ratio, which is unlikely in light of the preceding discussion and the differing isomer ratios observed during urban pollution plumes (see Sect. 4.5.1). Furthermore, an over-simplification was discovered in the derivation estimating

OH from the correlation of the ratio of benzene to toluene with the ratio of the pentane isomers. Therefore, a re-evaluation of this approach is required (S. Penkett, personal communication, 19 Jan 2011), and no such estimation was attempted here.

4.8 Conclusion

In an effort to better characterize the air chemistry and aerosol correlations and interactions of the boreal region, from July 12th until August 12th the participants of HUMPPA-COPEC 2010 measured a comprehensive suite of meteorological, air chemistry, and aerosol chemical and physical properties. In support of this endeavor, and to compliment these other measurements, FOTOS measured the C₄ and C₅ NMHCs at a 5.5 minute sampling frequency. An additional methane instrument (GC-FID) was operated at a 70 second sampling frequency. Despite environmental challenges and instrumentation issues, FOTOS achieved 67.6% data coverage for the whole of the campaign, and 91.4% coverage from a repair on July 29th until a major power outage on August 8th.

The alkane mixing ratios, together with the ratio of n- to iso-pentane, separated the campaign into five time periods. An initial period of low temporal variability was observed with well-defined peaks in alkane mixing ratios between periods of lower, stable baseline. The ratio of pentane isomers was low during these baseline periods, and usually peaked with the pentane mixing ratios. A second period with low alkane mixing ratios began on July 23rd as a cold front moved over the measurement site and brought in cleaner northern air that persisted for two days. Pentane mixing ratios fell to less than 20 pptv (but still well above the detection limit of the instrument), and the pentane isomer ratio rose dramatically. The ensuing period was dominated by two biomass burning plumes. This period was followed by a week of high temporal variability in the alkane mixing ratios, with significantly higher pentane isomer ratios than observed during the low variability period of the campaign. The final two days of measurements also observed a significant biomass burning plume. This characteristic grouping provided a framework for more detailed analysis.

Several periods of interest were identified within and across these groupings and analyzed in further detail. These periods included pollution events from St. Petersburg, Russia, and northern, mainland Europe, in addition to periods of low anthropogenic influence. Comparison with other anthropogenic tracers showed agreement, but also differences, indicating the importance of separate NMHC measurement for more complete anthropogenic filtering. These high frequency NMHC measurements highlighted the chemically distinct fingerprint of various anthropogenic sources. The two distinct groupings of the pentane isomer ratio were also apparent in the methane mixing ratios. The ratio of n-pentane to CO proved reliable at indicating periods of distant anthropogenic influence better than either value alone. The diel cycles of n-pentane and NO_x indicated a predominately traffic source for NO_x, which masked any diel input from natural sources. Finally, comparison with malonic acid, a secondary oxidation product, showed orthogonality indicating these compounds have truly independent sources.

Attempts to determine air mass aging from the pentane isomer ratio provided mixed results. In fact, this ratio often showed an anti-correlation to the ratio of NO_x to PAN or the concentration of malonic acid. The unique characteristics of summer at high latitudes (i.e. few hours of darkness and high levels of reactive VOCs), together with a wide range of pentane isomer emission ratios, resulted in a convolution of several factors that made aging determinations with the pentanes difficult. Furthermore, over-simplifications discovered in the method used by Penkett et al. to determine NO_3 concentrations precluded such analysis with this data set (S. Penkett, personal communication, 19 Jan 2011).

In conclusion, it was judged that even in the remote boreal forest, anthropogenic influences were frequent and significant. A variety of sources was indicated in the occasional correlation and anti-correlation of known anthropogenic tracers. Therefore, the measurement of the NMHCs, and their comparison with other tracers, provided additional, valuable information in the characterization of air masses. FOTOS was capable of measuring these compounds at higher frequency than typically realized, which provided an additional level of characterization and understanding.

Chapter 5

Future Directions

In the course of the campaigns and lab tests described in this work, several possibilities for further improving the robustness of FOTOS have become apparent. As mentioned in Sect. 2.4.1, the frailties exhibited by the fiberglass dewar could be addressed by switching to a metal dewar. Specifically, the chance of leaks in an all-metal system would be reduced, and any leaks that might arise could be more easily repaired. A metal dewar would also be easier to mount, as mounting connections could be welded to the dewar, eliminating the need for separate housing. A dewar matching these characteristics has been ordered from CryoVac GmbH & Co KG, Troisdorf, Germany. An additional improvement to the sampling system would be better heating of the transfer lines between the traps and multi-position (MuPo) valves. This could be accomplished by encasing the traps and MuPos within a single box heated to adequate temperatures (e.g. 70 °C). By incorporating the dewar “hat” into this box (as its base), the mounting of the traps on the dewar (and dewar in the rack) would be simplified. A final system improvement would be to design new traps that are more consistently and easily constructed and packed. These changes should also address the breakthrough seen in the C₂ and C₃ hydrocarbons mentioned in Sect. 2.8.2. Together, these changes to the cryogenic sampling system would increase performance and robustness of this critical element of FOTOS.

The experience gained in these initial uses of FOTOS emphasized the need for further optimization and characterization testing. One advantage of FOTOS is that all temperature, flow, and regulation settings are user-accessible. Time has not allowed careful analysis and optimization of all these parameters. Parameters such as trapping temperature and flow, injection temperature, MS dwell time, sample size, and MuPo bore size could all be more carefully addressed with further testing. Standard operating procedures for the testing and optimization of new traps would also improve the accessibility of this instrument to inexperienced users. Careful analysis of the stability of the system would be valuable for optimizing the calibration scheme employed. Factors such as frequency of calibrations and backgrounds, linearity checks, and data analysis automation could all potentially be further optimized, and these improvements will surely be necessary as new suites of VOC are pursued. Finally, while the intercomparison at Hohenpeißenberg indicated no obvious interferences from

humidity or ozone, focused interference tests of these and other environmental parameters could be enlightening and assist in optimizing the performance of the entire system.

Although FOTOS was only used for measuring NMHCs in this work, it was designed in such a way that the measurement of other VOCs should be attainable by using an appropriate GC column. For example, the installation of a DB-624 column would allow the measurement of many oxygenated and halogenated VOCs.

Recent experience has shown that conditioning of a cryogenic water trap like the one used in FOTOS is essential for accurate measurement of VOCs with higher solubility (e.g. acetone and methanol, Jobson and McCoskey, 2010). As the current configuration of traps in FOTOS does not allow for ambient air to pass through the water trap without also passing through the enrichment trap, a new sampling configuration is needed. An alternative configuration that would provide even more flexibility in sample flow paths is presented in Fig. 5.1. This new design has the uncommon benefits of being more simple and more flexible. During the period of water trap heating failure in the HUMPPA-COPEC campaign (see Sect. 4.3), it was observed that the cold water trap would function without heating for approximately 6 hours before significantly restricting sample flow. With this new design, the water trap need not be heated with each sampling cycle and could be flushed with ambient air during enrichment trap purging and cooling (Fig. 5.2). This change would increase the versatility of FOTOS, adding highly water soluble VOCs to the range of accessible compounds.

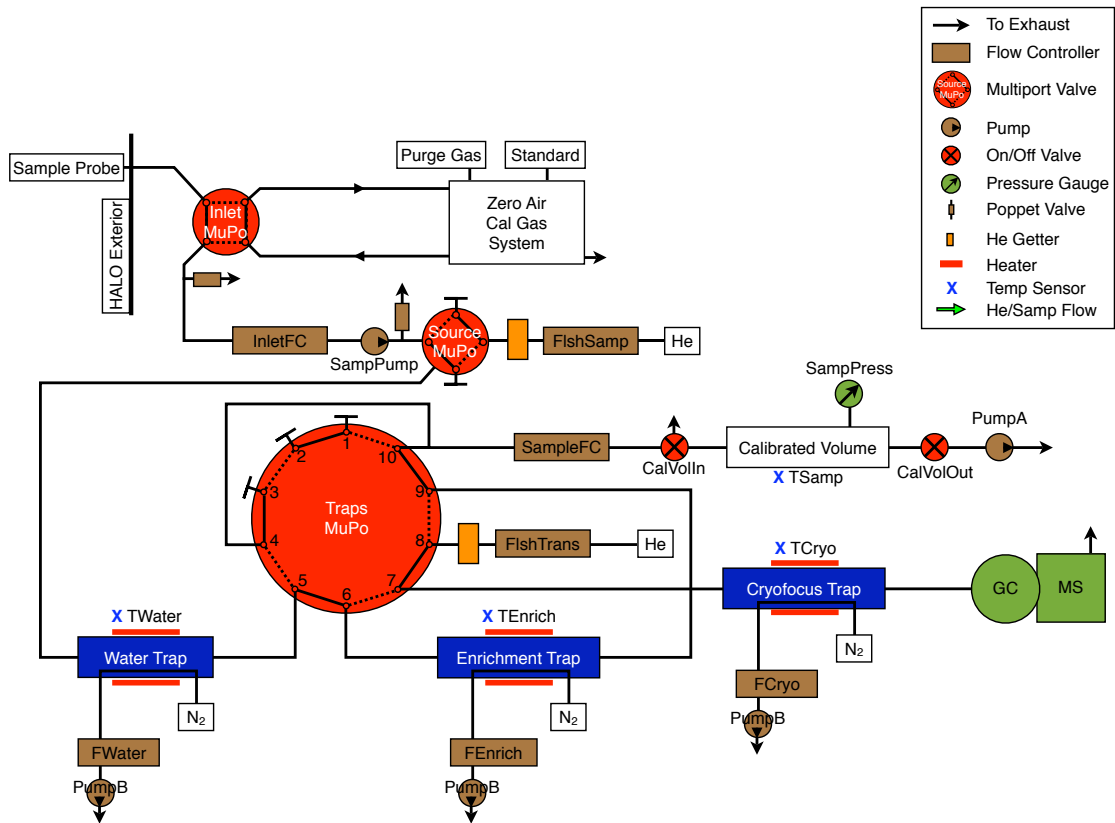


Figure 5.1: Gas flow schematic showing the alternative cryogenic sampling system.

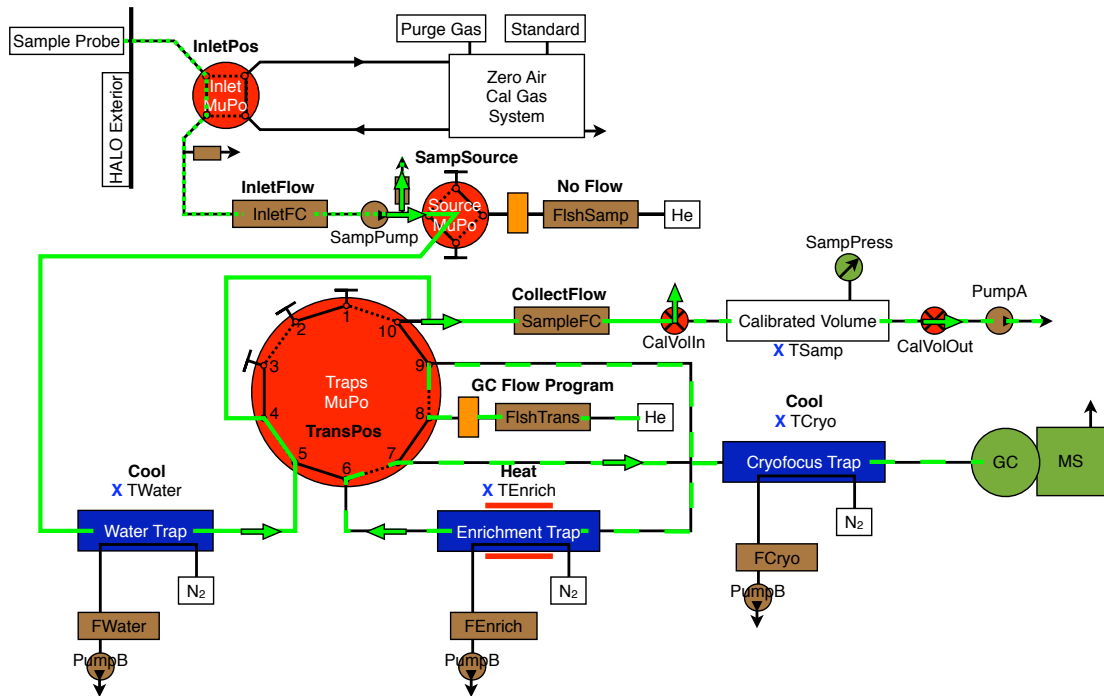


Figure 5.2: Alternative flow schematic for transferring the collected sample from the enrichment trap to the cryofocusing trap while conditioning the water trap with ambient air.

Chapter 6

Conclusions

Volatile Organic Compounds (VOCs), a class of minor atmospheric constituents, are present at levels below 0.5 ppmv down to a few pptv. Despite their trace levels, VOCs play an important role in atmospheric chemistry: influencing tropospheric ozone (and thereby urban smog and atmospheric oxidation capacity) and having direct and indirect effects on global climate change. The main sinks for VOCs are the oxidizing, atmospheric radicals: OH, NO₃, and O₃. These oxidation pathways have a net yield of ozone in the presence of NO_x. An important class of VOC is the non-methane hydrocarbons (NMHCs), some of which are predominately of an anthropogenic source, especially light alkanes and aromatics. Due to lower reactivities than biogenic emissions, these compounds have higher ambient concentrations and are ubiquitous throughout the troposphere and even into the lower stratosphere. For the past 50 years, VOCs have been measured off-line from samples collected in glass or metal flasks or on adsorbent cartridges. On-line GC measurements typically have a sampling frequency on the order of one hour. Therefore, an instrument capable of higher time resolution measurement of VOCs, including the NMHCs, would be desirable, especially for in situ measurement aboard research aircraft. To this end, the Fast Observation of Trace Organics System (FOTOS) was designed and built for use aboard the new High Altitude Long Range Scientific Aircraft (HALO).

FOTOS was designed and constructed with a custom, three-trap cryogenic sampling system and a modified, commercial, fast GC-MS. The goal of this design was to achieve maximum versatility, therefore no chemical dryers or adsorbents were employed for sample processing. Meeting the strict construction requirements for certification aboard HALO, FOTOS achieved 5.5 minute sampling frequency while measuring at least 13 different C₂ to C₅ NMHCs. In the initial sampling step, the sample was dried in an unpacked, cooled water trap (typically at -40 °C) and collected on a glass wool packed enrichment trap (typically at -135 °C). In the next step, the sample was then refocused on a cryofocusing trap (packed with glass wool or lined with a deactivated silica capillary at -135 °C). Finally, the sample was injected and separated on the GC while the next sample was being collected. An internal zero air and calibration system allowed for on-line calibration. The increased magnitude of data output was processed by a set of automated programs and procedures which proved to

be thorough and selective. Lab and internal consistency tests indicated that FOTOS was a fast, stable, precise, accurate, instrument with low background signal (less than 2% with the exception of high background alkene signal). The detection limit for n- and iso-pentane was determined to be 2.6 and 2.0 pptv, respectively. FOTOS was proven to be a versatile, robust, highly automated, precise, accurate, sensitive instrument, capable of in situ measurement of VOCs at sampling frequencies suitable for use aboard research aircraft, such as HALO.

To validate the performance of FOTOS, an intercomparison with the GC-FID system at the Meteorological Observatory at Hohenpeißenberg (MOHp), a WMO-GAW global station, was performed from January 26th to February 4th, 2010. A range of atmospheric conditions were sampled in this time, including a large pollution plume from Munich (56 km to the Northeast) and extended periods of cleaner air from the Southwest. Both systems ran at their maximum sampling frequency, which, at the time, was 6 minutes for FOTOS and 70 minutes for the MOHp GC-FID. The agreement between FOTOS and the MOHp system was determined by averaging the measurements from FOTOS made during the MOHp sampling times. Two compounds, iso-pentane and 1,3-butadiene, were found to be clipped by poor timing of the MS SIM grouping, and the values for comparison of these compounds were filtered by peak retention time. Thirteen different NMHCs were analyzed and compared within the framework of the GAW Data Quality Objectives (DQO). More than 80% of the C₄ and 100% of the C₅ alkane measurements satisfied these DQO. Additionally, 100% of the 1,3-butadiene and 95.7% of the propyne measurements were within the DQO. Propane, propene, ethyne, and the butene isomers showed significantly worse agreement. However, in the case of the butene isomers, this was likely complicated by low ambient mixing ratios (averages of less than 20 pptv) and the high system background previously mentioned. This first field campaign revealed the robustness and high accuracy of FOTOS, in addition to the advantage of higher sampling frequency, even in a ground-based measurement.

To demonstrate the capabilities of this new instrument (in lieu of an airborne campaign), FOTOS measured selected light NMHCs to complement the suite of measurements performed during a summer boreal forest campaign, HUMPPA-COPEC 2010. From July 12th to August 12th, 2010, an international consortium of institutes and instruments measured the physical and chemical properties of the gas and particle phase of the air over the boreal forest at the SMEAR II station near Hyytiälä, Finland. The boreal forest covers 8% of the Earth's land surface and represents 27% of all forests, therefore having a large potential impact on regional and global climate. As part of the HUMPPA-COPEC 2010 campaign, FOTOS sampled just above the canopy (16.8 meters) at a frequency of 5.5 minutes with a data coverage of 67.6% for the duration of the campaign. Methane was also measured with a separate GC-FID at 70 second intervals. Characteristics of the alkane mixing ratios and the pentane isomer ratio divided the campaign into five distinct periods: periods of low and high variability, a period of low alkane mixing ratios, and two periods of biomass burning. Comparisons of n-pentane and the pentane ratio with other anthropogenic tracers (CO, NO_x, and SO₂) revealed distinct sources of anthropogenic influence at the site and

allowed for distinguishing between local and distant sources. These measurements revealed the value of measuring the light NMHCs at high frequency, even in remote regions, as a specific marker of anthropogenic influence. These periods of influence were determined to be frequent and significant, even at this remote forest site. A significant correlation in the diel cycle of alkanes and NO_x was observed, suggesting minimal influence of natural sources on NO_x in this region of the boreal forest. Estimates of air mass aging with the pentane isomer ratio were anti-correlated to similar estimates from malonic acid concentrations and the ratio of NO_x to PAN. This result indicated that better understanding of the pentane isomer emission ratio, and perhaps the intricacies of photochemistry in the northern latitudes during the summer months, is needed.

List of Figures

2.1	The HALO aircraft	10
2.2	Mounting of FOTOS in HALO rack	11
2.3	Gas flow schematic	12
2.4	Inlet flow schematic for sampling	13
2.5	Flow schematic for sample drying and enrichment	14
2.6	Flow schematic for sample transfer	14
2.7	Flow schematic for sample injection	15
2.8	Flow schematic for purging the sample line	16
2.9	Diagram of cryogenic trap	17
2.10	Diagram of cryogenic dewar	18
2.11	Detail of a metal water trap	19
2.12	Wound trap during curing	21
2.13	Completed enrichment trap with housing	21
2.14	GC temperature and flow program	24
2.15	Schematic of the Zero Air Generator	24
2.16	PTR-MS signal of air scrubbed by the ZAG	26
2.17	Effect of retention time filter on intercomparison data set	27
2.18	Comparison of trap heating and cooling rates	29
2.19	Typical trap temperature cycling during the HUMPPA campaign	30
2.20	Chromatogram showing thirteen measured compounds	31
2.21	Trapping efficiency temperature tests	32
2.22	Nine successive measurements of n-butane	33
2.23	n-Butane signal from zero and sample runs	33
2.24	Error calculation for n-pentane	34
2.25	Time trace of calibration factors from HUMPPA	35
3.1	The inlet and sampling line connection at MOHp	38
3.2	Time trace of n-butane	39
3.3	Time trace of n-pentane agreement	41
3.4	Propane agreement	41
3.5	Propene agreement	42
3.6	iso-Butane agreement	43

3.7	n-Butane agreement	43
3.8	Ethyne agreement	44
3.9	iso-Butene agreement	45
3.10	Butene isomers agreement	45
3.11	iso-Pentane agreement	46
3.12	iso-Pentane agreement vs. retention time	46
3.13	n-Pentane agreement	47
3.14	Butadiene and propyne agreement	48
3.15	Butadiene and propyne agreement vs. retention time	48
3.16	Advantage of higher time resolution	50
4.1	Map of HUMPPA-COPEC site	54
4.2	Global model emission source map	55
4.3	Sampling inlets for FOTOS and methane GC-FID	57
4.4	Time series of n-pentane and pentane isomers ratio	59
4.5	Detail of first two urban pollution plumes	62
4.6	Back trajectories for the two urban pollution plumes	62
4.7	Detail of narrow pollution peaks	63
4.8	Back trajectories for narrow pollution peaks	63
4.9	Time series highlighting periods of low alkanes	64
4.10	Back trajectories for periods of low alkanes	64
4.11	Detail of biomass burning plume	67
4.12	Back trajectories for biomass burning plume	67
4.13	Pentane isomers ratio correlation with methane and time	68
4.14	Time series of n-pentane and CO	69
4.15	Histograms of wind direction, n-pentane and CO	69
4.16	Time series of n-pentane and SO ₂	70
4.17	Time series of n-pentane and NO _x	71
4.18	Diel cycle of n-pentane and NO _x	71
4.19	Time series of n-pentane and malonic acid	72
5.1	Alternative gas flow schematic	79
5.2	Alternative flow schematic for sample transfer	79

List of Tables

2.1	Trap design summary table	22
2.2	Partial composition of NPL standard with uncertainties	25
2.3	Selected properties of compounds measured at MOHp	31
3.1	Agreement of measurements between FOTOS and MOHp	49
4.1	Anthropogenic emission sources near SMEAR II station	56
4.2	HUMMPA Campaign Characteristic Grouping and Values	60
4.3	Aging comparison according to the characteristic grouping	73

List of Abbreviations

CCN	cloud condensation nuclei
CIMS	chemical ionization mass spectrometry
COPEC	Comprehensive Organic Particle and Environmental Chemistry
DQO	Data Quality Objectives
ECD	Electron Capture Detector
EDGAR	Emissions Database for Global Atmospheric Research
FID	Flame Ionization Detector
FOTOS	The Fast Observation of Trace Organics System
GAW	Global Atmosphere Watch
gC yr ⁻¹	grams of carbon per year
GC	gas chromatography
HALO	the High Altitude, LOng Range Research Aircraft
HUMPPA	Hyttiälä United Measurement of Photochemistry and Particles in Air
ID	inner diameter
LTM	Low Thermal Mass
m/z	mass to charge
MACH	Modular Accelerated Column Heater
MFC	mass flow controller
MOHp	Meteorological Observatory at Hohenpeißenberg
MS	mass spectrometry
MuPo	multi-position valve

NMHCs	non-methane hydrocarbons
NPL	National Physics Laboratory, UK
OD	outer diameter
PID	Photo-Ionization Detector
ppbv	parts per billion by volume or nmol/mol
ppmv	parts per million by volume or $\mu\text{mol/mol}$
pptv	parts per trillion by volume or pmol/mol
psi	pounds per square inch
PTFE	polytetrafluoroethylene
PTR	Proton Transfer Reaction
sccm	standard cubic centimeters
SIM	Select Ion Monitoring
SMEAR	Station for Measuring Forest Ecosystem-Atmosphere Relations
SOA	secondary organic aerosol
VOCs	volatile organic compounds
WMO	World Meteorological Organization

Schematic Parts List

CalVolIn	three-way solenoid valve allowing flow into the sample volume
CalVolOut	two-way solenoid valve allowing flow out of the sample volume
FCryo	cryofocusing trap cooling N ₂ mass flow controller
FEnrich	enrichment trap cooling N ₂ mass flow controller
FlshSamp	source He mass flow controller
FlshTrans	cryofocusing and GC He mass flow controller
FlshWater	water trap purging He mass flow controller
FWater	water trap cooling N ₂ mass flow controller
GC	gas chromatograph
Inlet MuPo	inlet two-position valve
InletFC	inlet mass flow controller
MS	mass spectrometer
N2PurgeFC	sample inlet purging nitrogen mass flow controller (for takeoff)
PumpA	sample volume evacuating pump
PumpB	cooling N ₂ mass flow controller backing pump
SampleFC	sample flow mass flow controller
SampPress	sample volume pressure gauge
SampPump	sample pump
Source MuPo	source multi-position valve
StandIn	two-way solenoid valve allowing standard gas into the zero air flow
TCryo	temperature of the cryofocusing trap
TEnrich	temperature of the enrichment trap
Traps MuPo	traps two-position valve
TSamp	sample volume temperature sensor
TWater	temperature of the water trap
ZAG	Zero Air Generator and calibration system

Bibliography

Altshuller, A. P. and C. A. Clemons. Gas chromatographic analysis of aromatic hydrocarbons at atmospheric concentrations using flame ionization detection. *Analytical Chemistry*, 34(4):466–472, 1962. doi:10.1021/ac60184a006.

Andreae, M. O. and P. Merlet. Emission of trace gases and aerosols from biomass burning. *Global Biogeochemical Cycles*, 15(4):955–966, 2001.

Apel, E. C., A. J. Hills, R. Lueb, S. Zindel, S. Eisele, and D. D. Riemer. A fast-GC/MS system to measure c-2 to c-4 carbonyls and methanol aboard aircraft. *Journal of Geophysical Research D: Atmospheres*, 108(D20), 2003. doi:10.1029/2002JD003199.

Atkinson, R. Gas-phase tropospheric chemistry of volatile organic compounds: 1. alkanes and alkenes. *Journal of Physical and Chemical Reference Data*, 26(2):215, 1997. doi:10.1063/1.556012.

Atkinson, R. Kinetics of the gas-phase reactions of OH radicals with alkanes and cycloalkanes. *Atmospheric Chemistry and Physics*, 3(6):2233–2307, 2003. doi:10.5194/acp-3-2233-2003.

Atkinson, R. and J. Arey. Atmospheric degradation of volatile organic compounds. *Chemical Reviews*, 103(12):4605–4638, 2003. doi:10.1021/cr0206420.

Baker, A. K., A. J. Beyersdorf, L. A. Doezema, A. Katzenstein, S. Meinardi, I. J. Simpson, D. R. Blake, and F. S. Rowland. Measurements of nonmethane hydrocarbons in 28 united states cities. *Atmospheric Environment*, 42(1):170–182, 2008. doi:10.1016/j.atmosenv.2007.09.007.

Baker, A. K., F. Slemr, and C. A. M. Brenninkmeijer. Analysis of non-methane hydrocarbons in air samples collected aboard the CARIBIC passenger aircraft. *Atmospheric Measurement Techniques*, 3(1):311–321, 2010. doi:10.5194/amt-3-311-2010.

Barrie, L. A. Arctic air pollution: An overview of current knowledge. *Atmospheric Environment*, 20(4):643–663, 1986. doi:10.1016/0004-6981(86)90180-0.

Bellar, T. A., M. F. Brown, and J. E. Sigsby. Determination of atmospheric pollutants in the part-per-billion range by gas chromatography. a simple trapping system for use with flame ionization detectors. *Analytical Chemistry*, 35(12):1924–1927, 1963. doi:10.1021/ac60205a041.

- Bon, D. M., I. M. Ulbrich, J. A. de Gouw, C. Warneke, W. C. Kuster, M. L. Alexander, A. Baker, A. J. Beyersdorf, D. Blake, R. Fall, J. L. Jimenez, S. C. Herndon, L. G. Huey, W. B. Knighton, J. Ortega, S. Springston, and O. Vargas. Measurements of volatile organic compounds at a suburban ground site (T1) in Mexico City during the MILAGRO 2006 campaign: measurement comparison, emission ratios, and source attribution. *Atmospheric Chemistry and Physics*, 11(6):2399–2421, 2011. doi:10.5194/acp-11-2399-2011.
- Burns, W. F., D. T. Tingey, R. C. Evans, and E. H. Bates. Problems with a Nafion[®] membrane dryer for drying chromatographic samples. *Journal of Chromatography A*, 269:1–9, 1983. doi:10.1016/S0021-9673(01)90777-0.
- Butler, T. M., M. G. Lawrence, B. R. Gurjar, J. van Aardenne, M. Schultz, and J. Lelieveld. The representation of emissions from megacities in global emission inventories. *Atmospheric Environment*, 42(4):703–719, 2008. doi:10.1016/j.atmosenv.2007.09.060.
- Carslaw, K. S., O. Boucher, D. V. Spracklen, G. W. Mann, J. G. L. Rae, S. Woodward, and M. Kulmala. A review of natural aerosol interactions and feedbacks within the earth system. *Atmospheric Chemistry and Physics*, 10(4):1701–1737, 2010. doi:10.5194/acp-10-1701-2010.
- Colman, J. J., A. L. Swanson, S. Meinardi, B. C. Sive, D. R. Blake, and F. S. Rowland. Description of the analysis of a wide range of volatile organic compounds in whole air samples collected during PEM-Tropics a and b. *Analytical Chemistry*, 73(15):3723–3731, 2001. doi:10.1021/ac010027g.
- Cramers, C. A. and P. A. Leclercq. Consideration on speed of separation, detection, and identification limits in capillary gc and gc/ms. *CRC Critical Reviews in Analytical Chemistry*, 20(2):117–147, 1988. doi:10.1080/00078988808048809.
- Cremer, S., M. F. Sledge, and J. Heinze. Chemical mimicry: Male ants disguised by the queen’s bouquet. *Nature*, 419(6910):897–897, 2002. doi:10.1038/419897a.
- Dandeneau, R. D. and E. H. Zerenner. An investigation of glasses for capillary chromatography. *Journal of High Resolution Chromatography*, 2(6):351–356, 1979. doi:10.1002/jhrc.1240020617.
- de Gouw, J. and C. Warneke. Measurements of volatile organic compounds in the earth’s atmosphere using proton-transfer-reaction mass spectrometry. *Mass Spectrometry Reviews*, 26(2):223–257, 2007. doi:10.1002/mas.20119.
- Desty, D., A. Goldup, and W. Swanton. In Brenner, N., J. Callen, and M. Weis, editors, *Gas Chromatography*, page 105. Academic Press, New York, 1962.
- Dettmer, K. and W. Engewald. Adsorbent materials commonly used in air analysis for adsorptive enrichment and thermal desorption of volatile organic compounds. *Analytical and Bioanalytical Chemistry*, 373(6):490–500, 2002. doi:10.1007/s00216-002-1352-5.

DLR. High altitude and long range research aircraft. 2009. Online: <http://www.halo.dlr.de>, accessed 18.04.2011.

DLR. 2011. Online: <http://www.dlr.de/en/Portaldata/1/Resources/luftfahrt/halo0903C.jpg>, accessed 18.04.2011.

Dlugokencky, E. J. Conversion of NOAA atmospheric dry air CH₄ mole fractions to a gravimetrically prepared standard scale. *Journal of Geophysical Research*, 110(D18), 2005. doi:10.1029/2005JD006035.

Draxler, R. and G. Rolph. 2011. HYSPLIT (HYbrid Single-Particle Lagrangian Integrated Trajectory) Model access via NOAA ARL READY Website (<http://ready.arl.noaa.gov/HYSPLIT.php>). NOAA Air Resources Laboratory, Silver Spring, MD.

Eerdeken, G., L. Ganzeveld, J. V. de Arellano, T. Klüpfel, V. Sinha, N. Yassaa, J. Williams, H. Harder, D. Kubistin, M. Martinez, and J. Lelieveld. Flux estimates of isoprene, methanol and acetone from airborne PTR-MS measurements over the tropical rainforest during the GABRIEL 2005 campaign. *Atmospheric Chemistry and Physics*, 9(13):4207–4227, 2009. doi:10.5194/acp-9-4207-2009.

Engel, A., H. Bönisch, and S. Sala. 2010. Institute for the Atmosphere and Environment, Goethe University, Frankfurt am Main. The analysis in this work was completed with iau_chrom version 3.5.

FAO. *Global forest resources assessment 2010 : main report*. Food and Agriculture Organization of the United Nations, Rome, 2010. ISBN 978-92-5-106654-6.

Fuentes, J. D., L. Gu, M. Lerdau, R. Atkinson, D. Baldocchi, J. W. Bottenheim, P. Ciccioli, B. Lamb, C. Geron, A. Guenther, T. D. Sharkey, and W. Stockwell. Biogenic hydrocarbons in the atmospheric boundary layer: A review. *Bulletin of the American Meteorological Society*, 81(7):1537–1575, 2000. doi:10.1175/1520-0477(2000)081<1537:BHITAB>2.3.CO;2.

Gebhardt, S., A. Colomb, R. Hofmann, J. Williams, and J. Lelieveld. Halogenated organic species over the tropical south american rainforest. *Atmospheric Chemistry and Physics*, 8(12):3185–3197, 2008. doi:10.5194/acp-8-3185-2008.

GFMC. Forest fires in the russian federation. Global Fire Monitoring Center / Fire Ecology Research Group, 2010. Online: <http://www.fire.uni-freiburg.de>, accessed 23.05.2011.

Greene, M. J. and D. M. Gordon. Social insects: Cuticular hydrocarbons inform task decisions. *Nature*, 423(6935):32, 2003. doi:10.1038/423032a.

Grenfell, R. J. P., M. J. T. Milton, A. M. Harling, G. M. Vargha, C. Brookes, P. G. Quincey, and P. T. Woods. Standard mixtures of ambient volatile organic compounds in synthetic

and whole air with stable reference values. *Journal of Geophysical Research*, 115(D14), 2010. doi:10.1029/2009JD012933.

Guenther, A. The contribution of reactive carbon emissions from vegetation to the carbon balance of terrestrial ecosystems. *Chemosphere*, 49(8):837–844, 2002. doi:10.1016/S0045-6535(02)00384-3.

Guenther, A., C. N. Hewitt, D. Erickson, R. Fall, C. Geron, T. Graedel, P. Harley, L. Klinger, M. Lerdau, W. A. Mckay, T. Pierce, B. Scholes, R. Steinbrecher, R. Tallamraju, J. Taylor, and P. Zimmerman. A global model of natural volatile organic compound emissions. *Journal of Geophysical Research*, 100(D5):8873–8892, 1995.

Harley, J., W. Nel, and V. Pretorius. Flame ionization detector for gas chromatography. *Nature*, 181(4603):177–178, 1958. doi:10.1038/181177a0.

Häseler, R., T. Brauers, F. Holland, and A. Wahner. Development and application of a new mobile LOPAP instrument for the measurement of HONO altitude profiles in the planetary boundary layer. *Atmospheric Measurement Techniques Discussions*, 2(4):2027–2054, 2009. doi:10.5194/amtd-2-2027-2009.

Helmig, D. Ozone removal techniques in the sampling of atmospheric volatile organic trace gases. *Atmospheric Environment*, 31(21):3635–3651, 1997. doi:10.1016/S1352-2310(97)00144-1.

Hewitt, C. *Reactive hydrocarbons in the atmosphere*. Academic Press, San Diego, 1999. ISBN 0-12-3460240-1.

Hooshiyar, P. A. and H. Niki. Rate constants for the gas-phase reactions of Cl-atoms with C₂–C₈ alkanes at T = 296 ± 2 K. *International Journal of Chemical Kinetics*, 27(12):1197–1206, 1995. doi:10.1002/kin.550271206.

IPCC. 2007. *Climate Change 2007: The Physical Science Basis. Contribution of Working Group I to the Fourth Assessment Report of the Intergovernmental Panel on Climate Change* [Solomon, S., D. Qin, M. Manning, Z. Chen, M. Marquis, K.B. Averyt, M. Tignor and H.L. Miller (eds.)]. Cambridge University Press, Cambridge, United Kingdom and New York, NY, USA, 996 pp.

Jacobson, M. Z. *Atmospheric pollution : history, science, and regulation*. Cambridge University Press, Cambridge UK, 2002. ISBN 0-521-01044-6.

Jobson, B. T. and J. K. McCoskey. Sample drying to improve HCHO measurements by PTR-MS instruments: laboratory and field measurements. *Atmospheric Chemistry and Physics*, 10(4):1821–1835, 2010. doi:10.5194/acp-10-1821-2010.

- Junkermann, W. The actinic UV-radiation budget during the ESCOMPTE campaign 2001: results of airborne measurements with the microlight research aircraft D-MIFU. *Atmospheric Research*, 74(1-4):461–475, 2005. doi:10.1016/j.atmosres.2004.06.009.
- Kesselmeier, J., P. Ciccioli, U. Kuhn, P. Stefani, T. Biesenthal, S. Rottenberger, A. Wolf, M. Vitullo, R. Valentini, A. Nobre, P. Kabat, and M. O. Andreae. Volatile organic compound emissions in relation to plant carbon fixation and the terrestrial carbon budget. *Global Biogeochemical Cycles*, 16(4), 2002. doi:10.1029/2001GB001813.
- Kesselmeier, J. and M. Staudt. Biogenic volatile organic compounds (voc): An overview on emission, physiology and ecology. *Journal of Atmospheric Chemistry*, 33:23–88, 1999. 10.1023/A:1006127516791.
- Kessler, A. and I. T. Baldwin. Defensive function of Herbivore-Induced plant volatile emissions in nature. *Science*, 291(5511):2141–2144, 2001. doi:10.1126/science.291.5511.2141.
- Korytar, P., H. Janssen, E. Matisova, and U. A. Brinkman. Practical fast gas chromatography: methods, instrumentation and applications. *Trends in Analytical Chemistry*, 21(9-10):558–572, 2002. doi:10.1016/S0165-9936(02)00811-7.
- Krieger, J. and H. Breer. Olfactory reception in invertebrates. *Science*, 286(5440):720–723, 1999. doi:10.1126/science.286.5440.720.
- Kulmala, M., H. Vehkamäki, T. Petäjä, M. Dalmaso, A. Lauri, V. Kerminen, W. Birmili, and P. McMurry. Formation and growth rates of ultrafine atmospheric particles: a review of observations. *Journal of Aerosol Science*, 35(2):143–176, 2004. doi:10.1016/j.jaerosci.2003.10.003.
- Kundu, S., K. Kawamura, and M. Lee. Seasonal variations of diacids, ketoacids, and -dicarbonyls in aerosols at Gosan, Jeju Island, South Korea: Implications for sources, formation, and degradation during long-range transport. *Journal of Geophysical Research*, 115(D19):D19307, 2010. doi:10.1029/2010JD013973.
- Kurten, T., M. Kulmala, M. D. Maso, T. Suni, A. Reissell, H. Vehkamäki, P. Hari, A. Laaksonen, Y. Viisanen, and T. Vesala. Estimation of different forest-related contributions to the radiative balance using observations in southern Finland. *Boreal Environment Research*, 8(4):275–285, 2003.
- Laube, J. C. *Determination of the distribution of halocarbons in the tropical upper troposphere and stratosphere*. PhD dissertation, Johann Wolfgang Goethe University, Frankfurt, Germany, 2008.
- Law, K. S. and A. Stohl. Arctic air pollution: Origins and impacts. *Science*, 315(5818):1537–1540, 2007. doi:10.1126/science.1137695.

- Leclercq, P. A. and C. A. Cramers. Optimum performance of capillary GC columns as a function of tube diameter and film thickness under various operating conditions. computer program for calculation of h- curves and minimum analysis times. *Journal of High Resolution Chromatography*, 8(11):764–771, 1985. doi:10.1002/jhrc.1240081112.
- Lindinger, W., A. Hansel, and A. Jordan. Proton-transfer-reaction mass spectrometry (ptr-ms): on-line monitoring of volatile organic compounds at pptv levels. *Chemical Society Reviews*, 27(5):347, 1998. doi:10.1039/a827347z.
- Liu, Z. and J. B. Phillips. High-speed gas chromatography using an on-column thermal desorption modulator. *Journal of Microcolumn Separations*, 1(5):249–256, 1989. doi:10.1002/mcs.1220010508.
- Lobert, J. M., D. H. Scharffe, W. M. Hao, and P. J. Crutzen. Importance of biomass burning in the atmospheric budgets of nitrogen-containing gases. *Nature*, 346(6284):552–554, 1990. doi:10.1038/346552a0.
- Lovelock, J. E. A sensitive detector for gas chromatography. *Journal of Chromatography A*, 1:35–46, 1958. doi:10.1016/S0021-9673(00)93398-3.
- Ludwig, J., F. X. Meixner, B. Vogel, and J. Förstner. Soil-air exchange of nitric oxide: An overview of processes, environmental factors, and modeling studies. *Biogeochemistry*, 52(3):225–257, 2001. doi:10.1023/A:1006424330555.
- Martin, A. J. P. The development of partition chromatography. In *Nobel Lectures, Chemistry 1942-1962*, pages 359–371. Elsevier Publishing Company, Amsterdam, 1964.
- Martin, A. J. P. and R. L. M. Synge. A new form of chromatogram employing two liquid phases i. a theory of chromatography 2. application to the micro-determination of the higher monoamino-acids in proteins. *Biochemical Journal*, 35:1358–1368, 1941.
- Matisová, E. and M. Dömötöróvá. Fast gas chromatography and its use in trace analysis. *Journal of Chromatography A*, 1000(1-2):199–221, 2003. doi:10.1016/S0021-9673(03)00310-8.
- Maštovská, K. and S. J. Lehotay. Practical approaches to fast gas chromatography-mass spectrometry. *Journal of Chromatography A*, 1000(1-2):153–180, 2003. doi:10.1016/S0021-9673(03)00448-5. A Century of Chromatography 1903-2003.
- Olivier, J. G. J., J. A. V. Aardenne, F. J. Dentener, V. Pagliari, L. N. Ganzeveld, and J. A. H. W. Peters. Recent trends in global greenhouse gas emissions: regional trends and spatial distribution of key sources in 2000. *Environmental Sciences*, 2(2-3):81–99, 2005. doi:10.1080/15693430500400345. The EDGAR version 3.2 Fast Track 2000 inventory is available at <http://www.mnp.nl/edgar/model/v32ft2000edgar>.
- Olivier, J. G. J., J. P. J. Bloos, J. J. M. Berdowski, A. J. H. Visschedijk, and A. F. Bouwman. A 1990 global emission inventory of anthropogenic sources of carbon monoxide on $1^\circ \times$

1° developed in the framework of EDGAR/GEIA. *Chemosphere - Global Change Science*, 1(1-3):1–17, 1999. doi:10.1016/S1465-9972(99)00019-7.

Penkett, S., R. Burgess, H. Coe, I. Coll, O. Hov, A. Lindskog, N. Schmidbauer, S. Solberg, M. Roemer, and T. Thijsse. Evidence for large average concentrations of the nitrate radical (NO₃) in western europe from the HANSA hydrocarbon database. *Atmospheric Environment*, 41(16):3465–3478, 2007. doi:10.1016/j.atmosenv.2006.11.055.

Plass-Dülmer, C., K. Michl, R. Ruf, and H. Berresheim. C₂-C₈ hydrocarbon measurement and quality control procedures at the global atmosphere watch observatory hohenpeissenberg. *Journal of Chromatography A*, 953(1-2):175–197, 2002. doi:10.1016/S0021-9673(02)00128-0.

Pollmann, J., D. Helmig, J. Hueber, C. Plass-Dülmer, and P. Tans. Sampling, storage, and analysis of C₂-C₇ non-methane hydrocarbons from the US national oceanic and atmospheric administration cooperative air sampling network glass flasks. *Journal of Chromatography A*, 1188(2):75–87, 2008. doi:10.1016/j.chroma.2008.02.059.

Pollmann, J., D. Helmig, J. Hueber, D. Tanner, and P. Tans. Evaluation of solid adsorbent materials for cryogen-free trapping—gas chromatographic analysis of atmospheric C₂–C₆ non-methane hydrocarbons. *Journal of Chromatography A*, 1134(1-2):1–15, 2006. doi:10.1016/j.chroma.2006.08.050.

Pollmann, J., J. Ortega, and D. Helmig. Analysis of atmospheric sesquiterpenes: Sampling losses and mitigation of ozone interferences. *Environmental Science & Technology*, 39(24):9620–9629, 2005. doi:10.1021/es050440w.

Pozzer, A., J. Pollmann, D. Taraborrelli, P. Jöckel, D. Helmig, P. Tans, J. Hueber, and J. Lelieveld. Observed and simulated global distribution and budget of atmospheric C₂–C₅ alkanes. *Atmospheric Chemistry and Physics*, 10(9):4403–4422, 2010. doi:10.5194/acp-10-4403-2010.

Rappenglück, B., E. Apel, M. Bauerfeind, J. Bottenheim, P. Brickell, P. Cavolka, J. Cech, L. Gatti, H. Hakola, and J. Honzak. The first voc intercomparison exercise within the global atmosphere watch (gaw). *Atmospheric Environment*, 40(39):7508–7527, 2006. doi:10.1016/j.atmosenv.2006.07.016.

Rinne, J., J. Bäck, and H. Hakola. Biogenic volatile organic compound emissions from the eurasian taiga: current knowledge and future directions. *Boreal Environment Research*, 14(4):807–826, 2009.

Schoenmakers, P. J., J. L. M. M. Oomen, J. Blomberg, W. Genuit, and G. van Velzen. Comparison of comprehensive two-dimensional gas chromatography and gas chromatography - mass spectrometry for the characterization of complex hydrocarbon mixtures. *Journal of Chromatography A*, 892(1-2):29–46, 2000. doi:10.1016/S0021-9673(00)00744-5.

- Shiojiri, K., T. Maeda, G. ichiro Arimura, R. Ozawa, T. Shimoda, and J. Takabayashi. Functions of plant infochemicals in tritrophic interactions between plants, herbivores and carnivorous natural enemies. *Japanese Journal of Applied Entomology and Zoology*, 46(3):117–133, 2002. doi:10.1303/jjaez.2002.117.
- Sihto, S., J. Mikkilä, J. Vanhanen, M. Ehn, L. Liao, K. Lehtipalo, P. P. Aalto, J. Duplissy, T. Petäjä, V. Kerminen, M. Boy, and M. Kulmala. Seasonal variation of CCN concentrations and aerosol activation properties in boreal forest. *Atmospheric Chemistry and Physics Discussions*, 10(11):28231–28272, 2010. doi:10.5194/acpd-10-28231-2010.
- Sillman, S. The relation between ozone, NO_x and hydrocarbons in urban and polluted rural environments. *Atmospheric Environment*, 33(12):1821–1845, 1999.
- Spracklen, D. V., B. Bonn, and K. S. Carslaw. Boreal forests, aerosols and the impacts on clouds and climate. *Philosophical Transactions of the Royal Society A*, 366(1885):4613–4626, 2008. doi:10.1098/rsta.2008.0201.
- Toon, G. C., J. Blavier, B. Sen, J. J. Margitan, C. R. Webster, R. D. May, D. Fahey, R. Gao, L. D. Negro, M. Proffitt, J. Elkins, P. A. Romashkin, D. F. Hurst, S. Oltmans, E. Atlas, S. Schauffler, F. Flocke, T. P. Bui, R. M. Stimpfle, G. P. Bonne, P. B. Voss, and R. C. Cohen. Comparison of MkIV balloon and ER-2 aircraft measurements of atmospheric trace gases. *Journal of Geophysical Research*, 104(D21):26779–26790, 1999. doi:10.1029/1999JD900379.
- Tunved, P., H. Hansson, V. Kerminen, J. Ström, M. D. Maso, H. Lihavainen, Y. Viisanen, P. P. Aalto, M. Komppula, and M. Kulmala. High natural aerosol loading over boreal forests. *Science*, 312(5771):261–263, 2006. doi:10.1126/science.1123052.
- Tunved, P., J. Ström, M. Kulmala, V. Kerminen, M. D. Maso, B. Svenningsson, C. Lunder, and H. Hansson. The natural aerosol over northern europe and its relation to anthropogenic emissions—implications of important climate feedbacks. *Tellus B*, 60(4):473–484, 2008. doi:10.1111/j.1600-0889.2008.00363.x.
- Warneke, C., S. A. McKeen, J. A. de Gouw, P. D. Goldan, W. C. Kuster, J. S. Holloway, E. J. Williams, B. M. Lerner, D. D. Parrish, M. Trainer, F. C. Fehsenfeld, S. Kato, E. L. Atlas, A. Baker, and D. R. Blake. Determination of urban volatile organic compound emission ratios and comparison with an emissions database. *Journal of Geophysical Research*, 112(D10), 2007. doi:10.1029/2006JD007930.
- Williams, J. Organic trace gases in the atmosphere: An overview. *Environmental Chemistry*, 1(3):125, 2004. doi:10.1071/EN04057.
- Williams, J., J. Crowley, H. Fischer, H. Harder, M. Martinez, T. Petäjä, J. Rinne, J. Bäck, M. Boy, M. D. Maso, J. Hakala, M. Kajos, P. Keronen, P. Rantala, J. Aalto, H. Aaltonen, J. Paatero, T. Vesala, H. Hakola, J. Levula, T. Pohja, F. Herrmann, J. Auld, E. Mesarchaki, W. Song, N. Yassaa, A. Nölscher, A. M. Johnson, T. Custer, V. Sinha, J. Thieser, N. Pouvesle,

D. Taraborrelli, M. J. Tang, H. Bozem, Z. Hosaynali-Beygi, R. Axinte, R. Oswald, A. Novelli, D. Kubistin, K. Hens, U. Javed, K. Trawny, C. Breitenberger, P. J. Hidalgo, C. J. Ebben, F. M. Geiger, A. L. Corrigan, L. M. Russell, H. Ouwersloot, J. V. de Arellano, L. Ganzeveld, A. Vogel, M. Beck, A. Bayerle, C. J. Kampf, M. Bertelmann, F. Köllner, T. Hoffmann, J. Valverde, D. González, M. Riekkola, M. Kulmala, and J. Lelieveld. The summertime boreal forest field measurement intensive (HUMPPA-COPEC-2010): an overview of meteorological and chemical influences. *Atmospheric Chemistry and Physics Discussions*, 11(5):15921–15973, 2011. doi:10.5194/acpd-11-15921-2011.

Williams, J., H. Fischer, G. W. Harris, P. J. Crutzen, P. Hoor, A. Hansel, R. Holzinger, C. Warneke, W. Lindinger, B. Scheeren, and J. Lelieveld. Variability-lifetime relationship for organic trace gases: A novel aid to compound identification and estimation of HO concentrations. *Journal of Geophysical Research*, 105(D16):20473–20486, 2000. doi:10.1029/2000JD900203.

Williams, J., V. Gros, E. Atlas, K. Maciejczyk, A. Batsaikhan, H. F. Schöler, C. Forster, B. Quack, N. Yassaa, R. Sander, and R. V. Dingenen. Possible evidence for a connection between methyl iodide emissions and saharan dust. *Journal of Geophysical Research*, 112(D7), 2007a. doi:10.1029/2005JD006702.

Williams, J., N. Yassaa, S. Bartenbach, and J. Lelieveld. Mirror image hydrocarbons from tropical and boreal forests. *Atmospheric Chemistry and Physics*, 7(3):973–980, 2007b. doi:10.5194/acp-7-973-2007.

Acknowledgements

For data security reasons, the acknowledgements have been removed from the online version.

Appendix A

A Comprehensive, Integrated, Modular Electronic Control System*

In any complicated analytic instrument, it is necessary to integrate many different devices, such as mass flow controllers, temperature sensors, pressure sensors, heaters, valves, and so forth. Unfortunately, if any commercial software exists to control these devices, it is often limited to a specific device with cumbersome communication to other software. Therefore, a single, comprehensive system to power and control all associated devices would be desired to simplify construction while increasing the performance and reliability of complicated instruments. The ability to log the readings from all associated devices is also necessary for later data analysis and quality control. Ideally, such a system would be based on modular control units, allowing the system to be customized to meet the needs of any particular instrument. Furthermore, a common, institute-wide system promotes synergies between research groups and pooling of experience.

Currently, many commercial solutions from the professional down to the hobbyist level are available. Professional examples include systems from National Instruments (NI Hardware plus LabView graphical programming environment) and Agilent (hardware + HP-VEE). The scientific software Mathworks MatLab/Simulink or Wavemetrics IGOR are also capable of input processing through third-party interfaces. On the hobbyist level, modular hardware systems available include systems similar to the BASIC driven C-Control from Conrad, which would still be applicable to some limited applications.

The vast majority of professional systems are optimized for big markets, such as automotive test benches, where many fast, medium resolution signals are to be captured. For economical and efficiency reasons, they are desktop computer based, support only low level input or output and are typically run in indoor environments on reliable high power grids. Size, weight, price, power consumption, scalability, outdoor ruggedness, application and programming flexibility are not of major concern.

*The author wishes to especially thank Frank Helleis for his input on this appendix. For more detailed construction details, including module schematics, please contact Frank Helleis at frank.helleis@mpic.de.

A.1 A New Process Control System

Therefore, to meet the needs of the Max Planck Institute for Chemistry, the Electronics Group developed a comprehensive, modular electronic control system, named after the x86 compatible host processor NEC V25. The hardware of the system consists of a small set of interface modules for the input from and output to analog devices. The main difference between this new hardware and the above mentioned commercial systems is the philosophy of complete integration of power supply, local preprocessing, fieldbus communication, and the analog front end on every interface module.

Each interface module has its own dc-dc-converter (input 12–48 Vdc) providing for all the voltages needed locally and galvanic isolation if necessary. This guarantees simple arbitrary expansion of the system without central power supply constraints or changes. Also, all power is only converted once in the system, and no converter needs to be over-sized, giving ultimate efficiency. Distributed power, quasi resonant design of the converters and cooling via the PC boards only eliminate the need for heat sinks, fans, and/or holes for air circulation.

All sensor modules provide galvanic isolation to the backplane power grid, therefore minimizing conducted noise interference from power modules within the same system. Temperature sensors, active and passive flow and pressure sensors and even controllers can easily be connected directly to one of two standard interface modules. For sensors, the general connectivity feature is common to all commercially available modular systems, while the galvanic isolation feature is not common at all.

Unlike commercial modular systems, the MPI system extends this hardware integration philosophy to actuators as well. Valves, pumps, fans, dc-, ac-, and stepper motors, filaments of ion sources, lenses, electron multipliers, diode lasers, discharge lamps and so on can all be connected directly without any glue circuitry to the appropriate interface module. Even line voltage modulators are available for regulation of kW Heaters and AC motors. A selection of five, redundantly-designed modules, most of them galvanically isolated with self-test features and output voltage and current read-out, serve for these purposes. For efficient local preprocessing and communication, each of the latest modules has at least one local embedded processor presenting a standard hardware (serial fieldbus) and software (public memory area) framework to the V25 host environment.

The flexibility of the V25 system is extended by the in-house developed host environment. With a core operating system transparent to the user, only the project specific object definitions and controlling procedures need be written for each individual instrument. Following this modular hardware and simplified software strategy, a system can be assembled and programmed for virtually any instrument application with minimum effort, running control procedures in parallel to monitoring signals, while logging selected values, typically at a frequency between 1 and 20 Hz.

This appendix will describe the function and capabilities of the V25 system used the FOTOS instrument. Section A.2 will discuss the standard hardware common to all V25 systems, including power requirements. Section A.3 will then detail the various modules

available. Section A.4 will discuss the various program files necessary for running a V25. Section A.5 will highlight the performance and capabilities of the V25 system with examples from the operation of FOTOS, which contains the most complex V25 to date.

A.2 Common Hardware and Construction

Each V25 consists of the same basic structure to which the modules are connected. The primary processing unit for the V25, called the V25Pro, consists of a processor unit (V25-Module), a COM port unit with up to 4 COM ports, and a PCMCIA flash storage disk. The V25-Module (MME Berlin) is an 8 MHz, Intel-compatible 8086 microcomputer, with 512 kB RAM, 512 kB Flash drive, watchdog and an 8 bit external bus interface. It can be configured with a Ram Disk of up to 256 kB and a removable flash memory card. Due to operating system limitations, only approximately 256 MB of the PCMCIA disk are accessible.

The V25Pro connects with a 10 MBit serial link to one or more backplanes, which in the first versions served as coprocessors and switches, in the newer versions only as switches. Each backplane is connected to an 8-port module bus, with 28, 5, ± 15 Vdc, an 8 bit general purpose bus, clock and reset signals available at each module port. The 8 bit general purpose bus is freely programmable by a field programmable gate array mounted on the backplane. Therefore, older modules with special backplane interfaces can be mixed with the latest modules, which are run by standard logic level serial interfaces.

The V25 is housed in a standard 19 inch, 3U rack and powered by a single 28 Vdc input. Communication with the V25 is possible via either the on-board display and six-key keypad or by serial RS232, USB, or LAN communication.

A.3 Input and Output Modules

The versatility of the V25 system lies in the set of easily exchangeable input and output modules. This system also enables the development of new modules that can be used alongside older models. Due to the difficulty and superfluity of updating every module with the newest model, some descriptions below will be somewhat redundant, but efforts will be made to clarify important differences. The FOTOS V25 consists of two backplanes containing four AIN8xC modules, two AIN8xE modules, three DCDC1x modules, two DC8x modules, two SCR3x modules, and three MFC4x modules, in addition to utilizing two RS232 communication ports.

A.3.1 AIN8xC

The AIN8x module receives analog input at eight channels. Each channel can be individually configured to read any one of a variety of sensors by means of a series of removable resistors and bridges, which produce the proper voltage division for the reading of changes in resistance, voltage, or current. Excited sensors with typically two supply conductors have to be connected in a specific way and use the resources of two adjacent channels. The temporal resolution of each channel of the AIN8xC module is 200 ms, and the resolution of the integrating converter is about 13 bits. This is more than sufficient for most applications. This module is generally

very robust and stable. Possible inputs include: thermistors, PT100 (two- or four-lead kinds), thermocouples, 0–5 Vdc, 0–10 Vdc, and 4–20 mA.

A.3.2 AIN8xE

The AIN8xE module is an update to the AIN8xC and takes advantage of an on-board processor which allows the module to provide much higher resolution. The temporal resolution of this module is 200 ms, and the analog to digital resolution is nominally 24 bits, realistically up to 20 bits. Thermocouples and voltage readings that required higher resolution (e.g. SamplePress) should be connected to an AIN8xE module. Care should be taken that sensors on coupled inputs (0&1, 2&3, 4&5, 6&7) are electrically isolated, or grounding loops between components will cause irregularities to the input signals. These modules have a tendency to show large, short spikes in the signal, but improvements in V25 programming have nearly eliminated their frequency and impact.

A.3.3 DCDC1x

The DCDC1x module provides one channel of DC output. The voltage and current output varies based on the requirements of the user and must be specified before construction and installation of the on-board transformer. These modules are typically used to directly, resistively heat cryogenic traps. These modules allow the user to set the voltage as well as the current. To achieve high current flow, the DCDC1x has two or four coupled output channels.

A.3.4 DC8x

The DC8x module is an update to the DCDC8x and DCDC4x modules and provides eight channels of DC output from 0-supply Voltage, at 2 A per channel. These modules are typically used to power DC heaters, fans, motors, even stepper motors and torbomolecular pumps with special software. There is one 6.3–8 A fuse per four channels. For higher currents the outputs can be connected in parallel. They do not have the low current limit problem of the DCDC8x module and have the additional advantage of being able to not just set a voltage but also read the output voltage and current. This is a good tool for trouble shooting: if you have voltage but no current, then you have got a broken circuit.

A.3.5 SCR3x

The SCR3x module regulates power from an external source, commonly an AC supply. The external source is connected to the first channel, and the remaining three channels can be used to power heaters or other devices requiring a higher, variable power supply. Each channel, input and output, has its own fuse, typically 6 A. For low power devices, some voltage leakage may be observed when the channel is turned off.

A.3.6 MFC4x

The MFC4x module controls four mass flow controllers (MFCs), or reads active capacitance pressure sensors. The first channel comes off the end of the module, and the other three are

connected with flat controller cable to the module. Therefore, these modules are typically mounted to position 6 or 7 of the backplane, providing space at the output for additional connections. In the FOTOS V25, several MFC controls are consolidated into one cable and plug, and these connections are also consolidated inside the V25 box.

A.4 Programming and Software

The V25 controller runs an extended Pascal developing environment on top of a tiny event driven multitasking operating system, both developed in-house. After years of experience developing process control systems and the corresponding user interfaces, it was recognized that the user interface consumes about 90 percent of the development and rework time when making changes. The logical consequence was to develop a canonical user interface generator, which can build both local and remote user interfaces from simple object definitions, which are generated by the programmer of the process control system anyway. This system is designed such that the individual user has as many resources available, while needing to interact with the least amount of code. Project development is greatly assisted by an available protected-mode, real-time, PC simulation for the system. A rudimentary console application, a DOS-like, command-line interface with optimized functionality, provides an interface for file handling, timer management, and debugging.

A.4.1 Common Software

The operating system consists of a purely event-driven round robin multitasking scheduler and a set of embedded drivers for serial communication, real-time clock, and disk support. The application programming interface is some forty system calls for task management, event handling, file handling, binary input/output, time/date support, math support and low level data conversion routines. Communication between tasks (system or application) is accomplished by means of system calls or events. Application programming almost exclusively uses absolutely timed or change-of-value events of user variables. This establishes an extremely simple and uniform data flow model as used in commercial graphical programming languages like LabVIEW.

The in-house designed Pascal Compiler makes use of these special features of the operating system extensively. By producing real machine code and the evaluation of the addresses of static variable structures at compile time, performance is optimized. Many lightweight tasks, rarely more than thirty lines of code, run in parallel to serve very specific jobs. Tasks are defined in a natural way as simple procedures, and multiple timers can be started within one task. Except for the installation of events and timers, the event driven nature of the system remains completely transparent to the user/programmer. Project-specific programming is further simplified by using a component-oriented programming strategy, providing trivial assignment of object structures to code. Multiple instances of the same objects can be run in parallel.

Fixed and floating point libraries are designed to be completely exception free, so even divisions by zero give reasonable results and do not crash the system. The built-in PID

regulator component eases process control design, one must simply connect input and output to the respective variables. Parameter menus are created automatically.

The necessary procedures for running every module, as well as a set of standard regulators and controllers, are found in the hardware and module driver file (currently `HardModH.pas`). This file contains a large set of variable types and menu structures, including all those necessary for incorporating all existing modules. These definitions are followed by various constant declarations and interpolation tables. The driver file concludes with over fifty procedures and functions for controlling the modules and other basic functions, such as input calibration and regulation and writing log files. A set of functions for communication with Vici multi-position valves via RS232 communication are also included. This file is maintained centrally, and therefore also transparent to the individual user.

A.4.2 Project Specific Software

The general tools created in the driver file are implemented for each specific project with the associated configuration file. This file follows a pattern similar to the driver file. It begins with type and structure declarations, followed by declarations linking menu items to hardware inputs and outputs, and finally the set of procedures and functions to run the connected modules. The structure declarations in this file set the menu structure for the operation of the V25 as shown on the on-board display and PC interface application. Using the six-button keypad or PC interface, the user can navigate through these menus, monitoring inputs or setting controls and set points. An example configuration file (that for FOTOS) can be seen in App. B.

There are a number of other files which may interact or be written by a V25 configuration file. While any menu item may be set during the initial booting of the system, any item can also be stored and loaded from a parameter file of arbitrary name. The configuration file defines the format and output of any number of desired log files. Duplication, and thereby overwriting, of log files is prevented by naming the files with the current time and logger specific extension, stored in a folder whose name is the current date. The reading and writing of other files is also possible, for example, reading in long or complicated control sequences or writing event (instead of time) triggered log files.

A.5 Performance and Capabilities

The performance and capabilities of the V25 can be demonstrated by examining one case study. The most complicated V25 to date is that for FOTOS, consisting of two full backplanes. This system currently controls and/or monitors eleven mass flow controllers, three high current heaters, eight valves and relays, five AC heaters, three DC heaters, five thermocouples, two pressure gauges, seven analog voltage inputs, two Pt100s, six thermistors, and three Vici multi-position valves. These values, along with a set of controlling and status variables, are recorded in four different log files of differing logging frequency. During the HUMPPA campaign in July and August of 2010 (see Chap. 4), this system ran continuously for five weeks. In that time, one module (a newly constructed DCDC1x, completed one week before

the campaign) needed repair* after two weeks of use. However, this module was quickly repaired and functioned the remaining two weeks without any sign of persisting problems. Otherwise, the only issue for this entire campaign was that on three different occasions, the communication between the V25 and one of the Vici multi-position valves failed. After the first occurrence, the configuration file was adjusted to perform a soft restart of the control program. This adjustment was successful in allowing the V25 to recover after the following two errors without user intervention, resulting in the loss of only a single measurement.

A.6 Conclusion

The comprehensive, integrated, modular electronic control system developed by the Electronics Group of the Max Planck Institute for Chemistry has been shown to meet the needs of a complex analytic instrument by incorporating the input and control of a wide range of devices into one system. Furthermore, the modular nature of this system allows it to be easily customized to the specific needs of a large variety of systems. These capabilities have been demonstrated clearly in the extended, reliable operation of FOTOS, a complex system requiring the integrated control of fifty-five different sensors, heaters, and other devices while logging over fifty different values at regular intervals (1–20 seconds).

*This was due to a known construction error. The copper sheet between the secondary coils and the output was not constructed to specifications and melted.

Appendix B

FastGCf2.pas

```
program main;

uses system, pidreg, vsio, HardModH;

type
TrapCtrlType = (off, manual, Cool, Heat, auto);
ProcedureType = (off, DewarFill, Purge, FlowMax, TakeOff, Prepare, Auto, Error);
PrepStateType = (off, FlowMax, Purge, TakeOff, DewarPrep, OKtoFill, Prepping, WtTZReady, Prepared);
SampStateType = (off, PrepTraps, Sampling, SampChase, WaitInjst, Transfer);
InjstStateType = (off, PrepInjst, InjstReady, WaitGCMS, Injecting);
FailType = (__, HeatError, DewarPres, N2LvlLow, TrapBox, InjstTime, SampTime, MupoPos);
SeqCtrlType = (Sample, Bottle, Zero, Calib, Curve, FileSeq);
StatusType = (busy, ready);

CyclStatStruct = object(AllInstanceRec)
  PrepState : PrepStateType; {wr=0}
  Running : OffOnType; {wr=0}
  SampState : SampStateType; {wr=0}
  SampTimer : TimeInst; {wr=0;show=timerel}
  InjstState : InjstStateType; {wr=0}
  InjstTimer : TimeInst; {wr=0;show=timerel}
  RunType : StringInst; {wr=0}
  NextRun : StringInst; {wr=0}
  FailState : FailType; {wr=0}
  FailCount : LongInst; {wr=0}
  LocalTime : TimeInst; {show=timesys}
end;

ViewStruct = object(AllInstanceRec)
  UTC : TimeInst; {wr=0;show=timesys}
  SampState : ^SampStateType;
  InjstState : ^InjstStateType;
  SampPress : ^SingleInst;
  TCryo : ^SingleInst;
  TEnrich : ^SingleInst;
  TWater : ^SingleInst;
  FlshWater : ^SingleInst;
  FlshTrans : ^SingleInst;
  FlshSamp : ^SingleInst;
  SampleFC : ^SingleInst;
  Valves : ^LongInst;
  TrapsMupo : ^MuposType;
  SourceMupo : ^MuposType;
  GCStatus : ^StatusType;
  MSSStatus : ^StatusType;
  TSamp : ^SingleInst;
  GCColTemp : ^SingleInst;
end;

TrapsLogStruct = object(AllInstanceRec)
  UTC : ^TimeInst; {show=timesys}
  TCryo : ^SingleInst;
  TCryoPo : ^SingleInst;
  FCryo : ^SingleInst;
  TEnrich : ^SingleInst;
  TEnrichPo : ^SingleInst;
  FEnrich : ^SingleInst;
  TWater : ^SingleInst;
  TWaterPo : ^SingleInst;
  FWater : ^SingleInst;
end;

Check1Struct = object(AllInstanceRec)
  UTC : ^TimeInst; {show=timesys}
  N2Press : ^SingleInst;
  N2PressPo : ^SingleInst;
  N2Temp : ^SingleInst;
  N2Level : ^SingleInst;
  TRackInlet : ^SingleInst;
end;
```

```

TCatalyst      : ^SingleInst;
TCatalyPo     : ^SingleInst;
ZeroAirFC     : ^SingleInst;
StandLoFC     : ^SingleInst;
StandHiFC     : ^SingleInst;
InletFC       : ^SingleInst;
InletMupo    : ^MuposType;
end;

Check2Struct   = object(AllInstanceRec)
  UTC          : ^TimeInst;    {show=timesys}
  TTMupo     : ^SingleInst;
  TTMupoPo   : ^SingleInst;
  TSMupo     : ^SingleInst;
  TSMupoPo   : ^SingleInst;
  TTBBoxH     : ^SingleInst;
  TTBBoxL     : ^SingleInst;
  TTBBox1Po   : ^SingleInst;
  TTBBox2Po   : ^SingleInst;
  TInjector   : ^SingleInst;
  TInjectPo   : ^SingleInst;
  TINlet1     : ^SingleInst;
  TINlet1Po   : ^SingleInst;
  TINlet2     : ^SingleInst;
  TINlet2Po   : ^SingleInst;
  TExtend     : ^SingleInst;
  TExtendPo   : ^SingleInst;
end;

ControlStruct  = object(AllInstanceRec) {task : Hd1Ctrl; stack:2048}
  AutoStart   : OffOnType;
  ProcCtrl    : ProcedureType;
  MainCtrl    : OffOnType;
  ThermZones  : ProcessType;
  ThermState  : StatusType; {wr=0}
  TrapsMain   : TrapCtrlType;
  LoggerMain  : ^OffOnType;
  Param       : ParamStruct;
  FailReset   : OffOnType;
  PurgeTime   : TimeInst;    {param=1;show=timerel}
  MaxSampTm   : TimeInst;    {param=1;show=timerel}
  MaxInjtTm   : TimeInst;    {param=1;show=timerel}
  MaxFail     : LongInst;    {param=1}
end;

ReadRunStruct  = object(AllInstanceRec)
  SeqLine     : LongInst;    {wr=0}
  Inlet       : LongInst;    {wr=0}
  SampType    : SeqCtrlType; {wr=0}
  CallLv1    : SingleInst;   {wr=0}
end;

RunSeqStruct   = object(AllInstanceRec) {task : Hd1RunSeq; stack:2048}
  SeqCtrl     : SeqCtrlType;
  RunSeqFile  : FileInst;    {param=1}
  CurveFile   : FileInst;    {param=1}
  FileStatus  : BoolInst;    {wr=0;range=___,loaded,notFound}
  NextLine    : LongInst;    {wr=0;min=1}
  NextInlet   : LongInst;    {min=1;max=2}
  NextSample  : SeqCtrlType; {wr=0}
  NextCallLv1 : SingleInst;  {min=0}
  ReadRun     : ReadRunStruct;
  Advance     : OffOnType;
  SetLine     : LongInst;    {min=0}
end;

EnvirStruct    = object(AllInstanceRec)
  N2Level     : ^SingleInst;
  N2Temp      : ^SingleInst;
  N2Press     : ^SingleInst;
  N2PressReg  : RegulStruct;
  MinN2Level  : SingleInst;   {param=1;min=0}
  PressTol    : SingleInst;   {param=1;min=0}
  AveInt      : SingleInst;   {param=1;min=1}
end;

HeatChkStruct  = object(AllInstanceRec) {task : HeaterCheck; stack:1024}
  Expected    : SingleInst;   {wr=0}
  Error       : SingleInst;   {wr=0}
  Tolerance   : SingleInst;   {param=1;max=0}
  HeatRate    : SingleInst;   {param=1;dec=3;min=0}
  HoldPower   : SingleInst;   {param=1;min=0}
  CutTime     : LongInst;    {param=1;min=200}
  MaxFail     : LongInst;    {param=1;min=1}
  FailCount   : LongInst;    {min=0}
  Heater      : ^RegulStruct;
end;

TrapStruct     = object(AllInstanceRec) {task : Hd1Trap; stack:1024}
  Temp        : ^SingleInst;
  Flow        : ^SingleInst;
  CycleCtrl   : TrapCtrlType;
  Status      : StatusType;   {wr=0}
  HeatCheck   : HeatChkStruct;
end;

```

```
HeatCtrl      : ^ProcessType;
CoolCtrl      : ^ProcessType;
PowerOut      : SingleInst;    {wr=0}
HeatMax       : SingleInst;    {param=1;min=0}
TempTol      : SingleInst;    {param=1;min=0}
MaxVolt      : SingleInst;    {wr=0}
SetVolt      : ^SingleInst;   {public=0}
HeatReg       : RegulStruct;
CoolReg       : RegulStruct;
TrapTemp     : TCalibStruct;
FC_N2        : ^MFCStruct;
end;

DewarStruct   = object(AllInstanceRec)
  Environment : EnvirStruct;
  CryoTrap    : TrapStruct;
  EnrichTrap  : TrapStruct;
  WaterTrap   : TrapStruct;
  PurgeWCtrl  : OffOnType;
end;

ViciStruct    = object(AllInstanceRec) {task : MupoServer; stack:4096}
  TrapsMupo  : MupoStruct;
  SourceMupo : MupoStruct;
  InletMupo  : MupoStruct;
  ComRs232   : FileInst;
  NewID      : LongInst;    {min=-1;max=9}
  SetID      : MuPoSetIDType;
  TTMupo   : ^SingleInst;
  TSMupo   : ^SingleInst;
  MupoTmOut : LongInst;    {Param=1}
end;

FlowsStruct   = object(AllInstanceRec)
  InletFC     : ^MFCStruct;
  ZeroAirFC   : ^MFCStruct;
  StandLoFC   : ^MFCStruct;
  StandHiFC   : ^MFCStruct;
  SampleFC    : ^MFCStruct;
  FlshWater   : ^MFCStruct;
  FlshTrans   : ^MFCStruct;
  FlshSamp    : ^MFCStruct;
  N2PurgeFC   : ^MFCStruct;
end;

AValve8Struct = object(AllInstanceRec) {alias : Valve8Struct}
  ValvePanel  : LongInst;    {show=bits8;param=1}
  CalVolIn    : ExtBitStruct;
  CalVolOut   : ExtBitStruct;
  InletSel    : ExtBitStruct;
  GCFan       : ExtBitStruct;
  ZABypass    : ExtBitStruct;
  StandIn     : ExtBitStruct;
  GCStart     : ExtBitStruct;
  MSStart     : ExtBitStruct;
end;

LineHeatStruct = object(AllInstanceRec) {task : HdlLines; stack:3072}
  TMupoReg   : RegulStruct;
  SMupoReg   : RegulStruct;
  TBox1Reg    : RegulStruct;
  TBox2Reg    : RegulStruct;
  InjectorReg : RegulStruct;
  Inlet1Reg   : RegulStruct;
  Inlet2Reg   : RegulStruct;
  ExtendReg   : RegulStruct;
  TTBoxH      : SingleInst;  {wr=0}
  TTBoxL      : SingleInst;  {wr=0}
  TBoxMin     : SingleInst;  {param=1}
end;

SamplingStruct = object(AllInstanceRec) {task : HdlCalVol; stack:1024}
  SampPress   : ^SingleInst;
  TSamp       : ^SingleInst;
  TRackInlet  : ^SingleInst;
  ViciMupos   : ViciStruct;
  Flows       : FlowsStruct;
  Valves      : AValve8Struct;
  LineHeaters : LineHeatStruct;
  PumpCalVol  : OffOnType;
  MinSmpPres  : SingleInst;  {param=1;min=0}
end;

GCMSStruct    = object(AllInstanceRec) {task:HdlGCMS; stack:1024}
  Start      : OffOnType;
  Status     : StatusType;   {wr=0}
  StatusIn   : UCalibStruct;
  StartOut   : ^ExtBitStruct;
  StatusHigh : LongInst;     {param=1}
  StartTime  : LongInst;     {param=1}
  StartSig   : ^SingleInst;
end;

ZACGStruct    = object(AllInstanceRec) {task : HdlZACG; stack:1024}
```

```

TCatalyst      : ^SingleInst;
ZeroRun        : OffOnType;
CalibRun       : OffOnType;
CalibLevel     : SingleInst;   {min=0}
CatStatus      : StatusType;   {wr=0}
CatSetTemp     : SingleInst;   {param=1}
CatTempTol    : SingleInst;   {param=1}
CatalystReg    : RegulStruct;
HeatCheck      : HeatChkStruct;
end;

ReadFlowStruct = object(AllInstanceRec)
  NextTime      : TimeInst;   {show=timerel;wr=0}
  NextValue     : SingleInst; {wr=0}
end;

GCFlowStruct   = object(AllInstanceRec) {task : Hd1GCFlow; stack:2048}
  GCFlowCtrl   : OffOnType;   {param=1}
  GCFlowTime   : TimeInst;   {show=timerel; wr=0}
  GCHeFlow     : ^SingleInst;
  GCHeSet      : ^SingleInst;
  GCCnstFlow   : SingleInst;  {param=1;min=0}
  InjectFlow   : SingleInst;  {param=1;min=0}
  GCFlowFile   : FileInst;    {param=1}
  FileStatus   : BoolInst;    {wr=0;range=___,loaded,notFound}
  GCFan        : ^ExtBitStruct;
  Running      : ^OffOnType;
  MSStartSig   : ^SingleInst;
  ReadFlow     : ReadFlowStruct;
end;

GCTempStruct   = object(AllInstanceRec)
  ColTemp      : ^SingleInst;
  Trans1       : ^SingleInst;
  Trans2       : ^SingleInst;
  GCSetTemp    : ^SingleInst;
end;

GCAuxStruct    = object(AllInstanceRec)
  GCFlowProg   : GCFlowStruct;
  GCTemps      : GCTempStruct;
end;

SampParaStruct = object(AllInstanceRec)
  SampSize     : SingleInst;  {param=1;min=0}
  CalVol       : SingleInst;  {param=1;min=0}
  ChaseTime    : TimeInst;    {param=1;show=timerel}
  TransTime    : TimeInst;    {param=1;show=timerel}
  WPurgeTime   : TimeInst;    {param=1;show=timerel}
  WaterCoolX   : TimeInst;    {param=1;show=timerel}
  InjectTime   : TimeInst;    {param=1;show=timerel}
  SamplePos    : MuposType;   {param=1}
  TransPos     : MuposType;   {param=1}
  PlugSource   : MuposType;   {param=1}
  HeSource     : MuposType;   {param=1}
  SampSource   : MuposType;   {param=1}
  Bot1Source   : MuposType;   {param=1}
  ZAG_Pos     : MuposType;   {param=1}
  InletPos     : MuposType;   {param=1}
end;

FlowParaStruct = object(AllInstanceRec)
  CollectF     : SingleInst;  {param=1;min=0}
  ChaseF       : SingleInst;  {param=1;min=0}
  CoolFlshF   : SingleInst;  {param=1;min=0}
  SampStdF    : SingleInst;  {param=1;min=0}
  WaterPurge  : SingleInst;  {param=1;min=0}
  WaterStdF   : SingleInst;  {param=1;min=0}
  InletF      : SingleInst;  {param=1;min=0}
  ZeroAirF    : SingleInst;  {param=1;min=0}
  N2PurgeF    : SingleInst;  {param=1;min=0}
end;

TempParaStruct = object(AllInstanceRec)
  TransTrig    : SingleInst;  {param=1;min=0;max=400}
  InjectTrig   : SingleInst;  {param=1;min=0;max=400}
  DewarSetP    : SingleInst;  {param=1;min=0}
  InjectSetT   : SingleInst;  {param=1;min=0}
  MupoSetT    : SingleInst;  {param=1;min=0}
  TBoxSetT    : SingleInst;  {param=1;min=0}
  InletSetT    : SingleInst;  {param=1;min=0}
  StdTemp     : SingleInst;  {param=1;dec=2;min=0}
  StdTOffSet  : SingleInst;  {param=1;dec=2;min=0}
  StdPress    : SingleInst;  {param=1;min=0}
end;

PhysicsStruct  = object(AllInstanceRec)
  Dewar        : DewarStruct;
  Sampling     : SamplingStruct;
  GC           : GCMSStruct;
  MS           : GCMSStruct;
  ZA_CG       : ZACGStruct;
  GC_Aux      : GCAuxStruct;
  SampParams   : SampParaStruct;

```



```

FlowParams : FlowParaStruct;
TempParams : TempParaStruct;
GCMS_Start : ProcessType;
end;

HardwareStruct = object(AllInstanceRec)
  BackPlanA : BackPlanStruct;
  BackPlanB : BackPlanStruct;
  Com2      : SIO;
end;

WorkUserStruct = object(AllInstanceRec)
  SampPress : UCalibStruct;
  N2Press   : UCalibStruct;
  N2Level   : UCalibStruct;
  ColTemp   : UCalibStruct;
  Trans1    : UCalibStruct;
  Trans2    : UCalibStruct;
  GCSetTemp : UCalibStruct;
end;

WorkTempStruct = object(AllInstanceRec) {task : HdlTemps; stack:4096}
  RefTemp : TCOffsuVStruct;
  TSamp   : TCalibStruct;
  TRackInlet : TCalibStruct;
  N2Temp  : TCalibStruct;
  TTBox1  : TCalibStruct;
  TTBox2  : TCalibStruct;
  TTMupo : TCalibStruct;
  TSMupo : TCalibStruct;
  TINjector : TCalibStruct;
  TINlet1  : TCalibStruct;
  TINlet2  : TCalibStruct;
  TExtend  : TCalibStruct;
  TCatalyst : TCalibStruct;
end;

WorkLogStruct = object(AllInstanceRec)
  LoggerMain : OffOnType;
  Viewer      : LoggerStruct;
  ViewState  : ^BoolInst;
  TrapsLogger : LoggerStruct;
  TrapsState  : ^BoolInst;
  Checker1    : LoggerStruct;
  Chk1State   : ^BoolInst;
  Checker2    : LoggerStruct;
  Chk2State   : ^BoolInst;
  ZALogHigh  : TimeInst; {param=1;show=timerel}
  ZALogLow   : TimeInst; {param=1;show=timerel}
end;

WorkStruct = object(AllInstanceRec) {task : HdlWork; stack:3072}
  TimeZone : TimeInst; {param=1;show=timerel}
  StartPress : SingleInst; {dec=2}
  RunList : FileInst; {param=1}
  FailList : FileInst; {param=1}
  DataDir : FileInst; {wr=0}
  BootTime : TimeInst; {wr=0;show=time}
  BootDate : TimeInst; {wr=0;show=date}
  LstSampTm : TimeInst; {wr=0;show=timerel}
  WorkUser : WorkUserStruct;
  WorkTemps : WorkTempStruct;
  WorkLogs : WorkLogStruct;
end;

UserStruct = object(AllInstanceRec)
  CycleStatus : CyclStatStruct;
  View        : ViewStruct;
  TrapsLog    : TrapsLogStruct;
  Check1      : Check1Struct;
  Check2      : Check2Struct;
  Control     : ControlStruct;
  Sequence    : RunSeqStruct;
  Physics     : PhysicsStruct;
  Hardware    : HardwareStruct;
  Work        : WorkStruct;
end;

const

UserData : UserStruct =
( View : ViewStruct =
  ( SampState : @CycleStatus.SampState;
    InjtState : @CycleStatus.InjtState;
    SampPress : @Physics.Sampling.SampPress;
    TCryo     : @Physics.Dewar.CryoTrap.Temp;
    TEnrich   : @Physics.Dewar.EnrichTrap.Temp;
    TWater    : @Physics.Dewar.WaterTrap.Temp;
    FlshWater : @Physics.Sampling.Flows.FlshWater.Flow;
    FlshTrans : @Physics.GC_Aux.GCFlowProg.GCHeFlow;
    FlshSamp  : @Physics.Sampling.Flows.FlshSamp.Flow;
    SampleFC  : @Physics.Sampling.Flows.SampleFC.Flow;
    Valves    : @Physics.Sampling.Valves.ValvePanel;
    TrapsMupo : @Physics.Sampling.ViciMupos.TrapsMupo.Position;
  )
)

```

```

SourceMupo : @Physics.Sampling.ViciMupos.SourceMupo.Position;
GCStatus   : @Physics.GC.Status;
MSStatus   : @Physics.MS.Status;
TSamp      : @Physics.Sampling.TSamp;
GCColTemp  : @Physics.GC_Aux.GCTemps.ColTemp;
);

TrapsLog : TrapsLogStruct =
(
  UTC       : @View.UTC;
  TCryo     : @Physics.Dewar.CryoTrap.Temp;
  TCryoPo   : @Physics.Dewar.CryoTrap.PowerOut;
  FCryo     : @Physics.Dewar.CryoTrap.Flow;
  TEnrich   : @Physics.Dewar.EnrichTrap.Temp;
  TEnrichPo : @Physics.Dewar.EnrichTrap.PowerOut;
  FEnrich   : @Physics.Dewar.EnrichTrap.Flow;
  TWater    : @Physics.Dewar.WaterTrap.Temp;
  TWaterPo  : @Physics.Dewar.WaterTrap.PowerOut;
  FWater    : @Physics.Dewar.WaterTrap.Flow;
);

Check1 : Check1Struct =
(
  UTC       : @View.UTC;
  N2Press   : @Physics.Dewar.Environment.N2Press;
  N2PressPo : @Physics.Dewar.Environment.N2PressReg.PowerFac;
  N2Temp    : @Physics.Dewar.Environment.N2Temp;
  N2Level   : @Physics.Dewar.Environment.N2Level;
  TRackInlet : @Physics.Sampling.TRackInlet;
  TCatalyst : @Physics.ZA_CG.TCatalyst;
  TCatalyPo : @Physics.ZA_CG.CatalystReg.PowerFac;
  ZeroAirFC : @Physics.Sampling.Flows.ZeroAirFC.Flow;
  StandLoFC : @Physics.Sampling.Flows.StandLoFC.Flow;
  StandHiFC : @Physics.Sampling.Flows.StandHiFC.Flow;
  InletFC   : @Physics.Sampling.Flows.InletFC.Flow;
  InletMupo : @Physics.Sampling.ViciMupos.InletMupo.Position;
);

Check2 : Check2Struct =
(
  UTC       : @View.UTC;
  TTMupo   : @Physics.Sampling.ViciMupos.TTMupo;
  TTMupoPo : @Physics.Sampling.LineHeaters.TMupoReg.PowerFac;
  TSMupo   : @Physics.Sampling.ViciMupos.TSMupo;
  TSMupoPo : @Physics.Sampling.LineHeaters.SMupoReg.PowerFac;
  TTBoxH    : @Physics.Sampling.LineHeaters.TTBoxH;
  TTBoxL    : @Physics.Sampling.LineHeaters.TTBoxL;
  TTBox1Po  : @Physics.Sampling.LineHeaters.TBox1Reg.PowerFac;
  TTBox2Po  : @Physics.Sampling.LineHeaters.TBox2Reg.PowerFac;
  TIinjector : @Physics.Sampling.LineHeaters.InjectorReg.Value;
  TIinjectPo : @Physics.Sampling.LineHeaters.InjectorReg.PowerFac;
  TInlet1   : @Physics.Sampling.LineHeaters.Inlet1Reg.Value;
  TInlet1Po : @Physics.Sampling.LineHeaters.Inlet1Reg.PowerFac;
  TInlet2   : @Physics.Sampling.LineHeaters.Inlet2Reg.Value;
  TInlet2Po : @Physics.Sampling.LineHeaters.Inlet2Reg.PowerFac;
  TExtend   : @Physics.Sampling.LineHeaters.ExtendReg.Value;
  TExtendPo : @Physics.Sampling.LineHeaters.ExtendReg.PowerFac;
);

Control : ControlStruct =
(
  LoggerMain : @Work.WorkLogs.LoggerMain;
  Param      : ParamStruct =
    (
      ParamFile : 'mc:UserData.ini';
      ParamData : @UserData;
    );
);

Physics : PhysicsStruct =
(
  Dewar : DewarStruct =
    (
      Environment : EnvirStruct =
        (
          N2Level : @Work.WorkUser.N2Level.Value;
          N2Temp  : @Work.WorkTemps.N2Temp.Temp;
          N2Press : @Physics.Dewar.Environment.N2PressReg.Value;
          N2PressReg : RegulStruct =
            (
              Value : @Work.WorkUser.N2Press.Value;
              Regulator : PID =
                (
                  PropBand : 10000;
                  IntTime  : 30000;
                  DiffTime : 0;
                  SamplePeriod : 200;
                );
            );
          HWHeatOut : @Hardware.BackPlanA.Modul3.Out0.SetVolt;
        );
    );
  CryoTrap : TrapStruct =
    (
      Temp : @Physics.Dewar.CryoTrap.TrapTemp.Temp;
      Flow : @Physics.Dewar.CryoTrap.FC_N2.Flow;
      HeatCheck : HeatChkStruct = (Heater : @Physics.Dewar.CryoTrap.HeatReg);
      HeatCtrl : @Physics.Dewar.CryoTrap.HeatReg.Control;
      CoolCtrl : @Physics.Dewar.CryoTrap.CoolReg.Control;
      MaxVolt : 1234.0;
      SetVolt : @Hardware.BackPlanA.Modul4.SetVolt;
      HeatReg : RegulStruct =
        (
          Value : @Physics.Dewar.CryoTrap.TrapTemp.Temp;
          Regulator : PID =
            (
              PropBand : 1800;
              IntTime  : 2000;
            );
        );
    );
);

```

```

        DiffTime      : 300;
        SamplePeriod  : 200;
    );
    HWHeatOut   : @Hardware.BackPlanA.Modul5.SetCurrent;
);
CoolReg       : RegulStruct =
( Value       : @Physics.Dewar.CryoTrap.TrapTemp.Temp;
  Regulator   : PID =
  ( PropBand  : 1800;
    IntTime   : 2000;
    DiffTime  : 300;
    SamplePeriod : 200;
  );
  HWCoolOut   : @Physics.Dewar.CryoTrap.FC_N2.SetFlow;
);
TrapTemp      : TCalibStruct =
( Sensor      : @Hardware.BackPlanB.Modul3.ConfCh1;
  HWCounts    : @Hardware.BackPlanB.Modul3.Ch1;
  TempOffsuV  : @Work.WorkTemps.RefTemp.TempOffsuV;
);
FC_N2        : @Hardware.BackPlanB.Modul7.MFC2;
);
EnrichTrap    : TrapStruct =
( Temp       : @Physics.Dewar.EnrichTrap.TrapTemp.Temp;
  Flow       : @Physics.Dewar.EnrichTrap.FC_N2.Flow;
  HeatCheck  : HeatChkStruct = (Heater : @Physics.Dewar.EnrichTrap.HeatReg);
  HeatCtrl   : @Physics.Dewar.EnrichTrap.HeatReg.Control;
  CoolCtrl   : @Physics.Dewar.EnrichTrap.CoolReg.Control;
  MaxVolt    : 1234.0;
  SetVolt    : @Hardware.BackPlanA.Modul5.SetVolt;
  HeatReg    : RegulStruct =
  ( Value     : @Physics.Dewar.EnrichTrap.TrapTemp.Temp;
    Regulator : PID =
    ( PropBand  : 1800;
      IntTime   : 2000;
      DiffTime  : 300;
      SamplePeriod : 200;
    );
    HWHeatOut  : @Hardware.BackPlanA.Modul4.SetCurrent;
  );
  CoolReg     : RegulStruct =
  ( Value     : @Physics.Dewar.EnrichTrap.TrapTemp.Temp;
    Regulator : PID =
    ( PropBand  : 1800;
      IntTime   : 2000;
      DiffTime  : 300;
      SamplePeriod : 200;
    );
    HWCoolOut  : @Physics.Dewar.EnrichTrap.FC_N2.SetFlow;
  );
  TrapTemp    : TCalibStruct =
  ( Sensor     : @Hardware.BackPlanB.Modul3.ConfCh2;
    HWCounts   : @Hardware.BackPlanB.Modul3.Ch2;
    TempOffsuV : @Work.WorkTemps.RefTemp.TempOffsuV;
  );
  FC_N2       : @Hardware.BackPlanB.Modul7.MFC3;
);
WaterTrap     : TrapStruct =
( Temp       : @Physics.Dewar.WaterTrap.TrapTemp.Temp;
  Flow       : @Physics.Dewar.WaterTrap.FC_N2.Flow;
  HeatCheck  : HeatChkStruct = (Heater : @Physics.Dewar.WaterTrap.HeatReg);
  HeatCtrl   : @Physics.Dewar.WaterTrap.HeatReg.Control;
  CoolCtrl   : @Physics.Dewar.WaterTrap.CoolReg.Control;
  MaxVolt    : 2.0;
  SetVolt    : @Hardware.BackPlanB.Modul5.SetVolt;
  HeatReg    : RegulStruct =
  ( Value     : @Physics.Dewar.WaterTrap.TrapTemp.Temp;
    Regulator : PID =
    ( PropBand  : 2000;
      IntTime   : 2500;
      DiffTime  : 300;
      SamplePeriod : 200;
    );
    HWHeatOut  : @Hardware.BackPlanB.Modul5.SetCurrent;
  );
  CoolReg     : RegulStruct =
  ( Value     : @Physics.Dewar.WaterTrap.TrapTemp.Temp;
    Regulator : PID =
    ( PropBand  : 2000;
      IntTime   : 2500;
      DiffTime  : 300;
      SamplePeriod : 200;
    );
    HWCoolOut  : @Physics.Dewar.WaterTrap.FC_N2.SetFlow;
  );
  TrapTemp    : TCalibStruct =
  ( Sensor     : @Hardware.BackPlanB.Modul3.ConfCh5;
    HWCounts   : @Hardware.BackPlanB.Modul3.Ch5;
    TempOffsuV : @Work.WorkTemps.RefTemp.TempOffsuV;
  );
  FC_N2       : @Hardware.BackPlanB.Modul7.MFC1;
);
);
Sampling      : SamplingStruct =

```

```

( SampPress : @Work.WorkUser.SampPress.Value;
  TSamp     : @Work.WorkTemps.TSamp.Temp;
  TRackInlet : @Work.WorkTemps.TRackInlet.Temp;
  ViciMupos : ViciStruct =
  ( TrapsMupo : MupoStruct =
    ( Position : @Physics.Sampling.ViciMupos.TrapsMupo.MupoEcho.IsPos;
      ID       : 1;
    );
    SourceMupo : MupoStruct =
    ( Position : @Physics.Sampling.ViciMupos.SourceMupo.MupoEcho.IsPos;
      ID       : 2;
    );
    InletMupo : MupoStruct =
    ( Position : @Physics.Sampling.ViciMupos.InletMupo.MupoEcho.IsPos;
      ID       : 3;
    );
    TTMupo    : @Physics.Sampling.LineHeaters.TMupoReg.Value;
    TSMupo    : @Physics.Sampling.LineHeaters.SMupoReg.Value;
  );
  Flows      : FlowsStruct =
  ( InletFC   : @Hardware.BackPlanA.Modul6.MFC0;
    ZeroAirFC : @Hardware.BackPlanA.Modul6.MFC3;
    StandLoFC : @Hardware.BackPlanA.Modul6.MFC2;
    StandHiFC : @Hardware.BackPlanA.Modul6.MFC1;
    SampleFC  : @Hardware.BackPlanA.Modul7.MFC0;
    FlshWater : @Hardware.BackPlanA.Modul7.MFC1;
    FlshTrans : @Hardware.BackPlanA.Modul7.MFC2;
    FlshSamp  : @Hardware.BackPlanA.Modul7.MFC3;
    N2PurgeFC : @Hardware.BackPlanB.Modul7.MFC0;
  );
  Valves     : AValve8Struct =
  ( CalVolIn  : ExtBitStruct = (HWOutput : @Hardware.BackPlanB.Modul4.Out2.SetVolt);
    CalVolOut : ExtBitStruct = (HWOutput : @Hardware.BackPlanB.Modul4.Out3.SetVolt);
    InletSel  : ExtBitStruct = (HWOutput : @Hardware.BackPlanA.Modul3.Out4.SetVolt);
    GCFan     : ExtBitStruct = (HWOutput : @Hardware.BackPlanB.Modul4.Out0.SetVolt);
    ZABypass  : ExtBitStruct = (HWOutput : @Hardware.BackPlanB.Modul4.Out4.SetVolt);
    StandIn   : ExtBitStruct = (HWOutput : @Hardware.BackPlanB.Modul4.Out5.SetVolt);
    GCStart   : ExtBitStruct = (HWOutput : @Hardware.BackPlanB.Modul4.Out7.SetVolt);
    MSStart   : ExtBitStruct = (HWOutput : @Hardware.BackPlanB.Modul4.Out6.SetVolt);
  );
  LineHeaters : LineHeatStruct =
  ( TMupoReg : RegulStruct =
    ( Value    : @Work.WorkTemps.TTMupo.Temp;
      Regulator : PID =
      ( PropBand : 1000;
        IntTime  : 20000;
        DiffTime : 0;
        SamplePeriod : 500;
      );
      HWHeatOut : @Hardware.BackPlanA.Modul2.Out0;
    );
  );
  SMupoReg   : RegulStruct =
  ( Value    : @Work.WorkTemps.TSMupo.Temp;
    Regulator : PID =
    ( PropBand : 1000;
      IntTime  : 20000;
      DiffTime : 0;
      SamplePeriod : 500;
    );
    HWHeatOut : @Hardware.BackPlanA.Modul2.Out1;
  );
  TBox1Reg    : RegulStruct =
  ( Value    : @Work.WorkTemps.TTBox1.Temp;
    Regulator : PID =
    ( PropBand : 1000;
      IntTime  : 30000;
      DiffTime : 0;
      SamplePeriod : 500;
    );
    HWHeatOut : @Hardware.BackPlanA.Modul3.Out5.SetVolt;
  );
  TBox2Reg    : RegulStruct =
  ( Value    : @Work.WorkTemps.TTBox2.Temp;
    Regulator : PID =
    ( PropBand : 1000;
      IntTime  : 30000;
      DiffTime : 0;
      SamplePeriod : 500;
    );
    HWHeatOut : @Hardware.BackPlanA.Modul3.Out6.SetVolt;
  );
  InjectorReg : RegulStruct =
  ( Value    : @Work.WorkTemps.TInjector.Temp;
    Regulator : PID =
    ( PropBand : 1000;
      IntTime  : 30000;
      DiffTime : 0;
      SamplePeriod : 500;
    );
    HWHeatOut : @Hardware.BackPlanA.Modul3.Out7.SetVolt;
  );
  Inlet1Reg   : RegulStruct =
  ( Value    : @Work.WorkTemps.TInlet1.Temp;
    Regulator : PID =

```

```

    ( PropBand      : 1000;
      IntTime       : 30000;
      DiffTime      : 0;
      SamplePeriod  : 500;
    );
    HWHeatOut      : @Hardware.BackPlanB.Modul6.Out0;
  );
  Inlet2Reg       : RegulStruct =
  ( Value          : @Work.WorkTemps.TInlet2.Temp;
    Regulator      : PID =
    ( PropBand      : 1000;
      IntTime       : 30000;
      DiffTime      : 0;
      SamplePeriod  : 500;
    );
    HWHeatOut      : @Hardware.BackPlanB.Modul6.Out1;
  );
  ExtendReg       : RegulStruct =
  ( Value          : @Work.WorkTemps.TExtend.Temp;
    Regulator      : PID =
    ( PropBand      : 1000;
      IntTime       : 30000;
      DiffTime      : 0;
      SamplePeriod  : 500;
    );
    HWHeatOut      : @Hardware.BackPlanB.Modul6.Out2;
  );
);
GC                : GCMSStruct =
( StatusIn        : UCalibStruct =
  ( Sensor         : @Hardware.BackPlanA.Modul0.ConfCh0;
    HWCounts       : @Hardware.BackPlanA.Modul0.Ch0;
  );
  StartOut        : @Physics.Sampling.Valves.GCStart;
  StartSig        : @Physics.GC.StartOut.HWOutput;
);
MS                : GCMSStruct =
( StatusIn        : UCalibStruct =
  ( Sensor         : @Hardware.BackPlanB.Modul0.ConfCh0;
    HWCounts       : @Hardware.BackPlanB.Modul0.Ch0;
  );
  StartOut        : @Physics.Sampling.Valves.MSStart;
  StartSig        : @Physics.MS.StartOut.HWOutput;
);
ZA.CG             : ZACGStruct =
( TCatalyst       : @Physics.ZA.CG.CatalystReg.Value;
  CatalystReg     : RegulStruct =
  ( Value          : @Work.WorkTemps.TCatalyst.Temp;
    Regulator      : PID =
    ( PropBand      : 1000;
      IntTime       : 5500;
      DiffTime      : 0;
      SamplePeriod  : 200;
    );
    HWHeatOut      : @Hardware.BackPlanA.Modul2.Out2;
  );
  HeatCheck       : HeatChkStruct = (Heater : @Physics.ZA.CG.CatalystReg);
);
GC_Aux           : GCAuxStruct =
( GCFlowProg     : GCFlowStruct =
  ( GCHeFlow      : @Physics.Sampling.Flows.FlshTrans.Flow;
    GCHeSet       : @Physics.Sampling.Flows.FlshTrans.SetFlow;
    GCFan         : @Physics.Sampling.Valves.GCFan;
    Running       : @CycleStatus.Running;
    MSStartSig    : @Physics.MS.StartSig;
  );
  GCTemps        : GCTempStruct =
  ( ColTemp       : @Work.WorkUser.ColTemp.Value;
    Trans1        : @Work.WorkUser.Trans1.Value;
    Trans2        : @Work.WorkUser.Trans2.Value;
    GCSetTemp     : @Work.WorkUser.GCSetTemp.Value;
  );
);
);
);
Hardware         : HardwareStruct =
( BackPlanA      : BackPlanStruct =
  ( Modul0        : Ain8xStruct   = (IOAdc : $A480);
    Modul1        : Ain8xStruct   = (IOAdc : $A4A0);
    Modul2        : SCR3xStruct   = (IOAdr  : $A410);
    Modul3        : DC8xStruct    = (IOAdr  : $A680);
    Modul4        : DCDC1xStruct  = (IOAdr  : $A600);
    Modul5        : DCDC1xStruct  = (IOAdr  : $A640);
    Modul6        : MFC4xStruct   = (AdcAdr : $A4C0; DacAdr : $A440; TbAdr : $A404);
    Modul7        : MFC4xStruct   = (AdcAdr : $A4E0; DacAdr : $A448; TbAdr : $A404);
  );
  BackPlanB      : BackPlanStruct =
  ( Modul0        : Ain8xStruct   = (IOAdc : $B480);
    Modul1        : Ain8xStruct   = (IOAdc : $B4A0; ConfCh2 : Thermist);
    Modul2        : Ain8xEStruct  = (IOAdr  : $B600; Power  : 240);
    Modul3        : Ain8xEStruct  = (IOAdr  : $B680; Power  : 240);
    Modul4        : DC8xStruct    = (IOAdr  : $B640);
    Modul5        : DC1xStruct    = (IOAdr  : $B6C0);
  );
);
);
);

```

```

Modul6      : SCR3xStruct = (IOAdr : $B410);
Modul7      : MFC4xStruct = (AdcAdr : $B4C0; DacAdr : $B440; TAdr : $B404);
);
Com2        : SIO =
( PortAddr   : 0;
  Baud       : 9600;
  Bits       : 8;
  StopBits   : 1;
  Parity     : none;
  Handshake  : XonXoff;
  Protocol   : MultiFile;
);
);
Work        : WorkStruct =
( WorkUser   : WorkUserStruct =
  ( SampPress : UCalibStruct =
    ( Sensor   : @Hardware.BackPlanB.Modul2.ConfCh7;
      HWCOUNTS : @Hardware.BackPlanB.Modul2.Ch7;
    );
  );
  N2Press    : UCalibStruct =
    ( Sensor   : @Hardware.BackPlanA.Modul1.ConfCh4;
      HWCOUNTS : @Hardware.BackPlanA.Modul1.Ch4;
    );
  N2Level    : UCalibStruct =
    ( Sensor   : @Hardware.BackPlanA.Modul1.ConfCh0;
      HWCOUNTS : @Hardware.BackPlanA.Modul1.Ch0;
    );
  ColTemp    : UCalibStruct =
    ( Sensor   : @Hardware.BackPlanB.Modul0.ConfCh4;
      HWCOUNTS : @Hardware.BackPlanB.Modul0.Ch4;
    );
  Trans1     : UCalibStruct =
    ( Sensor   : @Hardware.BackPlanB.Modul0.ConfCh5;
      HWCOUNTS : @Hardware.BackPlanB.Modul0.Ch5;
    );
  Trans2     : UCalibStruct =
    ( Sensor   : @Hardware.BackPlanB.Modul0.ConfCh6;
      HWCOUNTS : @Hardware.BackPlanB.Modul0.Ch6;
    );
  GCSetTemp  : UCalibStruct =
    ( Sensor   : @Hardware.BackPlanB.Modul0.ConfCh7;
      HWCOUNTS : @Hardware.BackPlanB.Modul0.Ch7;
    );
);
);
WorkTemps   : WorkTempStruct =
( RefTemp    : TCalibStruct =
  ( Sensor   : @Hardware.BackPlanB.Modul1.ConfCh3;
    HWCOUNTS : @Hardware.BackPlanB.Modul1.Ch3;
  );
  TSamp      : TCalibStruct =
    ( Sensor   : @Hardware.BackPlanB.Modul1.ConfCh2;
      HWCOUNTS : @Hardware.BackPlanB.Modul1.Ch2;
    );
  TRackInlet : TCalibStruct =
    ( Sensor   : @Hardware.BackPlanB.Modul1.ConfCh7;
      HWCOUNTS : @Hardware.BackPlanB.Modul1.Ch7;
    );
  TTBox1     : TCalibStruct =
    ( Sensor   : @Hardware.BackPlanB.Modul1.ConfCh5;
      HWCOUNTS : @Hardware.BackPlanB.Modul1.Ch5;
    );
  TTBox2     : TCalibStruct =
    ( Sensor   : @Hardware.BackPlanB.Modul1.ConfCh6;
      HWCOUNTS : @Hardware.BackPlanB.Modul1.Ch6;
    );
  N2Temp     : TCalibStruct =
    ( Sensor   : @Hardware.BackPlanB.Modul2.ConfCh3;
      HWCOUNTS : @Hardware.BackPlanB.Modul2.Ch3;
      TempOffsuV : @Work.WorkTemps.RefTemp.TempOffsuV;
    );
  ITMupo    : TCalibStruct =
    ( Sensor   : @Hardware.BackPlanA.Modul0.ConfCh5;
      HWCOUNTS : @Hardware.BackPlanA.Modul0.Ch5;
    );
  ITSMupo   : TCalibStruct =
    ( Sensor   : @Hardware.BackPlanA.Modul0.ConfCh7;
      HWCOUNTS : @Hardware.BackPlanA.Modul0.Ch7;
    );
  ITinjector : TCalibStruct =
    ( Sensor   : @Hardware.BackPlanB.Modul1.ConfCh4;
      HWCOUNTS : @Hardware.BackPlanB.Modul1.Ch4;
    );
  ITinlet1   : TCalibStruct =
    ( Sensor   : @Hardware.BackPlanA.Modul1.ConfCh1;
      HWCOUNTS : @Hardware.BackPlanA.Modul1.Ch1;
    );
  ITinlet2   : TCalibStruct =
    ( Sensor   : @Hardware.BackPlanA.Modul1.ConfCh2;
      HWCOUNTS : @Hardware.BackPlanA.Modul1.Ch2;
    );
  ITExtend   : TCalibStruct =
    ( Sensor   : @Hardware.BackPlanA.Modul0.ConfCh1;
      HWCOUNTS : @Hardware.BackPlanA.Modul0.Ch1;
    );
);
);

```

```

    );
    TCatalyst : TCalibStruct =
    ( Sensor      : @Hardware.BackPlanB.Modul2.ConfCh5;
      HWCOUNTS    : @Hardware.BackPlanB.Modul2.Ch5;
      TempOffsuV  : @Work.WorkTemps.RefTemp.TempOffsuV;
    );
  );
  WorkLogs : WorkLogStruct =
  ( Viewer      : LoggerStruct = (LoggData : @View);
    ViewState   : @Work.WorkLogs.Viewer.LoggState;
    TrapsLogger : LoggerStruct = (LoggData : @TrapsLog);
    TrapsState  : @Work.WorkLogs.TrapsLogger.LoggState;
    Checker1    : LoggerStruct = (LoggData : @Check1);
    Chk1State   : @Work.WorkLogs.Checker1.LoggState;
    Checker2    : LoggerStruct = (LoggData : @Check2);
    Chk2State   : @Work.WorkLogs.Checker2.LoggState;
  );
);
);

procedure MupoError (var MuPo : MupoStruct; MupoTmOut : LongInst);
begin
  with MuPo do begin
    if (Fail >= MupoTmOut) then begin
      UserData.CycleStatus.FailState := MupoPos;
      Fail := 0;
    end;
  end;
end;

procedure WriteStrLn (var DataDir: FileInst; var DataFile : FileInst; DataStr : StringInst);
var DataDate : StringInst; DateTime : StringInst; DataLine : StringInst; OutFile : FileInst;
begin
  OutFile := DataDir + '\ ' + DataFile;
  DataDate := JulianDate(BinDate(now),'.');
  DateTime := JulianTime(BinTime(now,0),':',0);
  DataLine := DataDate + ' ' + DateTime + ' ' + DataStr;
  Open(OutFile,AppendMode);
  WriteLn(OutFile,DataLine);
  Close(OutFile);
end;

procedure SetSample;
begin
  with UserData, Sequence, Physics, ZA_CG, Sampling.Valves do begin
    if (NextInlet = 2) then InletSel.Control := on else InletSel.Control := off;
    if (NextSample = Zero) or (NextSample = Calib) then begin
      if (NextSample = Zero) then CalibRun := off
      else begin
        CalibRun := on;
        CalibLevel := NextCalLvl;
      end;
      ZeroRun := on;
    end
    else ZeroRun := off;
  end;
end;

procedure Hd1Ctrl (var Control : ControlStruct);
var LocTime1 : TimeInst; LocTime2 : TimeInst;
begin
  with UserData, CycleStatus, Control, Physics, Dewar, Sampling, ZA_CG, Work, WorkLogs do begin
    with Environment, ViciMupos, Flows, LineHeaters, SampParams, FlowParams, TempParams do begin

      on MainCtrl do if (MainCtrl = off) then begin
        ThermZones := off;
        TrapsMain := off;
        ZeroRun := off;
        Running := off;
        PurgeWCtrl := off;
        PumpCalVol := off;
        LoggerMain := off;
        GCMS_Start := off;
        RunType := ' ';
        NextRun := ' ';
        Valves.ValvePanel := 0;
        FlshSamp.SetFlow := 0;
        FlshWater.SetFlow := 0;
        N2PurgeFC.SetFlow := 0;
        SampleFC.SetFlow := CollectF;
        InletFC.SetFlow := InletF;
        TrapsMupo.SetPos := SamplePos;
      end;

      on ThermZones do begin
        N2PressReg.SetValue := DewarSetP;
        TMupoReg.SetValue := MupoSetT;
        SMupoReg.SetValue := MupoSetT;
        TBox1Reg.SetValue := TBoxSetT;
        TBox2Reg.SetValue := TBoxSetT;
        InjectorReg.SetValue := InjectSetT;
        Inlet1Reg.SetValue := InletSetT;
        Inlet2Reg.SetValue := InletSetT;
        ExtendReg.SetValue := InletSetT;
      end;
    end;
  end;
end;

```

```

    CatalystReg.SetValue := CatSetTemp;
    N2PressReg.Control   := ThermZones;
    TMupoReg.Control    := ThermZones;
    SMupoReg.Control    := ThermZones;
    TBox1Reg.Control     := ThermZones;
    TBox2Reg.Control     := ThermZones;
    InjectorReg.Control  := ThermZones;
    ExtendReg.Control    := ThermZones;
    CatalystReg.Control  := ThermZones;
    if (ThermZones = auto) then begin
        Inlet1Reg.Control := auto;
        Inlet2Reg.Control := auto;
    end;
end;

on TTBoxL do if (TTBoxL >= TBoxMin) then ThermState := CatStatus else ThermState := busy;

on TrapsMain do begin
    if (TrapsMain < Heat) then begin
        CryoTrap.CycleCtrl := TrapsMain;
        EnrichTrap.CycleCtrl := TrapsMain;
        WaterTrap.CycleCtrl := TrapsMain;
    end;
    if (TrapsMain = Heat) then begin
        CryoTrap.CycleCtrl := TrapsMain;
        StartTimer(LocTime1,20000,fromNow);
    end;
end;

on LocTime1 do begin
    EnrichTrap.CycleCtrl := TrapsMain;
    StartTimer(LocTime2,20000,fromNow);
end;

on LocTime2 do WaterTrap.CycleCtrl := TrapsMain;

on LoggerMain do begin
    Viewer.LoggerCtrl := LoggerMain;
    TrapsLogger.LoggerCtrl := LoggerMain;
    Checker1.LoggerCtrl := LoggerMain;
    Checker2.LoggerCtrl := LoggerMain;
end;

end;
end;
while 0 = 0 do HandleEvents(1);
end;

procedure HdlTrap (var Trap : TrapStruct);
begin
    with Trap do begin

        SetVolt := MaxVolt;

        on Temp do begin
            PowerOut := HeatReg.PowerFac + CoolReg.PowerFac;
            if (CycleCtrl = Cool) and (abs(CoolReg.SetValue - Temp) <= TempTol) then Status := ready
            else if (CycleCtrl = Heat) and (abs(HeatReg.SetValue - Temp) <= TempTol) then Status := ready
            else Status := busy;
        end;

        on CycleCtrl do begin
            if (CycleCtrl < Cool) then begin
                HeatCtrl := CycleCtrl;
                CoolCtrl := CycleCtrl;
            end;
            if (CycleCtrl = Cool) then with CoolReg do begin
                HWOutMin := -FC_N2.Size;
                HeatCtrl := off;
                Control := auto;
            end;
            if (CycleCtrl = Heat) then with HeatReg do begin
                HWOutMax := HeatMax;
                Control := auto;
                CoolCtrl := off;
            end;
        end;

    end;

    while 0 = 0 do HandleEvents(1);
end;

procedure MupoServer (var ViciMupos : ViciStruct);
var LocTime1 : TimeInst; LocTime2 : TimeInst; LocTime3 : TimeInst;
begin
    with ViciMupos do begin

        with UserData.Control.Param do while ParamDone <> Done do waitfor(ParamDone);

        NewID := -1;
        on SetID do MuPoSetID2(ComRs232, SetID, NewID);

        on TrapsMupo.SetPos do MupoSetPos(ComRs232, TrapsMupo);
        on SourceMupo.SetPos do MupoSetPos(ComRs232, SourceMupo);
    end;
end;

```



```

    on InletMupo.SetPos do MupoSetPos(ComRs232, InletMupo);

ComRs232 := 'Com2';
Open(ComRs232,ReadMode or WriteMode);
SetDelimiter(ComRs232,$000D);

on LocTime1 do begin
    MupoGetPos(ComRs232, TrapsMupo);
    StartTimer(LocTime2,300,fromNow);
end;
on LocTime2 do begin
    MupoGetPos(ComRs232, SourceMupo);
    StartTimer(LocTime3,300,fromNow);
end;
on LocTime3 do begin
    MupoGetPos(ComRs232, InletMupo);
    StartTimer(LocTime1,300,fromNow);
end;

TrapsMupo.SetPos := TrapsMupo.DefaultPos;
SourceMupo.SetPos := SourceMupo.DefaultPos;
InletMupo.SetPos := InletMupo.DefaultPos;
LocTime1 := now;

end;
while 0 = 0 do HandleEvents(1);
end;

procedure Hdllines (var LineHeaters : LineHeatStruct);
begin
    with LineHeaters do begin
        on TBox1Reg.Value do begin
            if (TBox1Reg.Value <= TBox2Reg.Value) then begin
                TBoxL := TBox1Reg.Value;
                TBoxH := TBox2Reg.Value;
            end
            else begin
                TBoxL := TBox2Reg.Value;
                TBoxH := TBox1Reg.Value;
            end;
        end;
    end;
    while 0 = 0 do HandleEvents(1);
end;

procedure HdLGCMS (var GC : GCMSStruct);
var LocTimer : TimeInst;
begin
    with GC, StartOut do begin

        On LocTimer do begin
            Control := off;
            Start := off;
        end;

        On Start do begin
            if Start = on then begin
                if Status = busy then Start := off else Control := on;
                StartTimer (LocTimer,StartTime,fromNow);
            end;
        end;

        On StatusIn.Value do if StatusIn.Value > StatusHigh then Status := ready else Status := busy;

        LocTimer := now;

    end;
    while 0 = 0 do HandleEvents(1);
end;

procedure HdLZACG (var ZA_CG : ZACGStruct);
begin
    with UserData, Physics, ZA_CG, Sampling, ViciMupos, Flows, Valves, SampParams, FlowParams do begin
        on TCatalyst do begin
            if (abs(CatSetTemp - TCatalyst) <= CatTempTol) then CatStatus := ready else CatStatus := busy;
        end;

        on ZeroRun do begin
            if (ZeroRun = on) then begin
                ZeroAirFC.SetFlow := ZeroAirF;
                InletMupo.SetPos := ZAG_Pos;
                ZABypass.Control := off;
                if (CalibRun = on) then begin
                    if (CalibLevel < StandLoFC.Size) then begin
                        StandLoFC.SetFlow := CalibLevel;
                        StandHiFC.SetFlow := 0;
                    end
                    else begin
                        StandLoFC.SetFlow := 0;
                        StandHiFC.SetFlow := CalibLevel;
                    end;
                end;
            end;
        end;
    end;
end;

```

```

        StandIn.Control := on;
    end
    else begin
        StandLoFC.SetFlow := 0;
        StandHiFC.SetFlow := 0;
        StandIn.Control := off;
    end;
end;
end
else begin
    ZeroAirFC.SetFlow := 0;
    StandLoFC.SetFlow := 0;
    StandHiFC.SetFlow := 0;
    StandIn.Control := off;
    InletMupo.SetPos := InletPos;
end;
end;

end;
while 0 = 0 do HandleEvents(1);
end;

procedure HdlTemps (var WorkTemps : WorkTempStruct);
begin
    with WorkTemps, UserData.Hardware do begin

        with BackPlanB.Modul4 do on Out0.SetVolt do begin
            Out1.SetVolt := Out0.SetVolt;
        end;

        with BackPlanA.Modul3 do on Out0.SetVolt do begin
            Out1.SetVolt := Out0.SetVolt;
            Out2.SetVolt := Out0.SetVolt;
        end;

    end;
    while 0 = 0 do HandleEvents(1);
end;

procedure HdlWork (var Work : WorkStruct);
begin
    with UserData, Work, WorkLogs, Checker1, Physics do begin

        on LoggDir do DataDir := LoggDir;

        with ZA_CG do on ZeroRun do begin
            if (ZeroRun = on) then LoggPeriod := ZALogHigh else LoggPeriod := ZALogLow;
        end;

        with View do begin
            on UTC do CycleStatus.LocalTime := UTC + TimeZone;
            on GCStatus do if (GCStatus = ready) then Sampling.Valves.GCFan.Control := off;
        end;

    end;
    while 0 = 0 do HandleEvents(1);
end;

procedure HdlRunSeq (var Sequence : RunSeqStruct);
var LocTime : TimeInst;
begin
    while 0 = 0 do with Sequence, ReadRun do begin

        while SeqCtrl < Curve do begin
            NextSample := SeqCtrl;
            SetSample;
            waitfor(SeqCtrl);
        end;

        while SeqCtrl = Curve do begin
            Advance := off;
            if (Open(CurveFile,ReadMode) <> 0) then begin
                FileStatus := notFound;
                SeqCtrl := Sample;
            end
            else begin
                FileStatus := loaded;
                ReadRecord(CurveFile,ReadRun,100);
                while ReadRecord(CurveFile,ReadRun,1000) = 0 do begin
                    NextLine := SeqLine;
                    NextInlet := Inlet;
                    NextSample := SampType;
                    NextCallLvl := CallLvl;
                    while SeqCtrl = Curve do begin
                        if (SetLine > 0) and (SetLine <> NextLine) then break;
                        SetLine := 0;
                        StartTimer(LocTime,1000,fromNow);
                        waitfor(LocTime);
                        if (Advance = on) then break;
                    end;
                    Advance := off;
                    if (SeqCtrl <> Curve) then break;
                end;
                FileStatus := ___;
            end;
        end;
    end;
end;

```

```
    Close(CurveFile);
    if (SeqCtrl = Curve) then SeqCtrl := Sample; SetLine := 0;
end;

while SeqCtrl = FileSeq do begin
  Advance := off;
  if (Open(RunSeqFile,ReadMode) <> 0) then begin
    FileStatus := notFound;
    SeqCtrl := Sample;
  end
  else begin
    FileStatus := loaded;
    ReadRecord(RunSeqFile,ReadRun,100);
    while ReadRecord(RunSeqFile,ReadRun,1000) = 0 do begin
      NextLine := SeqLine;
      NextInlet := Inlet;
      NextSample := SampType;
      NextCallLvl := CallLvl;
      while SeqCtrl = FileSeq do begin
        if (SetLine > 0) and (SetLine <> NextLine) then break;
        SetLine := 0;
        StartTimer(LocTime,1000,fromNow);
        waitfor(LocTime);
        if (Advance = on) then break;
      end;
      Advance := off;
      if (SeqCtrl <> FileSeq) then break;
    end;
    if (SetLine > NextLine) then SetLine := 0;
    FileStatus := ___;
  end;
  Close(RunSeqFile);
end;

end;
end;

procedure HeaterCheck (var HeatCheck : HeatChkStruct);
var LocTime : TimeInst; ScaledPower : SingleInst;
begin
  while 0 = 0 do with HeatCheck, Heater do begin

    if (Control <> auto) then waitfor(Control);

    if (HeatRate = 0) then HeatRate := 0.001;
    while Control = auto do begin
      if (FailCount >= MaxFail) then begin
        Control := Fail;
        break;
      end;
      ScaledPower := (PowerFac - HoldPower) / (100 - HoldPower);
      if (ScaledPower < 0) then ScaledPower := 0;
      Expected := Value + (HeatRate * ScaledPower * (CutTime / 1000));
      LocTime := now + CutTime;
      waitfor(LocTime);
      if (Control <> auto) then break;
      Error := Value - Expected;
      if (Error < Tolerance) then FailCount := FailCount + 1 else FailCount := 0;
    end;

  end;
end

procedure Hd1CalVol (var Sampling : SamplingStruct);
begin
  while 0 = 0 do with Sampling, Valves do begin

    while PumpCalVol = off do begin
      CalVolOut.Control := off;
      waitfor(PumpCalVol);
    end;

    if (PumpCalVol = on) then begin
      CalVolOut.Control := on;
      while PumpCalVol = on do begin
        if (SampPress <= MinSmpPres) then break;
        waitfor(TSamp);
      end;
      PumpCalVol := off;
    end;

  end;
end;

procedure Hd1GCFFlow (var GCFFlowProg : GCFFlowStruct);
var LocTime : TimeInst; TimeDiff : LongInst; dSetFlow : SingleInst;
begin
  while 0 = 0 do with GCFFlowProg, ReadFlow do begin

    while GCFFlowCtrl = off do begin
      GCHeSet := GCCnstFlow;
      GCFFlowTime := 0;
      waitfor(GCHeFlow);
    end;

  end;

end;
```

```

while GCFlowCtrl = on do begin
  GCFlowTime := 0;
  while GCFlowCtrl = on do begin
    if (Running = on) then GCHeSet := InjectFlow else GCHeSet := GCCnstFlow;
    waitfor(GCHeFlow);
    if (MSStartSig > 0) then break;
  end;
  if (GCFlowCtrl <> on) then break;

  GCFan.Control := off;
  if (Open(GCFlowFile,ReadMode) <> 0) then FileStatus := notFound
  else begin
    FileStatus := loaded;
    LocTime := now;
    while ReadRecord(GCFlowFile,ReadFlow,1000) = 0 do begin
      TimeDiff := NextTime - GCFlowTime;
      dSetFlow := (NextValue - GCHeSet) * 500 / TimeDiff;
      while GCFlowTime < NextTime do begin
        GCHeSet := GCHeSet + dSetFlow;
        GCFlowTime := GCFlowTime + 500;
        LocTime := LocTime + 500;
        waitfor(LocTime);
        if (GCFlowCtrl <> on) then break;
      end;
      if (GCFlowCtrl <> on) then break;
    end;
    GCFan.Control := on;
    FileStatus := ___;
  end;
  Close(GCFlowFile);
end;

end;
end;

procedure Interlock;
var FailStr : StringInst; OldPress : SingleInst; DiffSum1 : SingleInst; DiffSum2 : SingleInst;
begin
  with UserData, CycleStatus, Control, Physics, Dewar, Environment, Work do begin
    with Sampling, ViciMupos, LineHeaters do begin

      with CryoTrap do on HeatCtrl do if (HeatCtrl = Fail) then FailState := HeatError;
      with EnrichTrap do on HeatCtrl do if (HeatCtrl = Fail) then FailState := HeatError;
      with WaterTrap do on HeatCtrl do if (HeatCtrl = Fail) then FailState := HeatError;

      on N2Press do begin
        DiffSum2 := DiffSum1;
        DiffSum1 := (OldPress - N2Press + DiffSum2 * (AveInt - 1)) / AveInt;
        if ((DiffSum1 + DiffSum2) > (PressTol * (2 * AveInt - 1) / (AveInt * AveInt))) then begin
          FailState := DewarPres;
        end;
        OldPress := N2Press;
      end;

      on N2Level do if (N2Level <= MinN2Level) then FailState := N2LvlLow;
      on TBoxL do if (TBoxL <= TBoxMin) then FailState := TrapBox;
      on InjtTimer do if (InjtTimer >= MaxInjtTm) then FailState := InjtTime;
      on SampTimer do if (SampTimer >= MaxSampTm) and (ProcCtrl > Purge) then FailState := SampTime;

      on TrapsMupo.Fail do MupoError(TrapsMupo, MupoTmOut);
      on SourceMupo.Fail do MupoError(SourceMupo, MupoTmOut);
      on InletMupo.Fail do MupoError(InletMupo, MupoTmOut);

      on FailState do if (FailState <> __) then begin
        if (FailState = HeatError) or (ProcCtrl > Purge) then begin
          FailStr := str(FailState);
          WriteStrLn(DataDir,FailList,FailStr);
          FailCount := FailCount + 1;
          if (FailState <= N2LvlLow) then ProcCtrl := off
          else begin
            if (FailCount >= MaxFail) then ProcCtrl := off else ProcCtrl := Error;
          end;
        end;
      end;

      on FailReset do if (FailReset = on) then begin
        FailState := __;
        FailCount := 0;
        FailReset := off;
      end;

    end;
  end;
  while 0 = 0 do HandleEvents(1);
end;

procedure HdlRemote;
begin
  while 0 = 0 do with UserData, CycleStatus, Physics, Work do begin
    if (GCMS_Start > stdby) then GCMS_Start := off;

    while GCMS_Start = stdby do begin

```

```
    if (GC.Status = ready) and (MS.Status = ready) then begin
        GCMS_Start := manual;
        break;
    end;
    waitfor(View.TSamp);
end;

if (GCMS_Start = manual) then begin
    GC.Start := on;
    MS.Start := on;
    WriteStrLn(DataDir,RunList,RunType);
    GCMS_Start := off;
end;

if (GCMS_Start = off) then waitfor(GCMS_Start);

end;
end;

procedure Hd1Start;
begin
    while 0 = 0 do with UserData, CycleStatus, Control do begin

        if (AutoStart = off) then waitfor(AutoStart);

        while AutoStart = on do begin
            ProcCtrl := Prepare;
            while Autostart = on do begin
                if (PrepState = Prepared) then break;
                waitfor(PrepState);
            end;
            if (Autostart <> on) then break;
            ProcCtrl := Auto;
            AutoStart := off;
        end;

    end;
end;

procedure PurgeWater;
var LocTime : TimeInst;
begin
    while 0 = 0 do with UserData, Physics, Dewar, WaterTrap do begin
        with Sampling.Flows.F1shWater, SampParams, FlowParams do begin

            if (PurgeWCtrl = off) then waitfor(PurgeWCtrl);

            while PurgeWCtrl = on do begin
                SetFlow := WaterPurge;
                CycleCtrl := Heat;
                LocTime := now + WPurgeTime;
                while PurgeWCtrl = on do begin
                    if (now > LocTime) then break;
                    waitfor(Temp);
                end;
                if (PurgeWCtrl <> on) then break;

                SetFlow := WaterStdF;
                LocTime := now + TransTime - WPurgeTime - WaterCoolX;
                while PurgeWCtrl = on do begin
                    if (now > LocTime) then break;
                    waitfor(Temp);
                end;
                if (PurgeWCtrl <> on) then break;

                CycleCtrl := Cool;
                PurgeWCtrl := off;
            end;

        end;
    end;
end;

procedure PrepLoop;
var LocTime : TimeInst;
begin
    while 0 = 0 do with UserData, CycleStatus, Control, Physics, Dewar, Sampling, ZA_CG, GC_Aux do begin
        with Environment, ViciMupos, Flows, Valves, SampParams, FlowParams, TempParams do begin

            while ProcCtrl = off do begin
                PrepState := off;
                MainCtrl := off;
                AutoStart := off;
                SourceMupo.SetPos := PlugSource;
                waitfor(ProcCtrl);
            end;

            while ProcCtrl = DewarFill do begin
                if (Running = off) then ProcCtrl := Purge;
                PrepState := DewarPrep;
                while ProcCtrl = DewarFill do begin
                    if (InjtState = Injecting) then break;
                    waitfor(TSamp);
                end;
            end;
        end;
    end;
end;
```

```

if (ProcCtrl <> DewarFill) then break;

N2PressReg.Control := off;
SourceMupo.SetPos := HeSource;
TrapsMupo.SetPos := SamplePos;
FlshSamp.SetFlow := SampStdF;
TrapsMain := Heat;
ZeroRun := on;
LoggerMain := off;
Running := off;
PrepState := UKtoFill;
GCMS_Start := stdby;

while ProcCtrl = DewarFill do begin
  if (GCMS_Start <> stdby) then break;
  waitfor(TSamp);
end;
if (ProcCtrl <> DewarFill) then break;

RunType := ' ';
NextRun := ' ';
while ProcCtrl = DewarFill do begin
  GCMS_Start := stdby;
  DewarSetP := N2Press + 100.0;
  waitfor(TSamp);
end;
end;

while ProcCtrl = Purge do begin
  PrepState := Purge;
  MainCtrl := off;
  waitfor(TSamp);

  SourceMupo.SetPos := HeSource;
  FlshSamp.SetFlow := SampStdF;
  TrapsMain := Heat;
  ZeroRun := on;
  ThermZones := auto;
  waitfor(TSamp);
  N2PressReg.Control := off;

  LocTime := now + PurgeTime;
  while ProcCtrl = Purge do begin
    SampTimer := LocTime - now;
    GCMS_Start := stdby;
    waitfor(TSamp);
    if (now > LocTime) then ProcCtrl := off;
  end;
  SampTimer := 0;
end;

while ProcCtrl = FlowMax do begin
  PrepState := FlowMax;
  MainCtrl := off;
  waitfor(TSamp);

  SourceMupo.SetPos := HeSource;
  FlshSamp.SetFlow := SampStdF;
  TrapsMain := manual;
  ThermZones := auto;
  waitfor(TSamp);

  with EnrichTrap, FC_N2 do SetFlow := Size;
  with WaterTrap, FC_N2 do SetFlow := Size;
  with CryoTrap, FC_N2 do SetFlow := Size;

  waitfor(ProcCtrl);
end;

while ProcCtrl = TakeOff do begin
  PrepState := TakeOff;
  MainCtrl := off;
  waitfor(TSamp);

  ZABypass.Control := on;
  N2PurgeFC.SetFlow := N2PurgeF;
  InletFC.SetFlow := 0;
  InletMupo.SetPos := ZAG_Pos;
  SourceMupo.SetPos := HeSource;
  FlshSamp.SetFlow := SampStdF;
  ThermZones := auto;
  TrapsMain := Heat;

  waitfor(ProcCtrl);
end;

while ProcCtrl = Prepare do begin
  SampTimer := 0;
  waitfor(TSamp);

  PrepState := Prepping;
  LocTime := now;
  PurgeWCtrl := off;
  RunType := ' ';

```

```
NextRun      := ' ';
ZeroRun      := off;
ThermZones   := auto;
TrapsMain    := Cool;
PumpCalVol   := on;
LoggerMain   := on;
FlshWater.SetFlow := 0;
N2PurgeFC.SetFlow := 0;
SampleFC.SetFlow := CollectF;
InletFC.SetFlow := InletF;
TrapsMupo.SetPos := SamplePos;
SourceMupo.SetPos := HeSource;
GCFlowProg.GCFlowCtrl := on;
waitfor(TSamp);

FlshSamp.SetFlow := SampStdF;
while ProcCtrl = Prepare do begin
  GCMS_Start := stdby;
  SampTimer := now - LocTime;
  if (PumpCalVol = off) then break;
  waitfor(TSamp);
end;

PrepState := WtTZReady;
while ProcCtrl = Prepare do begin
  GCMS_Start := stdby;
  SampTimer := now - LocTime;
  if (ThermState = ready) then break;
  waitfor(TSamp);
end;
SampTimer := 0;
if (ProcCtrl <> Prepare) then break;

PrepState := Prepared;
waitfor(ProcCtrl);
end;

while ProcCtrl = Auto do begin
  if (PrepState <> Prepared) then ProcCtrl := Prepare
  else begin
    LoggerMain := on;
    TrapsMain := auto;
    GCMS_Start := stdby;
    waitfor(TSamp);
    Running := on;
    waitfor(ProcCtrl);
  end;
end;

while ProcCtrl = Error do begin
  PrepState := off;
  AutoStart := off;
  StartTimer(LocTime,2000,fromNow);
  waitfor(LocTime);
  SampTimer := 0;
  InjTTimer := 0;
  AutoStart := on;
  waitfor(ProcCtrl);
end;

end;
end;
end;

procedure SampleLoop;
var LocTime : TimeInst; EndPress : SingleInst; dum1 : LongInst; dum2 : LongInst;
begin
  while 0 = 0 do with UserData, CycleStatus, Physics, Dewar, Sampling, ZA_CG, Sequence do begin
    with ViciMupos, Flows, Valves, SampParams, FlowParams, TempParams, Work do begin

      while Running = off do begin
        SampState := off;
        waitfor(Running);
      end;

      SetSample;
      while Running = on do begin
        SampState := PrepTraps;
        TrapsMupo.SetPos := SamplePos;
        FlshSamp.SetFlow := CoolFlshF;
        FlshWater.SetFlow := 0;
        EnrichTrap.CycleCtrl := Cool;
        WaterTrap.CycleCtrl := Cool;
        waitfor(TSamp);

        LocTime := now;
        while Running = on do begin
          if (EnrichTrap.Status = ready) and (WaterTrap.Status = ready) then break;
          SampTimer := now - LocTime;
          waitfor(TSamp);
        end;

        while Running = on do begin
          if (PumpCalVol = off) then break;
```

```

    SampTimer := now - LocTime;
    waitfor(TSamp);
end;
SampTimer := 0;
if (Running <> on) then break;

SampState := Sampling;
StartPress := (SampPress / StdPress) * (StdTemp / (TSamp + StdTOffSet));
if (NextSample = Bottle) then SourceMupo.SetPos := BotlSource else SourceMupo.SetPos := SampSource;
CalVolIn.Control := on;
SampleFC.SetFlow := CollectF;
FlshSamp.SetFlow := 0;

LocTime := now;
while Running = on do begin
    EndPress := StdPress * ((TSamp + StdTOffSet) / StdTemp) * (SampSize / CalVol + StartPress);
    if (SampPress >= EndPress) then break;
    SampTimer := now - LocTime;
    waitfor(TSamp);
end;
LstSampTm := SampTimer;
SampTimer := 0;
if (Running <> on) then break;

SampState := SampChase;
CalVolIn.Control := off;
SourceMupo.SetPos := HeSource;
FlshSamp.SetFlow := ChaseF;
LocTime := now + ChaseTime;

SetSample;
Advance := on;

while Running = on do begin
    if (now > LocTime) then break;
    waitfor(TSamp);
    SampTimer := LocTime - now;
end;
SampTimer := 0;
if (Running <> on) then break;

SampState := WaitInjt;
PumpCalVol := on;
while Running = on do begin
    if (InjtState = InjtReady) then break;
    SampTimer := now - LocTime;
    waitfor(TSamp);
end;
if (Running <> on) then break;

SampState := Transfer;
FlshSamp.SetFlow := SampStdF;
TrapsMupo.SetPos := TransPos;
PurgeWCtrl := on;
EnrichTrap.CycleCtrl := Heat;

LocTime := now + TransTime;
while Running = on do begin
    if (now > LocTime) then break;
    SampTimer := LocTime - now;
    waitfor(TSamp);
end;
SampTimer := 0;
if (Running <> on) then break;

RunType := NextRun;
if (ZeroRun = off) then begin
    if (NextSample = Bottle) then NextRun := 'Bottle' else NextRun := 'Sample'
end
else begin
    if (CalibRun = off) then NextRun := 'Zero' else NextRun := 'Calib' + Str(CalibLevel);
end;

InjtState := WaitGCMS;
end;

end;
end;

procedure InjectLoop;
var LocTime : TimeInst;
begin
    while 0 = 0 do with UserData, CycleStatus, Physics, Dewar do begin
        with CryoTrap, TempParams, GC_Aux, GCTemps do begin

            while Running = off do begin
                InjtState := off;
                waitfor(Running);
            end;

            while Running = on do begin
                InjtState := PrepInjt;
                CycleCtrl := Cool;

```



```
    waitfor(Temp)

    LocTime := now;
    while Running = on do begin
        if (Status = ready) then break;
        InjtTimer := now - LocTime;
        waitfor(Temp);
    end;
    InjtTimer := 0;

    while Running = on do begin
        if (ColTemp >= TransTrig) then break;
        waitfor(Temp);
    end;
    if (Running <> on) then break;
    InjtState := InjtReady;

    LocTime := now;
    while Running = on do begin
        if (InjtState = WaitGCMS) then break;
        InjtTimer := now - LocTime;
        waitfor(Temp);
    end;

    LocTime := now;
    while Running = on do begin
        if (ColTemp <= InjectTrig) then break;
        InjtTimer := now - LocTime;
        waitfor(Temp);
    end;
    InjtTimer := 0;
    if (Running <> on) then break;

    InjtState := Injecting;
    GCMS_Start := stdby;
    CycleCtrl := Heat;
    waitfor(Temp);

    LocTime := now + SampParams.InjectTime;
    while Running = on do begin
        if (now > LocTime) then break;
        waitfor(Temp);
        InjtTimer := LocTime - now;
    end;
    InjtTimer := 0;
end;

end;
end;

begin
    with UserData, Control, Work do begin

        BootTime := now;
        MClock (View.UTC);
        MParamSave (Param);

        CreateThread ('Interlock', 1024, Interlock);
        CreateThread ('HdlRemote', 2048, HdlRemote);
        CreateThread ('HdlStart', 1024, HdlStart);
        CreateThread ('PurgeWater', 1024, PurgeWater);
        CreateThread ('PrepLoop', 1024, PrepLoop);
        CreateThread ('SampleLoop', 1024, SampleLoop);
        CreateThread ('InjectLoop', 1024, InjectLoop);

        WriteWord (DispTastLED, 1);

        MakeDateDir(DataDir, yymmdd);

    end;
    while 0 = 0 do HandleEvents(1);
end;
```


Curriculum Vitae

Education:

- Max Planck Institute for Chemistry, Ph.D. Chemistry, July 2011 (Estimated)
- University of California – Berkeley, M.S. Chemistry, Dec 2007 (3.78 GPA)
- University of North Carolina – Chapel Hill, Jun–Dec 2005 (4.00 GPA)
- Brigham Young University, B.S. Chemistry, Cum Laude, April 2005 (3.83 GPA)
- 20 publications and presentations

Awards and Honors:

- Outstanding Graduate Student Instructor Award - Chem 1A Winter 2006 (UCB)
 - Top 10% of University GSI's
- Francis P. Venable Award - Sept 2005 (UNC)
 - Merit award for new graduate students
- Venable Summer Research Fellowship - Jun–Aug 2005 (UNC)
 - For early research before beginning graduate school
- Office of Research and Creative Activities Grant - Feb 2004 (BYU)
 - Awarded based on written proposal and experience
- Chemistry Department Undergraduate Research Awards - May 2003–Dec 2004 (BYU)
 - Merit based undergraduate research awards
- Dean's List, College of Physical and Mathematical Sciences - 4 semesters (BYU)
 - Top 5% of students in College
- Heritage Scholar - Mar 1999 (BYU)
 - 4-year full-tuition merit scholarship

Teaching Experience:

- One semester and one term as General Chemistry Lab Instructor
- Two semesters as Physical Chemistry Lab Teacher's Assistant
- Four semesters as General Chemistry Lab Teacher's Assistant

Common Responsibilities and Goals:

- Graded lab reports and exams.
- Provided short pre-lab instruction as well as lecture summaries.
- Held test reviews and had office hours for providing one-on-one assistance.
- Helped students see connections between academic principles and real-world applications.

Department of Chemistry, University of California, Berkeley

Graduate Student Instructor, Chem 125 - Physical Chemistry Lab Sept–Dec 2006

Supervisors: Haw Yang and Edmundo Angeles

- Supervised several different experiments each class period.
- Administered oral lab reports to determine students full range of subject mastery.

Graduate Student Instructor, Chem 1A - General Chemistry Jan–May 2006
Supervisor: Mark Kubinec

- Worked through homework problems and administered quizzes.
- Developed a mid-semester instructor evaluation.

Department of Chemistry, University of North Carolina, Chapel Hill

Teaching Assistant, Chem 181L - Physical Chemistry Lab I Sept–Dec 2005
Supervisor: Carribeth Bliem

- Taught a lecture on computational molecular modeling and basis sets to 60 students.
- Provided support for mathematical and modeling software.

Department of Chemistry and Biochemistry, Brigham Young University, Provo, UT

Laboratory Instructor, Chem 107 - General Chemistry Lab Apr–June 2004
Faculty Mentor: Philip R. Brown Jan–Apr 2005

- Supervised and trained Teaching Assistants.
- Presented introduction to course and safety training to class of 120 students.
- Coordinated course materials with stockroom.
- Wrote exams and assigned final grades.
- Addressed student issues and enforced Honor Code.

Teaching Assistant, Chem 107 - General Chemistry Lab Aug 2002–Apr 2004
Supervisor: Philip R. Brown

Private Tutor

One-on-one mentoring one semester for a college Junior in Physical Chemistry II and one semester for a high school chemistry student.

Computer and Instrumental Skills:

- Programming languages: Pascal, Igor, Visual Basic, Java, Matlab, LabView, Mathcad, Perl
- Instrument experience: MS and isotope ratio MS, GC, Cryogenic concentrators, TD-GC, Raman and UV/Vis spectrometers, NMR, FTIR (including step-scan modifications), YAG laser and optics, vacuum systems, computer interfaced transducers, XPS, ICP, HPLC-DAD, ISE, DSC, PPLN-OPO

Research Experience:

Max Planck Institute for Chemistry, Mainz, Germany

Jonathan Williams, Advisor Jan 2008–present

- Participated in field campaigns and performed laboratory measurements.
- Developed and constructed a fast GC-MS system for in situ VOC measurement.
- Designed innovative cryogenic sampling system.
- Prepared fast GC-MS for use aboard HALO scientific aircraft.
- Developed automated data handling and analysis routines.

Department of Chemistry, University of California, Berkeley

Kristie A. Boering, Advisor

Feb 2006–Sep 2007

- Measured and analyzed stable isotope ratios of N₂O isotopologues.
- Investigated stratospheric dynamics and mixing across the polar winter vortex.
- Constrained magnitude of tropospheric sources of greenhouse gases.
- Maintained and serviced a MAT 252 isotope ratio mass spectrometer.

Department of Chemistry, University of North Carolina

Roger E. Miller, Advisor (Deceased Nov 2005)

Jun–Dec 2005

- Developed ion source for doping helium nanodroplets.

Department of Chemistry and Biochemistry, Brigham Young University

Matthew C. Asplund, Advisor

May 2004–May 2005

- Discovered important ligand exchange through temperature resolved experiments.
- Performed time-resolved FTIR experiments on nano- and millisecond time scales.
- Studied the dynamics of solvent-ligand exchange in coordination to metal complexes.
- Measured quantum yield of photochemistry reactions.
- Performed computer modeling of chemicals studied using ECCE (Gaussian interface).

Randall B. Shirts, Advisor

Aug 2002–Aug 2004

- Investigated hard sphere (HS) classical systems to determine equations of state.
- Investigated HS probability distributions of energy and velocity.
- Wrote 4000+ line macro for simulation data analysis.

Special Training:

Autumn School

Oct 2008

for Climate Change: Causes and Impacts in Paphos, Cyprus

Sponsored by the Energy, Environment and Water Research Centre, Cyprus, and the Max Planck Institute for Chemistry in Mainz, Germany

- Discussed causes of climate change and how they are measured.
- Discussed impacts of climate change and how they are modeled on global and local levels.
- Researched and presented impacts of climate change on North American regions.

Agilent Training Courses, Cheadle, UK

Feb 2008

ChemStation operation and GC-MS maintenance and troubleshooting

Autumn School

Oct 2006

for Measurement Techniques in Atmospheric Chemistry in Oberwesel, Germany

Sponsored by the University of Utrecht and the Max Planck Institute for Chemistry in Mainz

- Discussed wide range of measurement techniques currently employed in research field.
- Co-wrote a summary of one lecture for publication (see below).

Personal:

Born: 14 November 1980 in Saint Joseph, Missouri, USA

Publications:

- Williams, J., et al. The summertime boreal forest field measurement intensive (HUMPPA-COPEC-2010): an overview of meteorological and chemical influences. *Atmos. Chem. Phys. Discuss.*, 2011. In Print.
- Arduini, Jgor; Comfort, Lauren; Johnson, Aaron M.; and Holzinger, Rupert. Mass Spectrometry in Atmospheric Chemistry. "2. Mass Spectrometry in Atmospheric Chemistry." **Proceedings of the Autumn School for Measurement Techniques in Atmospheric Chemistry**. 2007.
- Shirts, R. B.; Burt, S. R.; Johnson, A. M. Periodic boundary condition induced breakdown of the equipartition principle and other kinetic effects of finite sample size in classical hard-sphere molecular dynamics simulation. *J. Chem. Phys.* 2006, *125*, 164102.
- Asplund, M. C.; Johnson, A. M.; Jakeman, J. A. Time-Resolved Infrared Dynamics of C–F Bond Activation by a Tungsten Metal–Carbonyl. *J. Phys. Chem. B* 2006, *110*, 20–24.

Selected Presentations: (presenter underlined)

- Aaron M. Johnson. Advancements in Airborne Fast GC-MS: A FACT Collaboration Project, (Poster). Autumn School for Climate Change: Causes and Impacts, Paphos, Cyprus, October 2008.
- Aaron M. Johnson. Advancements in Airborne Fast GC-MS: A FACT Collaboration Project, (Oral). IMPRS Days, Mainz, Germany, July 2008.
- Aaron M. Johnson. Isotopic Measurements of Nitrous Oxide: Stratospheric Transport and Arctic Ozone Loss, (Oral). Graduate Research Conference, Berkeley, CA, Feb. 2007.
- M. C. Asplund, J. A. Jakeman, A. M. Johnson. Time resolved studies of C–F bond activation using organometallics, (Poster). Charles Harris Symposium, Berkeley, CA, 2005.
- Matthew C. Asplund, Jared A. Jakeman, and Aaron M. Johnson. Time resolved infrared spectroscopy of a C-F bond activation reaction, (Oral INOR 791). ACS National Meeting, San Diego, CA, March 2005.
- Randall B. Shirts, Scott R. Burt, Aaron M. Johnson. Small-system effects in molecular dynamics simulations, (Oral COMP 020). ACS National Meeting, San Diego, CA, March 2005.
- Randall B. Shirts, Scott R. Burt, Aaron M. Johnson. Corrections to the microcanonical hard-sphere virial expansion for small numbers of particles and for small enclosures in both periodic and reflecting boundary conditions, (Poster PHYS 274). ACS National Meeting, San Diego, CA, March 2005.
- Matthew C. Asplund, Aaron M. Johnson, and Jared A. Jakeman. Influence of metal-solvent binding of C-F bond activation using a tungsten organometallic, (Poster PHYS 389). ACS National Meeting, San Diego, CA, March 2005.
- Randall B. Shirts, Aaron M. Johnson, and Scott R. Burt. Corrections to microcanonical hard-sphere virial coefficients for small numbers of particles and for small enclosures, (Poster PHYS 432). ACS National Meeting, Anaheim, CA, March 2004.
- Aaron M. Johnson, Randall B. Shirts. Corrections to Hard Sphere Virial Coefficients for Finite Systems, (Oral). BYU College of Physical and Mathematical Sciences, Spring Research